On Diffusion Transport Properties in Fuel Cell Gas Diffusion Layers Using the Lattice Boltzmann Method

Espinoza Andaluz, Mayken

2017

Document Version:
Publisher's PDF, also known as Version of record

On Diffusion Transport Properties in Fuel Cell Gas Diffusion Layers Using the Lattice Boltzmann Method

MAYKEN ESPINOZA ANDALUZ
DEPARTMENT OF ENERGY SCIENCES | LUND UNIVERSITY 2017

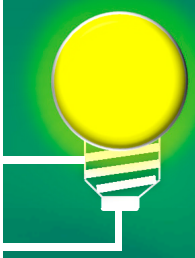

On Diffusion Transport Properties in Fuel Cell Gas Diffusion Layers Using the Lattice Boltzmann Method

On Diffusion Transport Properties in Fuel Cell Gas Diffusion Layers Using the Lattice Boltzmann Method

Mayken Stalin Espinoza Andaluz

LUND
UNIVERSITY

AKADEMISK AVHANDLING/DOCTORAL DISSERTATION

för avläggande av teknologie doktorsexamen vid Tekniska Fakulteten, Lunds Universitet att offentligen försvaras fredagen den 19:e maj kl. 10:15 i hörsal E, M-huset, Ole Römers väg 1, Lund, Sverige.

by due permission of the Faculty of Engineering at Lund University, will be defended on Friday 19th of May at 10:15 a.m. in Lecture Hall E in the M-building, Ole Römers väg 1, Lund, Sweden.

Fakultetsopponet/Faculty opponent
Associate Professor Erik Kjeang
Simon Fraser University
Vancouver, Canada

Organization	Document name
LUND UNIVERSITY Department of Energy Sciences	DOCTORAL DISSERTATION
	Date of issue 2017-04-10
Author(s) **Mayken Stalin Espinoza Andaluz**	Sponsoring organization Secretary of Higher Education, Science, Technology and Innovation – SENESCYT and ESPOL (Ecuador)

Title and subtitle

On Diffusion Transport Properties in Fuel Cell Gas Diffusion Layers Using the Lattice Boltzmann Method

Abstract

The polymer electrolyte fuel cell (PEFC) is considered as one of the most promising devices for providing efficient, clean and noiseless conversion of chemical energy to electrical energy. This device can provide electrical and thermal energy for transport, mobile and stationary applications ranging in a wide range of power requirements. However, in spite of its promising potential and increasing presence during recent years, the PEFCs are still not widely commercialized around the world. The competition with current technologies is hard, especially due to the high cost involved in the PEFC production and degradation issues.

The energy conversion within the PEFCs is maintained by different multi-physics and multi-chemical phenomena that occur at different length and time scales. The reactant gases and the electrons, products of the electrochemical reactions, flow through complex and anisotropic geometries which make their description difficult, especially when a pore-scale analysis is considered. As part of a PEFC, the gas diffusion layer (GDL) plays an important role in the energy conversion process, giving mechanical support to the cell and providing a structure to which the reactant and product fluids can flow; as well as it allows the flow of electrons from the active sites to the current collectors and vice versa.

A complete understanding of the diffusion transport properties, considering the morphological configuration at the pore-scale level, can give an insight to improve certain characteristics of the GDLs and eventually enhance the behavior of the whole system. Considering that a pore-scale and in-situ experiment represents a considerable investment of resources, computational tools to describe the different transport phenomena through the GDLs offer a unique opportunity to study the diffusion transport phenomena and estimate the properties of the GDLs.

Two- and three-dimensional models representing GDLs have been developed to analyze the impact of morphological configurations on certain diffusion transport properties, as well as the fluid behavior and mass transport through the mentioned layers when they are subjected to different conditions of compression, morphological configurations or inflow. Due to the complexity of the GDLs, the Lattice Boltzmann method (LBM) was chosen as the computational tool to describe and analyze the fluid flow behavior and the mass transport phenomena through the GDLs. This methodology can be applied not only to the mentioned layer in PEFCs, but also to the porous media found in other type of FC such as solid oxide fuel cells (SOFCs).

The GDLs are stochastically created and the diffusion transport parameters such as porosity, gas-phase tortuosity, permeability, inertial coefficient and normalized diffusivitiy are analyzed from a pore-scale point of view. This thesis not only provides insightful information about the different diffusion transport GDL parameters, but also offers an analysis of the effects of morphological configurations on the mentioned properties. Several correlations for gas-phase tortuosity, permeability and diffusibility among others, are proposed to predict the behavior of the mentioned parameters. The computation of the parameters is supported by single-phase Lattice Boltzmann models which allow a deep analysis of the fluid behavior and the mass transport phenomena through the digitally created GDLs. The GDL generation and the LB models are completely developed by the author.

Key words

PEFC, Lattice Boltzmann method, gas diffusion layers, porosity, gas-phase tortuosity, permeability, inertial coefficient, diffusibility, pore-scale modeling.

Classification system and/or index terms (if any)

Supplementary bibliographical information	Language English
ISSN and key title ISRN LUTMDN/TMHP-17/1129-SE	ISBN 978-91-7753-236-1 (print) 978-91-7753-237-8 (pdf)
Recipient's notes / Number of pages 168	Price
Security classification	

Signature  Date 2017-04-10

On Diffusion Transport Properties in Fuel Cell Gas Diffusion Layers Using the Lattice Boltzmann Method

Mayken Stalin Espinoza Andaluz

LUND
UNIVERSITY

Department of Energy Sciences
Faculty of Engineering (LTH)
Lund University
www.energy.lth.se

Thesis for the degree of Doctor of Philosophy in Engineering.

Coverphoto by Mayken Stalin Espinoza Andaluz

Department of Energy Sciences
Faculty of Engineering
Lund University
Box 118
SE-221 00 LUND
SWEDEN

ISBN 978-91-7753-236-1 (print)
ISBN 978-91-7753-237-8 (pdf)
ISRN LUTMDN/TMHP-17/1129-SE
ISSN 0282-1990

Printed in Sweden by Media-Tryck, Lund University
Lund 2017

"Si en lugar de afrontar el peligro,
hubiera yo cometido la vileza de pasarme
al enemigo, habríamos tenido paz,
***Mu**cha paz: **L**a paz del coloniaje"*
E. Alfaro

Abstract

The polymer electrolyte fuel cell (PEFC) is considered as one of the most promising devices for providing efficient, clean and noiseless conversion of chemical energy to electrical energy. This device can provide electrical and thermal energy for transport, mobile and stationary applications ranging in a wide range of power requirements. However, in spite of its promising potential and increasing presence during recent years, the PEFCs are still not widely commercialized around the world. The competition with current technologies is hard, especially due to the high cost involved in the PEFC production and degradation issues.

The energy conversion within the PEFCs is maintained by different multi-physics and multi-chemical phenomena that occur at different length and time scales. The reactant gases and the electrons, products of the electrochemical reactions, flow through complex and anisotropic geometries which make their description difficult, especially when a pore-scale analysis is considered. As part of a PEFC, the gas diffusion layer (GDL) plays an important role in the energy conversion process, giving mechanical support to the cell and providing a structure to which the reactant and product fluids can flow; as well as it allows the flow of electrons from the active sites to the current collectors and vice versa.

A complete understanding of the diffusion transport properties, considering the morphological configuration at the pore-scale level, can give an insight to improve certain characteristics of the GDLs and eventually enhance the behavior of the whole system. Considering that a pore-scale and in-situ experiment represents a considerable investment of resources, computational tools to describe the different transport phenomena through the GDLs offer a unique opportunity to study the diffusion transport phenomena and estimate the properties of the GDLs.

Two- and three-dimensional models representing GDLs have been developed to analyze the impact of morphological configurations on certain diffusion transport properties, as well as the fluid behavior and mass transport through the mentioned layers when they are subjected to different conditions of compression, morphological configurations or inflow. Due to the complexity of the GDLs, the Lattice Boltzmann method (LBM) was chosen as the computational tool to describe and analyze the fluid flow behavior and the mass transport phenomena through the GDLs. This methodology can be applied not only to the mentioned layer in PEFCs, but also to the porous media found in other type of FC such as solid oxide fuel cells (SOFCs).

The GDLs are stochastically created and the diffusion transport parameters such as porosity, gas-phase tortuosity, permeability, inertial coefficient and normalized

diffusivitiy are analyzed from a pore-scale point of view. This thesis not only provides insightful information about the different diffusion transport GDL parameters, but also offers an analysis of the effects of morphological configurations on the mentioned properties. Several correlations for gas-phase tortuosity, permeability and diffusibility among others, are proposed to predict the behavior of the mentioned parameters. The computation of the parameters is supported by single-phase Lattice Boltzmann models which allow a deep analysis of the fluid behavior and the mass transport phenomena through the digitally created GDLs. The GDL generation and the LB models are completely developed by the author.

Keywords: PEFC, Lattice Boltzmann method, gas diffusion layers, porosity, gas-phase tortuosity, permeability, inertial coefficient, diffusibility, pore-scale modeling.

Popular Science Summary

Cars delivering to the atmosphere water instead of contaminants? Back-up supply energy not emitting pollutants? Yes, it is possible!

Fuel cells (FCs) can supply electrical and thermal energy producing just water as product. During the process, the electrical energy is produced in a noiseless and efficient manner. Although FCs are not a new concept, there are still some issues that have to be clearly understood inside them.

FCs are normally designed in the range of tens of centimeters, and one of the most important elements is the so-called gas diffusion layer (GDL). This layer helps the energy conversion process to be performed by facilitating the flow of gases and electrons. Its structure is very complex and its thickness is in the range of micrometers.

This thesis provides a better understanding of the different diffusion transport properties found in the GDLs. This improved understanding is a door for finding better material configurations, and eventually to reduce production costs of the FCs which will help this device to increase its presence and use.

To provide useful information about the different diffusion properties of the GDLs, especially because of its really small size and complex structure, computational tools are employed. The geometries for analyzing the GDLs are digitally created, and the simulation model to mimic the fluid behavior is completely developed.

The results presented in this work will assist to predict the behavior of a complete FC based on computational tools. Such predictions can be used to propose better and improved material configurations for the different parts of the FCs, and finally give the FC a push forward in the world energy system.

For a cleaner world in which our next generations can live in!

Resumen de Divulgación Científica

¿Automóviles emitiendo a la atmósfera agua en lugar de contaminantes? ¿Suministro de respaldo de energía que no emita contaminantes? Si, es posible!

Las celdas de combustible pueden suministrar energía eléctrica y térmica produciendo como resultado únicamente agua. Durante el proceso, la energía eléctrica es producida sin ruido y de manera eficiente. Aunque el concepto de las celdas de combustible no es nuevo, hay algunos asuntos que deben ser claramente entendidos dentro de ellas.

Las celdas de combustible son normalmente diseñadas en el rango de las decenas de centímetros, y uno de los elementos mas importantes para su funcionamiento es la también llamada capa difusora de gases. Esta capa ayuda a que el proceso de conversión de la energía pueda efectuarse facilitando el flujo de gases y electrones. Su estructura es muy compleja y su espesor está en el rango de los micrómetros.

Esta tesis provee un mejor entendimiento de las diferentes propiedades de difusión encontradas en las capas difusoras de gases. Este mejorado entendimiento es una puerta para encontrar mejores configuraciones de los materiales, y eventualmene reducir el costo de producción de las celdas de combustible lo cual ayudará a incrementar su presencia y uso.

Para proveer información útil acerca de los diferentes parámetros de difusión de las capas difusoras de gases, especialmente debido a su tamaño muy pequeño y estructura compleja, herramientas computacionales son empleadas. Las modelos geométricos para analizar las capas difusoras de gases son digitalmente creados, y el modelo de simulación para imitar el comportamiento de los fluidos es completamente desarrollado.

Los resultados presentados en este trabajo asisten en la predicción del comportamiento de una celda de combustible completamente basado en modelos computacionales. Estas predicciones pueden ser usadas para proponer mejores y mejoradas configuraciones de materiales para las diferentes partes de las celdas de combustible, y finalmente darle a las celdas de combustible el avance en los sistemas de energía en el mundo.

Por un planeta mas limpio en el que nuestras próximas generaciones puedan vivir!

Acknowledgments

This work has been carried out at the Department of Energy Sciences, Faculty of Engineering of Lund University. Lund, Sweden.

I am very grateful to my supervisors Martin Andersson and Bengt Sundén. Their guidance, academic confidence, and all the support that I have received from them have been crucial during this period in Sweden. Several discussions with Jinliang Yuan are also kindly acknowledged.

In addition, I would like to express my gratitude to all my fellow PhD students, the current and the former ones, academic staff members and administrators at the Department of Energy Sciences for a nice working environment and cooperation during this time.

The current work was financially supported by the Secretary of Higher Education, Science, Technology and Innovation (Senescyt, Ecuador) on behalf of the Ecuadorian people. Additional support from ESPOL was also received which is gratefully acknowledged. Special thanks to Vinnova VINNMER (2015-01485) project, which made possible to have short-research-stay-visits at Forschungszentrum Jülich, Germany and allowed me to present some of the results at scientific conferences.

Finally, I would really like to mention all the people that made this happen, however; there is no memory to remember, and there is no space to write a complete, ordered and detailed list… I perhaps would need several pages for such a list. To all of you, to whose who contributed to a greater or lesser extent to achieve this goal, from near or from far away...

Tack så mycket!, Thank you very much!, Muchas gracias!

List of publications

The following publications are included in the thesis and are referenced by roman numerals in the body text of the thesis:

I. **Espinoza-Andaluz, M.**, Sundén, B., & Andersson, M. (2014). Highlights of Fuel Cell Modeling From a Lattice Boltzmann Method Point of View. *Volume 6A: Energy*. DOI:10.1115/imece2014-37010

II. **Espinoza-Andaluz, M.**, Andersson, M., Yuan, J., & Sundén, B. (2015). Compress effects on porosity, gas-phase tortuosity, and gas permeability in a simulated PEM gas diffusion layer. *International Journal of Energy Research*, **39**(11), 1528–1536. DOI:10.1002/er.3348

III. **Espinoza-Andaluz, M.**, Andersson, M., & Sundén, B. (2016). Predicting transport parameters in PEFC gas diffusion layers considering micro-architectural variations using the Lattice Boltzmann method. *International Journal of Energy Research*. **41**(4), 565-578 DOI:10.1002/er.3661

IV. **Espinoza-Andaluz, M.**, Sundén, B., & Andersson, M. (2016). Impact on Diffusion Parameters Computation in Gas Diffusion Layers, Considering the Land/Channel Region, Using the Lattice Boltzmann Method. *ECS Transactions*, **75**(14), 521–530. DOI:10.1149/07514.0521ecst

V. **Espinoza-Andaluz, M.**, Andersson, M., & Sundén, B. (2017). Comparing through-plane diffusibility correlations in PEFC gas diffusion layers using the lattice Boltzmann method. *International Journal of Hydrogen Energy*. Article in Press. DOI: 10.1016/j.ijhydene.2017.02.096

Author contribution

For Papers **I** and **II**, the co-authors jointly defined the research questions. For Papers **III**, **IV** and **V**, the thesis author was main responsible of defining the research questions.

For all papers, the thesis author was responsible for developing the computational code, performing simulations, analysis of the results and writing the papers.

List of publications not included in the thesis

I. **Espinoza-Andaluz, M.**, Sundén, B., & Andersson, M. (2014). Lattice Boltzmann Modeling From the Macro-to the Microscale-An Approximation to the Porous Media in Fuel Cells. *In REGenerative Energien und WAsserstofftechnologie-Symposium, REGWA 2014*.

II. **Espinoza-Andaluz, M.**, Sunden, B., Andersson, M., & Yuan, J. (2015). Analysis of Porosity and Tortuosity in a 2D Selected Region of Solid Oxide Fuel Cell Cathode Using the Lattice Boltzmann Method. *ECS Transactions*, **65**(1), 59–73.
DOI:10.1149/06501.0059ecst

III. **Espinoza-Andaluz M.** (2015). On Microstructural Analysis of Porous Media Existing in Fuel Cells Using the Lattice Boltzmann Method. Licentiate dissertation, Division of Heat Transfer, Department of Energy Sciences, Lund University.

IV. **Espinoza-Andaluz, M.**, Andersson, M., & Sundén, B. (2016). Computational time and domain size analysis of porous media flows using the lattice Boltzmann method. *Computers & Mathematics with Applications*. Article in press.
DOI:10.1016/j.camwa.2016.12.001

V. **Espinoza-Andaluz, M.**, Sunden, B., & Andersson, M. (2016). Incidence of the particle size over the tortuosity in a porous medium using the lattice Boltzmann method. *Technological Journal-ESPOL*, **29**(1).

VI. **Espinoza-Andaluz, M.**, Andersson, M., & Sundén, B. (2016). Potential of Lattice Boltzmann Method to Determine the Ohmic Resistance in Porous Materials. *Journal of Physics: Conference Series*, **738**, 012090.
DOI:10.1088/1742-6596/738/1/012090

VII. Andersson, M., Beale, S. B., **Espinoza-Andaluz, M.**, Wu, Z., & Lehnert, W. (2016). A review of cell-scale multiphase flow modeling, including water management, in polymer electrolyte fuel cells. *Applied Energy*, **180**, 757–778.
DOI:10.1016/j.apenergy.2016.08.010

VIII. **Espinoza-Andaluz, M.**, Andersson, M., & Sundén, B. (2017). Modeling of a Gradient Porosity SOFC Anode Using the Lattice Boltzmann Method. *Energy Procedia*, **150C**, 1333 – 1339.

DOI:10.1016/j.egypro.2017.03.484

IX. **Espinoza-Andaluz, M.**, Sunden, B., & Andersson, M. (2017). Pore-scale analysis of transport parameters in modeled SOFC anodes with gradient porosity in the main flow direction. ECS transactions.
Accepted for publication.

X. **Espinoza-Andaluz, M.**, Andersson, M., & Sundén, B. (2017). Impact of Carbon Deposition on Diffusion Parameters in Porous Anodes of Solid Oxide Fuel Cells Using the Lattice Boltzmann Method.
To be submitted.

Table of Contents

Nomenclature

A	Area, [L^2]
C	Mass concentration, [M]
c	Basic speed on the lattice [lu ts^{-1}]
D	Diffusion coefficient, [L^2 T^{-1}]
e	Velocity vector, [M L^{-1}]
f	Particle distribution function
g	Particle distribution function, mass LB model
j	Local diffusive flux, [M L^{-2} T^{-1}]
l	Length, [L]
L	Thickness of a layer, [L]
K	Permeability, [L^2]
Q	Diffusibility, [-]
q	Darcy flux, [L T^{-1}]
p	Pressure, [M L^{-1} T^{-2}]
r	Position vector, [L]
Re	Reynolds number, [-]
S	Source term
t	Time, [T]
u	Macroscopic velocity [LT^{-1}]
$\mathbf{v}$	Velocity field, [LT^{-1}]
v	Velocity field in one direction, [LT^{-1}]
w	Weighting factor
V	Volume, [L^3]
x	Distance in x direction, [L]
χ	Position for phase function

Chemicals

e^-	Electrons
H_2	Hydrogen
H_2O	Water
H^+	Hydrogen ion
O_2	Oxygen

Greek Symbols

β	Inertial coefficient, [L^{-1}]
γ	Function of characteristic lengths
Δ	Change of a quantity
δ	Percentage of inclined fibers
ϑ	Land/channel ratio
ε	Porosity, [-]
ϕ	Scalar parameter

φ	Phase function
μ	Micro-, x10^{-6}
μ	Dynamic viscosity, [M L^{-1} T^{-1}]
ν	Kinematic viscosity, [M^2 T^{-1}]
ϱ	Density, [M L^{-3}]
τ	Tortuosity, [-]
τ	Relaxation time, ts
∇	Gradient of a function/variable
Ω	Collision operator
ς	Ratio between the actual and initial thickness

Abbreviations

2D/3D	Two/three-dimensional
AIMD	Ab initio Molecular Dynamics
BGK	Bhatnagar, Gross and Krook
BTE	Boltzmann transport equation
CC	Carbon cloth
CP	Carbon paper
DFT	Density functional theory
DM	Diffusion media
DmQn	Scheme used in LBM
FC	Fuel cell
GDL	Gas diffusion layer
HOR	Hydrogen oxidation reaction
IP	In-plane direction
LGA	Lattice gas automata
LBE	Lattice Boltzmann equation
LBM	Lattice Boltzmann method
MC	Monte Carlo
MD	Molecular Dynamics
MPL	Micro-porous layer
MRT	Multiple-relaxation-time
NS	Navier-Stokes
ORR	Oxygen reduction reaction
PDF	Particle distribution function
PEFC	Polymer electrolyte fuel cell
PEM	Polymer electrolyte membrane
PTFE	Polytetrafluoroethylene
RMSE	root-mean-squared error
SEM	Scanning electron microscope
SOFC	Solid oxide fuel cell
SRT	Single-relaxation-time
SSE	Sums of squares due to error

TP	Through-plane direction

Subscripts

2D	Two-dimensional case
g	Gas-phase
i	ith-direction
T	Total
||	Parallel direction
c	Constant parameter
in	Inlet
out	Outlet
R	Relaxation time
eff	Effective
bulk	Bulk
v	Relative to fluid flow LB
m	Relative to mass transport LB

Superscripts

eq	Equilibrium

List of Figures

List of Tables

"Water will be the coal of the future!"
J. Verne, 1874

1 Introduction

Together with the population increase, the energy demand has also been increasing during the last decades. There are some countries in which the energy demand surpasses the energy production into the country [1]. Although this mismatch between the demand and production of energy can be solved, the important issue that our society faces is the increasing amount of the emissions of polluting gases to the atmosphere. The mentioned situation occurs because the consumed energy is mainly coming from the combustion of fossil fuels [2, 3].

Considering the mentioned scenario, one of the considered strategies to decrease the emission of polluting gases is the utilization of renewable energies. During the last years, the use of different kind of renewable energies, i.e., wind, solar, biomass, etc., has increased around the world [4, 5]. However, due to some technical and financial issues, as well as the availability of fossil fuels, the presence of renewable energies in the world is still low [6].

To avoid the use of fossil fuels and to decrease the emission of polluting gases, the useful energy should be generated by clean devices. A clean, efficient, noiseless and compact device is the fuel cell (FC). This electrochemical device converts the chemical energy present in the fuel, i.e., pure hydrogen or any compound with hydrogen as constitutive element, into electrical and thermal energy. During the last years, in the world, the amount of power produced coming from FCs has been increased as depicted in Figure 1.

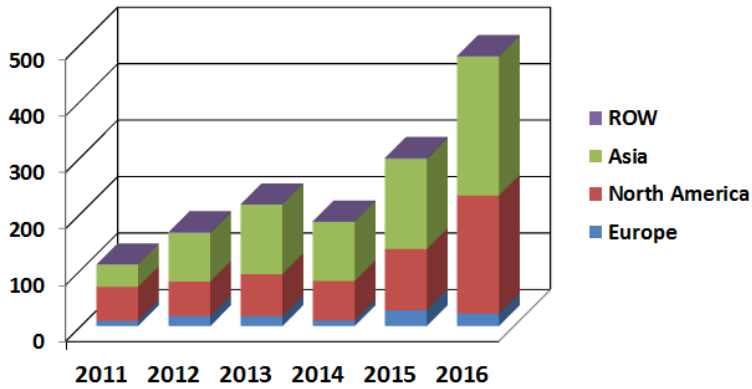

Figure 1.1 Megawatts by Region generated by FCs
The megawatts usage from FCs has increased during the last years with more presence in Asia and North America. Figure adapted from [7]

The FCs, in a general point of view, are constituted by an anode (fuel side) and an cathode (oxidant side) sandwiching the electrolyte. Although FCs can be classified in different ways, i.e., working temperature, output power, typical applications or electrolyte used, the last mentioned characteristic is the most widespread employed to classify them. Among the FC types, the most widely used are the polymer electrolyte fuel cell (PEFC) and solid oxide fuel cell (SOFC). The power contribution of PEFC as percentage in comparison to the total amount of power provided by FCs in 2016 is around 65%, according to the Fuel Cell Industry Review 2016 [7].

Albeit FCs have been gaining presence in several applications, their market presence in comparison with the total energy demand is still low; a demand that is expected to be double in approximately 30 years [8]. This is mainly because the FC technology is still expensive, especially due to the materials involved in its construction and failures related to aging and thermal balance [9]. Nonetheless, the solution for a cheaper and better FC can be achieved from the basics, the fundamental properties of the different FC elements. Although the functioning of a FC is apparently simple, the system itself is a complex, inhomogeneous, multi-physics, and multi-scale system in which all the physical, chemical and thermal phenomena are interrelated.

An important element in PEFCs is the so-called gas diffusion layer (GDL), which gives mechanical support of the cell and help to distribute reactant gases from the flow plates to the active sites among other characteristics that are detailed in Chapter 2. Explaining the transport phenomena and evaluating transport parameters of GDLs are not an easy task, especially due to the small length scale and complex geometries found in these layers. From a research point of view, modeling appears as a suitable option when the analysis and study can not be carried out in-situ because of running operations and too small length scales. Additionally, numerical models can eventually

help to predict the behavior of the different systems as a first step of the manufacturing process saving time and production cost.

During the last years, the Lattice Boltzmann method (LBM) has demonstrated to be a powerful tool to simulate phenomena in a wide range of applications such as acoustic [10], electromagnetic [11], or even medical research [12]. Because of its ability for mimicking different transport phenomena through complex geometries with considerable accuracy, LBM is considered in the present thesis. LBM helps us to recover the fluid flow behavior and mass transport phenomena at the pore-scale level decreasing the commonly assumed characteristics or properties when a complete length scale model is achieved. Analyzing the properties of the GDLs from a micro-scale point of view places us a step forward in the way of getting a much more realistic model coupling the different scales present in FCs.

1.1 Research Objectives

The main objective of this thesis is to obtain an increased understanding of the fluid behavior through the GDLs and their transport diffusion properties from a pore-scale point of view. This objective is achieved by resolving and/or obtaining numerical models of GDLs to analyze the different gas diffusion transport properties from a micro-scale point of view supported, and developing the code for applying the LBM. In detail, the different steps to reach the objective are:

- to develop a code to digitally create GDLs (2D and 3D) based on realistic porous media found in PEFCs.
- to develop a fluid flow and mass transport Lattice Boltzmann (LB) model, to be applied in the simulated GDLs.
- to propose different correlations between the diffusion transport properties of the GDLs and microstructural configurations.
- to compute diffusion transport properties that can be used as input parameters in a full length scale PEFC model.
- to compare previous effective diffusion correlations with the obtained ones from a micro-scale modeling point of view.

The digitally created GDLs were used to analyze the behavior of the fluid flow and mass transport phenomena, to determine the effects of: the physical compressions, microstructural morphological variations, and land/channel considerations. Diffusion transport properties such as porosity, gas-phase tortuosity, permeability, effective diffusion coefficient and others are considered in the present thesis.

1.2 Methodology

First of all, porous media with physical characteristics similar to what is found in realistic GDLs are required, and therefore; a computer code to digitally create such layers are developed. In this work, 2D and 3D geometrical representations of the GDLs were digitally created to analyze the involved properties.

Computing the different diffusion transport properties in complex geometries requires the development and implementation of fluid flow LB models and mass transport LB models. The corresponding steps to obtain the fluid flow behavior and mass transport phenomena through the digitally created GDLs was developed (2D and 3D) in Matlab®. Several boundary conditions for the fluid flow and mass transport LB models were implemented and evaluated, and the developed computer code was benchmarked with fundamental physical problems.

According to the transport phenomena analyzed, the boundary conditions of the LBM are implemented. The porous media representing the GDLs are also modified to evaluate the impact of such variations on the different diffusion transport properties.

Once the fluid flow behavior and mass transport phenomena through the digitally created GDLs are obtained, the diffusion transport properties are evaluated. Taking into account physical modifications, morphological configurations and microstructural architecture, correlations for predicting the different diffusion transport properties are proposed.

1.3 Thesis Outline

The thesis is divided in two parts. The first part is related to the main concepts and definitions as well as the methodology and processes required to reach the objectives. The current **Chapter 1** gives a general insight to the research objectives and the methodology applied. A literature review focusing on PEFCs and GDLs, as well as the transport properties considered in the present thesis are given in **Chapter 2**. General aspects about FC modeling and GDL generation is presented in **Chapter 3**, detailed information about the LBM, the fluid flow LB model and the mass transport LB model are also included. **Chapter 4** presents the obtained results based on the GDL generation, the LB model application and computation of the parameters. **Chapter 5** discusses the conclusions of the present study, and **Chapter 6** provides suggested possible future studies based on the achieved results.

The second part of the thesis compiles the appended publications. More specifically, the papers concern:

Paper I – A review paper in which the potential of LBM to study the diffusion transport parameters in GDLs is analyzed.

Paper II – A two-dimensional study on the compression effect on porosity, gas-phase tortuosity and permeability, in GDLs.

Paper III – A two-dimensional study in which effects of morphological considerations over the different diffusion transport properties in GDLs are analyzed.

Paper IV – The effect on diffusion transport parameters considering the land/channel region in a three-dimensional model representing the GDLs is carried out.

Paper V – A detailed comparison of the most widely used correlations to predict the diffusibility in GDLs is carried out in a three-dimensional study.

2 Fuel Cells

A fuel cell (FC) is an electrochemical device that converts energy stored in a fuel into electrical and thermal energy due to an electrochemical reaction. As mentioned, there are different types of FCs, and they are commonly classified according to the electrolyte sandwiched between the electrodes. The present chapter aims to describe in detail the PEFC, with a focus on the specific layer which is the core of this study, i.e., GDL, and the main diffusion transport parameters to be analyzed.

2.1 Polymer Electrolyte Fuel Cell

High electrical efficiency, no emission of polluting gases, modularity and fast start-up can be mentioned as some of the advantages of the PEFCs. Their efficiency can be as high as 60%, and if co-generation is considered it can reach around 80% [13]. The electrochemical reaction for the energy conversion is carried out due to the assembly of the different constitutive elements of the PEFCs. The reactant and reactive gases have to pass through different layers which play important roles in the electronic and ionic transport phenomena, as well as for the mass diffusion process. The catalyst layer (CL) and GDLs are placed on both sides of the polymer electrolyte membrane (PEM) as shown in Figure 2.1.

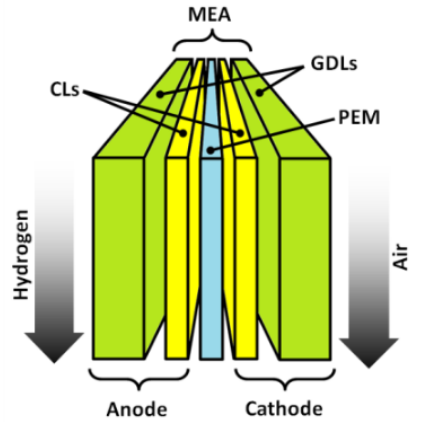

Figure 2.1 Main constitutive elements of PEFCs
The polymer membrane is sandwiched with the anode and cathode. The fuel (H_2) flows on the anode side while the oxygen (O_2) flows on the cathode side.

Hydrogen flows from the flow plates at the anode side to the membrane passing through the GDL and reach the active sites in order to take part in the electrochemical reaction. At anode side, the hydrogen is oxidized to produce protons and electrons in an electrochemical reaction named hydrogen oxidation reaction (HOR). At this stage, only the positive ions (H^+) are allowed to pass through the polymer membrane which is commonly a Nafion® membrane type. The free electrons produced from the mentioned electrochemical reaction are able to be used in electrical external appliances. At the same time, on the cathode side, the oxygen molecules reacts with the electrons which are received from the external circuit and the positive ions producing water (H_2O) in an electrochemical reaction named oxygen reduction reaction (ORR). The electrochemical reactions involved in the energy conversion process are expressed as:

Anode side (HOR): $$H_2 \rightarrow 2H^+ + 2e^- \quad (2.1)$$

Cathode side (ORR): $$\frac{1}{2}O_2 + 2H^+ + 2e^- \rightarrow H_2O \quad (2.2)$$

As expected, the overall reaction inside the FCs considers the water and heat as products. Heat is generated because the electrochemical reaction inside the FC is highly exothermic.

PEFC's operating temperature falls in a range of 50 – 100° C [14], making them suitable for transport and portable applications. The transport application has been developed with considerable emphasis during recent years, especially in the automotive market [15]. On the other hand, portable applications are also promising;

in which laptops, cellphones and radio communication devices can be energized using PEFCs [16]. In addition, to take advantage of the generated heat during the energy conversion process, co-generation is applied to use this heat, and therefore significantly increases the overall efficiency of PEFC systems [17].

Although PEFCs present several advantages, there are still some barriers that have to be faced in order to wide-spread the use this device around the world, for example the durability and the cost. According to [18], by 2015 the related cost for the GDLs represents around one third of the total cost of the system, and just below of the cost related to the membrane. In this sense, a complete understanding of momentum/mass/heat transfer, ionic/electronic transport and electrochemical reactions in the GDLs can help to improve the microstructural configuration materials in order to achieve the desirable durability and also decrease the production cost. Considering the last mentioned matter, fundamental research represents an important link between the current state-of-the-art of FCs and their future applicability.

2.2 Gas Diffusion Layer

The GDLs play an important role during the energy conversion process that occur inside the PEFCs. Some of the main functions of GDLs are [19, 20]:

- Offer mechanical support to the PEFC.
- Allow diffusion of reactant gases from the flow channel to the active sites.
- Help to remove the excess water on the cathode side.
- Allow electronic transport, resulting from the hydrogen oxidation, from the active sites to the current collectors.
- Help to remove heat at the anode and the cathode sides.
- Protect the catalyst layers of corrosion or erosion

Physical characteristics which allow the mentioned functions have to be analyzed and completely understood in order to obtain the most suitable behavior during PEFC operation. The most recent years have seen an increased interest of placing the GDLs together with the so-called micro-porous layers (MPL) to improve the physical behavior of the PEFCs, improving the electrical contact and helping in the water removal task, during the energy conversion process [21]. These two layers together, i.e., GDL and MPL, are commonly called diffusion media (DM). The micro-porous layer can act as an interface between the GDL and the CL as depicted in Figure 2.2.

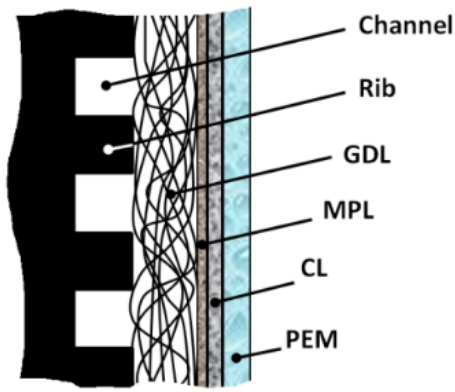

Figure 2.2 Diffusion media on the anode side of a PEFC
Schematic representation of different layers helping to distribute the reactant gases, transport of electrons during the energy conversion process.

The MPL can be placed adjacent to the GDL, and it can also be fully or partially integrated to the GDL. However, it is a current topic of discussion to find the most suitable configuration of this DM [22]. The present thesis focuses on the diffusion transport parameters of the GDL itself.

From a morphological point of view, there are several types of GDLs according to the way in which the carbon fibers are arranged. In PEFC applications, the two most commonly used GDLs are the carbon paper (CP) and carbon cloth type (CC) [23 - 26]. The CP type can be seen as an arrangement of straight carbon fibers, while the CC type has a woven fabric nature. Figure 2.3 shows scanning electron microscope (SEM) pictures of both GDL types [27].

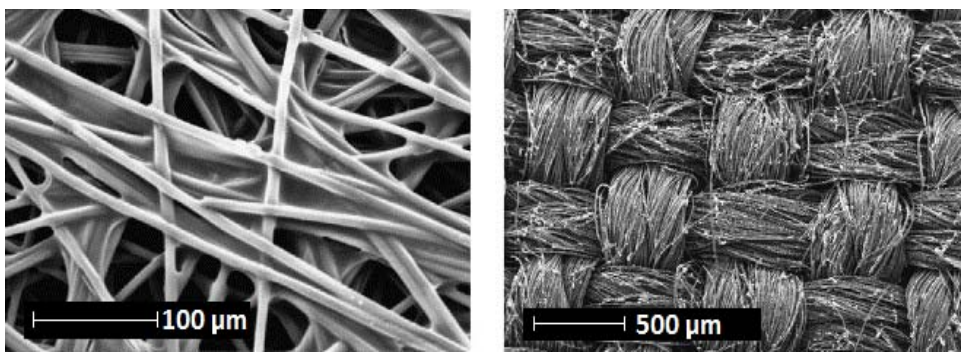

Figure 2.3 Most widely used GDL types
SEM image of CP (left side) and CC (right side) GDLs. Image reproduced by permission of Elsevier ®.

Both, CC and CP, are commercially available as reported in [28]. When the GDL is not compressed because of the FC assembly, its thickness is in the range of tens of microns to around 1500 μm [29 - 31]. There are certain treatments applied to the GDLs, all of them with the aim of improving certain physical characteristics. However, the implementation of these treatments can also affect other parameters at the same time. To allow the flexibility of the GDL, a binder is added during the manufacturing process [32], while polytetrafluoroethylene (PTFE) can be added to increase its hydrophobicity [33, 34]. Table 2.1 shows examples of commercial CP GDLs with their respective properties.

Table 2.1 List of selected commercially available CP GDLs
Information presented in this table are from [28, 31].

Product name	Thickness (μm)	Bulk density (g/cm^3)	PTFE Treated	MPL
AvCarb EP40	200	0.20	No	No
AvCarb MGL 370	370	0.46	No	No
Toray 090	280	0.45	No	No
AvCarb GDS1120 P50	184	0.40	Yes	Yes
GD65055T	1500	0.45	Yes	No
GDS2120	260	0.40	No	Yes
TGP-H030	110	0.40	No	No

Due to its complex nature and physical inhomogeneous properties, a microscopical study of the physical parameters considering the arrangement of the fibers can help to understand in detail the transport phenomena through the GDLs. All the parameters analyzed, the way to determine them, as well as typical values of the diffusion transport parameters are detailed in the following section. It is important to notice that the investigations in the present work are focused on the CP GDL type.

2.3 Diffusion Transport Properties

Before defining the properties considered in the present thesis, it should be mentioned that most of the parameters are directional dependent, i.e., they show different values according to the direction in which are measured, especially because the non-homogeneity and anisotropic nature of the GDLs. In a 3D domain, the in-plane (IP) and through-plane (TP) directions can be identified. Figure 2.4 shows the scheme in which the directions are described.

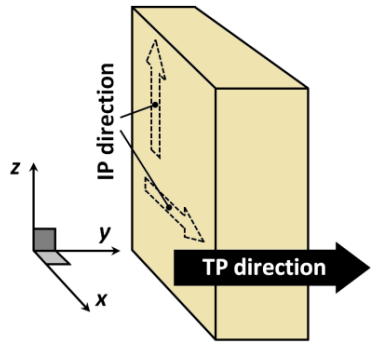

Figure 2.4 Schematic showing the IP and TP direction
Most of the diffusion parameters are directional dependent. In the scheme, the TP direction is parallel to the *y* axis.

In both, 2D and 3D cases, the TP direction is considered in the current thesis because of the importance of the transport phenomena in that direction. In 2D cases, the GDL is represented in the yz plane, according to Figure 2.4.

2.3.1 Porosity

The void space in the GDLs allow the reactant gases to flow from the flow plates to the active sites where the electrochemical reactions occur. Additionally, the water produced at the cathode side can flow from the CL to the air channel. Therefore, the higher the amount of void spaces is more easily can the reactant/product gases pass through the GDLs. However, having a higher porosity decreases the mechanical strength of the MEA, and it can result in an increment of the thermal and electrical resistance. By definition, the porosity can be determined as the ratio between the void space and the total space occupied by the volume considered in the study. Equation (2.3) defines the porosity.

$$\varepsilon = \frac{V_g}{V_T} \tag{2.3}$$

where V_g represents the void space, i.e., the space that can be occupied by the fluid, and V_T corresponds to the total volume. It is a dimensionless quantity and can be expressed in percent. If the analyzed domain is a 2D case [35, 36], a modified version to compute the porosity can be used:

$$\varepsilon_{2D} = \frac{A_g}{A_T} \tag{2.4}$$

here A_g is the area representing the hypothetical space that can be occupied by the fluid and A_T the total area of the studied domain. The GDL porosity, also known as bulk porosity, is in the range of around 50% to 90% [28, 31, 37].

In a porous media, such as GDLs, if there are isolated pores or totally obstructed pathways, one can define an effective porosity. In the current thesis, it is assumed that all the void spaces are occupied by the fluid; and therefore, the effective porosity and bulk porosity achieve the same value. In the open literature, definition of a local porosity can be found. It is a measure of the porosity in a selected region or part of the total GDL [38].

2.3.2 Gas-phase tortuosity

Another important property describing the diffusion process in GDLs is the gas-phase tortuosity (from now on, it is mentioned only as tortuosity). The tortuosity can be defined as a measure of the complexity of the porous medium through which the fluid is passing. If there is no presence of solid obstacles/particles/material in the analyzed domain, the fluid tends to flow along a straight line. However, in porous media as found in GDLs, the fluid has to follow the pathways according to the microstructural configuration of the medium. It can be determined, geometrically, as the ratio between the actual length of the pathway followed by the fluid and the shortest distance length:

$$\tau_{\mathrm{g}} = \frac{\Delta l}{\Delta x} \tag{2.5}$$

where Δl and Δx are lengths represented in Figure 2.5. According to Eq. (2.5), the tortuosity quantity is non-dimensional, and in the GDLs it has to be greater than unity.

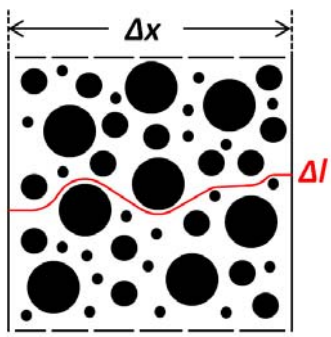

Figure 2.5 Illustration of a tortuous path through a porous medium
The ratio between *Δl* and *Δx*, i.e., the tortuosity, in a porous medium is always greater than unity.

Given the complexity of the medium, and considering the difficulty of evaluating all the possible pathways followed by the fluid, the tortuosity is often approximated as a function of the porosity. Several attempts to determine a suitable tortuosity-porosity correlation based on experimental and theoretical studies can be found in [39]. Table 2.2 shows previous tortuosity-porosity correlations which are often applied to GDLs.

Table 2.2 Selected tortuosity-porosity correlations applied in porous media
The selected correlations are often used in GDL modeling.

Correlation	Authors	Remarks
$\tau = \varepsilon^{-0.5}$	Bruggeman [40]	Derived from the electrical conductivity and based on uniformly distributed spheres.
$\tau = 1 - 0.49\, Ln(\varepsilon)$	Barrande et al. [41]	Homogeneous assembly of particles, spheres or fibers with uniform porosity distribution.
$\tau = \frac{3-\varepsilon}{2}$	Neale and Nader [42]	Random homogeneous of isotropic sphere packings.
$\tau = \left(\frac{\varepsilon-\varepsilon_c}{1-\varepsilon_c}\right)^{\gamma}$	Ghanbarian and Cheng [43]	Based on the percolation theory a power law form is proposed. ε_c is a constant porosity and γ is a function of characteristic lengths.

However, most of the previous studies do not specifically describe the porous media as the ones found in GDLs, therefore; one of the possible ways to determine the tortuosity based on the fluid behavior through the GDLs is by knowing the pore-velocity in such porous media. If the velocity of the fluid is known, the tortuosity can be determined as explained by Koponen et al. [44]:

$$\tau_g = \frac{\langle |\mathbf{v}| \rangle}{\langle v_{||} \rangle} \tag{2.6}$$

here $|\mathbf{v}|$ represents the absolute value of flow velocity field, $v_{||}$ is the component of that velocity in the main flow direction, and $< >$ denotes the spatial average over the pore space. In GDLs, the tortuosity can fall in a range from slightly greater than unity up to around 2.5 [45].

2.3.3 Permeability

Permeability is an important property to be evaluated in the porous GDLs. It represents the ability of a GDL to allow the flow of the fluid through the layer. Again, due to its complex geometry and the difficulty of describe the behavior of the fluid through the GDLs, several attempts to determine the permeability have been carried out. The most common correlations relate the permeability with the porosity, but there are some relationships in which the fiber diameter is also considered [46, 47]. As expected, all the proposed relationships show that higher porosities provide higher GDL permeability.

However, if the velocity field as well as the pressure gradient between the inlet and outlet is known, and considering the low Reynolds numbers ($Re < 1$) that are found in the flows through the GDLs [48 , 49], the permeability K can be computed by means of the Darcy's law [50]:

$$K = -\frac{\mu\, q}{\nabla p} = -\frac{\mu\, q}{(p_{out} - p_{in})/L} \tag{2.7}$$

where μ is the dynamic viscosity, q is the so-called Darcy flux, and ∇p is the pressure gradient. In GDLs the permeability can reach values in the order of 10^{-13} and 10^{-8} m^2 [51, 52].

2.3.4 Inertial Coefficient

In normal conditions, the regime of the flow through the GDL is creeping flow, and the Darcy's law can be applied to determine the permeability. Nonetheless, if the velocities become relatively high, the Darcy equation is no longer applicable and it should be modified to the Forchheimer equation [53]. The Forchheimer equation to represent non-Darcy flows in one-dimensional single phase flow through a porous medium is expressed as:

$$-\nabla p = \frac{\mu}{K} q + \beta \rho q^2 \tag{2.8}$$

where β is the inertial coefficient often called the non-Darcy coefficient, and ρ is the density of the fluid.

According to the study developed by Liu et al. [54], the dimensional group: inertial coefficient, permeability, and porosity divided with tortuosity, appears to be a universal constant. Based on a wide variety of data from porous media of different nature, they proposed the following expression to describe the inertial coefficient:

$$\beta = 2.88x10^{-6}\frac{\tau}{\varepsilon\, K} \tag{2.9}$$

where the constant $2.88x10^{-6}$ is in length units. The inertial coefficient has been considered in the study including PTFE in GDLs applied to FCs [55], and in the permeability study of GDLs presented by Gostick et al. [56]. However, in the last mentioned study the tortuosity is not computed, but it is estimated by means of the Bruggeman approximation.

2.3.5 Normalized Effective Diffusivity

The diffusivity measured in a porous medium (D_{eff}) differs from the diffusivity measured in the free space (D_{bulk}). The ratio between the effective diffusion coefficient and the bulk diffusion coefficient is often called the obstruction factor [57], and there have been several attempts to establish this ratio as a function of the porosity [58]. According to Hoogschagen [59], the ratio between the effective diffusion coefficient and the bulk diffusion coefficient, i.e., a normalized effective diffusivity, can be introduced and called diffusibility (Q):

$$Q = \frac{D_{eff}}{D_{bulk}} \tag{2.10}$$

As mentioned, there are many correlations to determine the diffusibility as a function of the porosity. In Table 2.3 the most common correlations applied to GDLs are presented.

Table 2.3 Most commonly diffusibility correlations used in GDLs
The selected correlations are often used in GDL modeling. Table adapted from [58].

Correlation (Q)	Authors	Remarks
$\varepsilon^{1..5}$	Bruggeman [40]	Effective medium approximation
$\frac{2\varepsilon}{3-\varepsilon}$	Neale and Nader [42]	Effective medium approximation
$\left(\frac{\varepsilon-0.037}{1-0.037}\right)^{0.661}$	Tomadakis and Sotirchos [60]	Percolation theory
$\left(\frac{\varepsilon-0.11}{1-0.11}\right)^{0.785}$	Nam and Kaviany [61]	Percolation theory
$1-\left[\frac{3(1-\varepsilon)}{3-\varepsilon}\right]$	Das et al. [62]	Effective medium approximation

All the correlations present similar trend, i.e., if the porosity increases the diffusibility increases. Considering the possible values which the GDL porosity can reach, Figure 2.6 is elaborated based on the mentioned correlations.

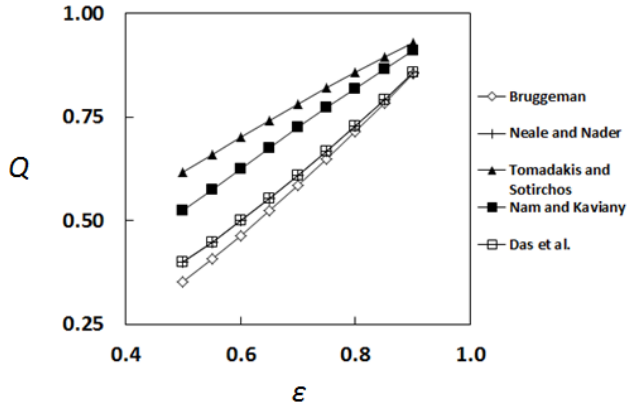

Figure 2.6 Normalized effective diffusion coefficient for GLDs
The porosity values considered are in the range in which the GDL porosity can be.

The correlations presented in Table 2.3 can help to predict the diffusibility as a function of the porosity with a higher or lower degree of accuracy. However, from a pore-scale point of view, the diffusibility can also be determined if the mass concentration is known in the pore-space of the GDLs. Considering the porous characteristic of the GDLs, the Fick's law can be applied to determine the diffusibility:

$$\frac{D_{eff}}{D_{bulk}} = \frac{\iint_A j\, dA}{A\left(\frac{D_{bulk}\,\Delta C}{L}\right)} \tag{2.11}$$

where A is the cross-sectional area of the analyzed GDL domain, j the local diffusive flux, ΔC the concentration difference between the inlet and outlet, and L the thickness of the GDL considered during the analysis.

Computational tools can help to analyze the diffusion transport parameters defined in the present chapter. A pore-scale analysis can give us a more detailed information about the fluid behavior and mass transport phenomena through the GDLs. The following chapter is mainly focusing on the applied methodology and porous media generation used in the current thesis.

3 Fuel Cell Modeling

Modeling and simulation provide opportunities to study and analyze the FC electrodes to obtain vital information which allow us to improve several properties in the different layers. To date, there is not a complete, 3D, dynamic, full length and time scale model available to predict the behavior of a FC. However, the coupling of the different scales is a task on which researchers are focusing. In the present chapter, fundamentals of the methodology applied in the current work, as well as the description of the GDL generation is given.

3.1 Computational Approaches

As mentioned, the FC modeling embraces a wide range of phenomena at different length scales. There are different approaches for modeling the transport phenomena in FCs, each of them can be specific for solving problems in certain length scales. At the same time, the time scale and the computational cost are parameters to be considered. Modeling and simulation from the electronic scale, such as Ab Initio Molecular Dynamics (AIMD), to cell scale based on the volume average method offer a unique opportunity to understand and improve the FC performance from a different perspective.

All the physical, chemical, mechanical, thermal and related phenomena cannot be described by a single approach. However, obtaining physical properties of a certain length scale can be used as input parameter for a higher length scale. Among the different approaches, ordered from the smaller length scale to the higher length scale

are mentioned as: Ab Initio Molecular Dynamics (AIMD), Ab Initio based on the density functional theory (DFT), Molecular Dynamics (MD) and Monte Carlo (MC), discrete elements and phase field methods, Lattice Boltzmann method (LBM) and volume average methods, i.e., finite volume method and finite difference method [63]. The suitable methodology for a specific length scale is based on the phenomena to be described, the time scale at which the phenomena are occurring and the computational cost. Figure 3.1 shows a schematic with the different approaches applied to FC modeling.

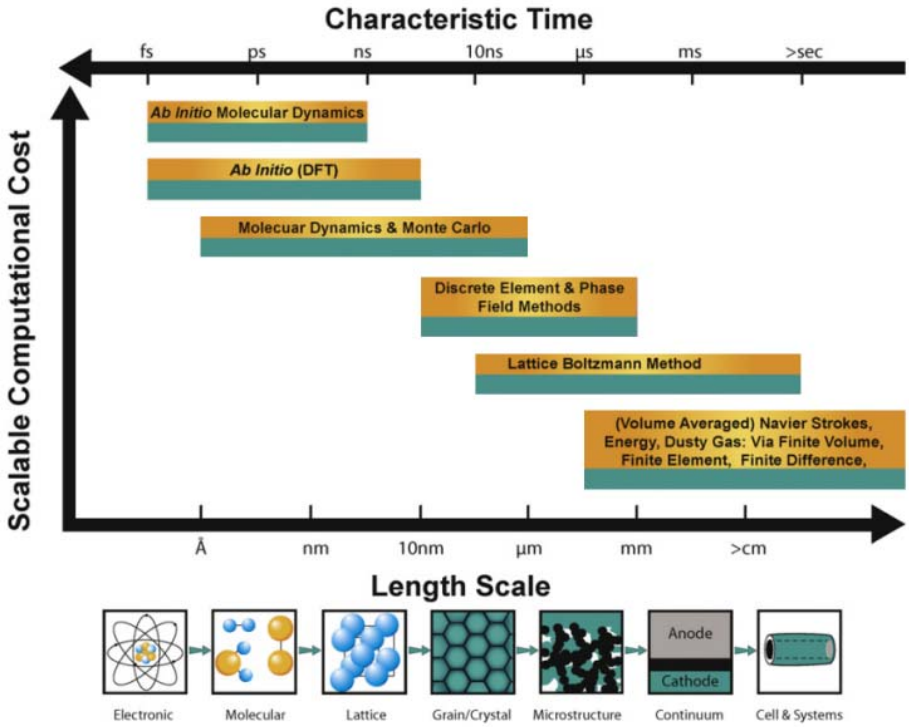

Figure 3.1 Length scale, time scale and computational cost for different approaches in FC modeling
Scheme modified from Ref. [64] with permission of Elsevier.

3.2 Fundamentals of Lattice Boltzmann Method

During the last years, the development of strategies for solving and describing fluid flows and transport phenomena in complex geometries has been increased. LBM originally comes from the lattice gas automata (LGA) method, an MD model in which space, time and velocities are discretized [65]. LBM has proven to be a useful

tool for modeling fluid flow behavior and transport phenomena in porous media with complex geometries and/or mobile boundary conditions such as found in GDLs [66 - 68]. Among the advantages of using the LBM, it can be mentioned: easy implementation of several transport phenomena, and the conservation laws are held automatically with no additional efforts [69].

The application of LBM relies on the discretization of the total domain to be analyzed. Each element receives the name of *"lattice node"* or *"lattice element"* and has a direct connection with its neighboring nodes. When a transport phenomenon is described by using the LBM, it is common to define the number of linked connections between the nodes., i.e., the lattice scheme. The lattice scheme has the structure *DmQn*, where *m* represents the spatial lattice arrangement (it defines if the problem is analyzed in one-, two-, or three dimensions), and *n* defines the number of linked connections between the analyzed node and its vicinity. Thus, a *D2Q4* means a two-dimensional model in which each lattice node has four linked connections. Several schemes can be used when the LBM is applied as presented in [70]. The most common schemes when applying LBM are *D2Q9* and *D3Q19*, and their graphical representations are shown in Figure 3.2.

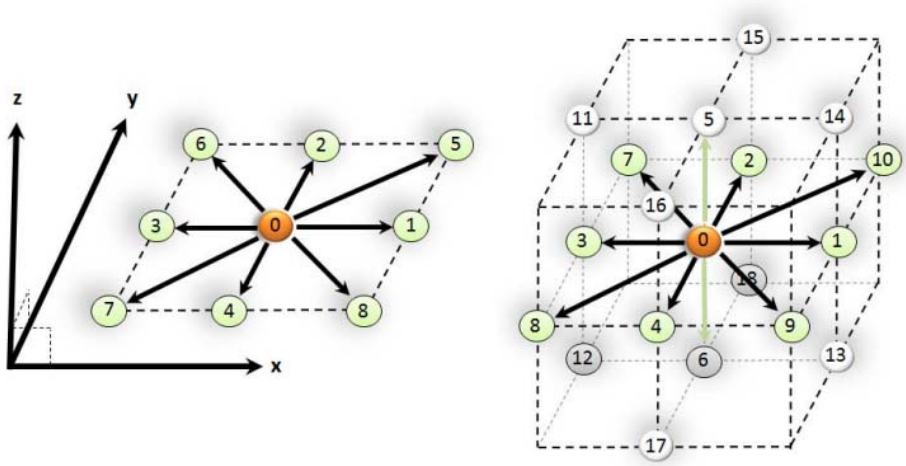

Figure 3.2 Most common schemes using in LBM for modeling
Left side represents the D2Q9 scheme while the right side is the D3Q19 scheme.

The properties of each node are represented by the particle distribution function (PDF). The mentioned function is equivalent to a group of particles in a certain region of the domain within a range of velocities at a certain time. The connection between each lattice node depends on the scheme used, and each connection has different weight factors as shown in Table 3.1

Table 3.1 Weighting factors for the most common LBM schemes

The highest value of the weight is assigned to the analyzed node and decreases according to the distance to its neighbor direction. The sum of all the w_i must always be the unity. Table adapted from [65].

Scheme	Linked direction	w_i
D2Q9	i = 0	4/9
	i = 1 – 4	1/9
	i = 5 – 8	1/36
D3Q19	i = 0	1/3
	i = 1 – 6	1/18
	i = 7 – 18	1/36

The backbone of the LBM is the Boltzmann equation, which is an integro-differential equation and its solution is not an easy task. The Boltzmann transport equation (BTE) can be expressed as:

$$\frac{\partial f(r,t)}{\partial t} + e.\nabla f(r,t) = \Omega \tag{3.1}$$

where f represents the particle distribution function, r the position vector, t the time and e the velocity vector. The term on the right-hand side of Eq. (3.1) represents the so-called collision operator which eventually is expressed as a function of f.

Several studies relative to the collision operator, and how it is defined, have been developed in order to obtain the most suitable approximation to model different transport phenomena. The single-relaxation-time (SRT) and multiple-relaxation-time (MRT) have been widely investigated, and although the MRT has more degrees of freedom, the simplicity and lower computational cost of the SRT makes it one of the most applicable models, especially for several phenomena at low Reynolds numbers [71, 72]. In the study performed by Bhatnagar, Gross and Krook [73], the collision operator of the BTE is expressed in a simple manner considering the terms of the conservation laws or mass, momentum and energy. They proposed the following approximation to determine the collision parameter:

$$\Omega = \frac{1}{\tau_R}[f^{eq}(r,t) - f(r,t)] \tag{3.2}$$

here τ_R is the so-called relaxation time which is related to the transport properties, i.e., viscosity, mass diffusion coefficient, thermal diffusivity, etc., corresponding to the analyzed phenomena, and f^{eq} is the equilibrium distribution function. Based on the

research about PEFC modeling, specifically transport phenomena studies of GDL and CL, where the Bhatnagar, Gross and Krook (BGK) approximation has been widely used [74 - 76], the present study considers the BGK approximation during the modeling and simulation process.

Replacing Eq. (3.2) in Eq. (3.1), and considering the discretization of the domain, the Lattice Boltzmann equation (LBE) can be expressed as follows:

$$\frac{\partial f_i(r,t)}{\partial t} + e_i.\nabla f_i(r,t) = \frac{1}{\tau_R}\left[f_i^{eq}(r,t) - f_i(r,t)\right] \tag{3.3}$$

where the subscript *i* corresponds to the ith-direction in which the properties are going to be propagated, i.e., the number of linked connections between the lattice element in the domain. The equilibrium particle distribution is defined according to the transport phenomena analyzed. The general form of the equilibrium PDF can be expressed as [77]:

$$f_i^{eq} = \phi w_i[a + b\, e_i\,.u + c(e_i\,.u)^2 + d\, u^2] \tag{3.4}$$

where *u* is the macroscopic flow velocity vector; *a*, *b*, *c* and *d* are constants that have to be determined according to the conservation principle, i.e., momentum, mass or energy. The parameter ϕ represents the scalar parameter to be considered, i.e, density, species concentration or temperature.

Independen of the transport phenomena to be analyzed, LBM follows an algorithm to compute the macroscopic variables involved in the simulation process. The algorithm can be divided, in a simplified way, into four main steps: collision step, streaming step, boundary conditions and calculation of the macroscopic quantities. All the mentioned steps must be effected at every time step, besides the initialization of the involved parameters (only once) and the convergence criteria. Figure 3.3 shows the algorithm with the simplified LBM scheme.

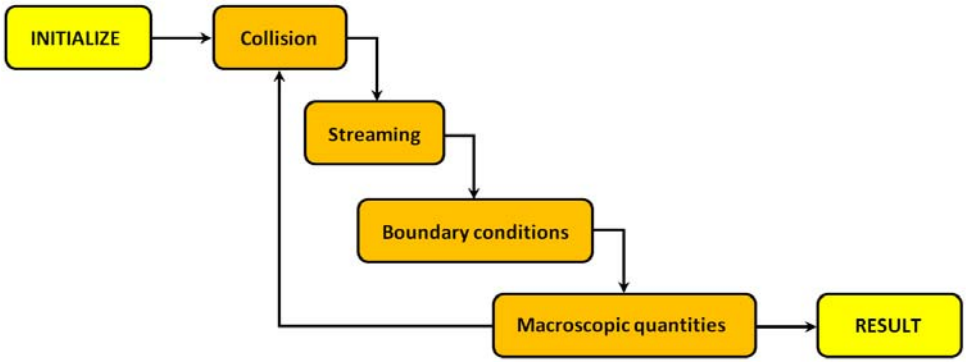

Figure 3.3 Main steps in the algorithm of the LBM
Orange blocks represent the steps that have to be followed at every iterative step.

The collision step, i.e., relaxation towards local equilibrium, is achieved by using the BGK approximation. In the streaming step, the direction-specific PDFs are moved to the nearest neighbor lattice nodes. The boundary conditions should be specified at the fluid/solid interface, inlet and outlet as well as the boundaries of the analyzed domain. The computation of the macroscopic quantities is required because they have to be updated at every time step [78]. More detailed information for each specific model, i.e., fluid flow or mass transport, is given in the following sub-sections.

3.2.1 Fluid flow LB model

From a macroscopic point of view, the fluid flow is governed by the Navier-Stokes (NS) equation, and therefore; the NS equation for conservation of momentum is considered and continuity equation must be satisfied [79]:

$$\frac{\partial u}{\partial t} + (u.\nabla)u + \nabla p - \nu\nabla^2 u = 0 \tag{3.5}$$

$$\nabla . u = 0 \tag{3.6}$$

where p is the pressure on the fluid and ν is the kinematic viscosity. To obtain the fluid flow behavior by using the LBM, Eq. (3.3) can be discretized in time and expressed as follows:

$$f_i(r + e_i\,\Delta t, t + \Delta t) - f_i(r,t) = \frac{1}{\tau_\nu}\left[f_i^{eq}(r,t) - f_i(r,t)\right]. \tag{3.7}$$

As mentioned, the equilibrium particle distribution function (f^{eq}) has to be defined according to the transport phenomena to be analyzed, and the relaxation parameter (τ_ν) is related to the kinematic viscosity of the fluid. Quian et al. [80] defines the equilibrium PDF for solving the fluid behavior as:

$$f_i^{eq} = \rho w_i\left[1 + 3\frac{e_i.u}{c^2} + \frac{9}{2}\frac{(e_i.u)^2}{c^4} - \frac{3}{2}\frac{u^2}{c^2}\right] \tag{3.8}$$

here c is the basic speed in the lattice, and u is the macroscopic velocity of the fluid. The relaxation time and the kinematic viscosity are related:

$$\tau_\nu = 3\nu + 0.5 \tag{3.9}$$

At every time step, the macroscopic quantities must be updated, the local density and the velocity can be computed based on the particle distribution function in each lattice element:

$$\rho = \sum_i f_i \tag{3.10}$$

$$\rho u = \sum_i e_i f_i \tag{3.11}$$

Fluid Flow Boundary Conditions

To model the fluid flow through the porous media, different boundary conditions should be implemented. The following boundary conditions are the most commonly applied in the fluid flow LB model [78, 81]:

- Dirichlet boundaries: It is also known as "pressure" boundary condition. Commonly applied at the inlet/outlet of the studied domain. To implement this boundary condition, the density is specified and then the velocity can be computed.
- Von Neumann boundaries: This boundary condition constrains the flux at the boundaries. The velocity vector is specified when this boundary condition is implemented. It is normally applied at the inlet/outlet of the studied domain.

- Bounceback boundaries: These represent a fundamental boundary condition to be implemented in the media with complex geometries as found in GDLs. It is applied when a fluid/solid interface appears. The PDF coming towards the solid boundary bounces back into the flow domain.
- Periodic boundaries: When the whole domain is not modeled, but a selected representative region; periodic boundary conditions are implemented at the sides of the domain which are parallel to the main flow direction. It can be explained as follows: for the unknown boundary nodes, neighboring nodes are at the opposite boundary.

For the inlet and outlet boundaries, when neither the velocity nor the pressure is known, the best choice is to approximate the unknown PDFs in the boundary by using the second derivative approximation based on the Taylor polynomial expansion. In addition to the mentioned boundary conditions, the symmetric boundary condition can be added to the list. However, considering the anisotropic nature of the GDLs, this kind of boundary is not employed in the current study.

3.2.2 Mass transport LB model

The mass transport phenomena through the GDLs can be explained, in general terms, with the help of the following reaction-diffusion equation [82]:

$$\frac{\partial C}{\partial t} - \nabla(D\,\nabla C) = S \tag{3.12}$$

here S represents the source term, which for the current study is equal to zero. At the same time, the solution is obtained at steady state and therefore the concentration C is not changing with the time. The evolution equation of the particle distribution function to model the mass transport phenomena using the LBM is similar to Eq. (3.7) with a change of the nomenclature:

$$g_i(r + e_i\,\Delta t, t + \Delta t) - g_i(r,t) = \frac{1}{\tau_m}\left[g_i^{eq}(r,t) - g_i(r,t)\right] \tag{3.13}$$

where g is the PDF employed in the mass transport LB model, g^{eq} represents the equilibrium PDF for the mass transport model and the relaxation parameter (τ_m) is related to the mass diffusion coefficient. According to the work reported in [83, 84], the equilibrium PDF for the mass transport model using the LBM can be determined as:

$$g_i^{eq} = Cw_i\left[1 + 3\frac{e_i.u}{c^2}\right] \tag{3.14}$$

here the mass concentration (C) can be defined similarly as for the fluid flow LB model:

$$C = \sum_i g_i. \tag{3.15}$$

The relaxation parameter is related to the mass diffusion coefficient with the following expression:

$$\tau_m = 3D + 0.5. \tag{3.16}$$

In addition, the mass flux is a required parameter to be computed in the mass transport LB model. It can be obtained through the Chapman-Enskog asymptotic analysis of Eq. (3.13) [85, 86], and it is computed as follows:

$$j = \left(1 - \frac{1}{2\tau_m}\right)\sum_i e_i\, g_i \tag{3.17}$$

Mass Transfer Boundary Conditions

Similar to the fluid flow LBM model, the boundary conditions for the mass transport LB model have to be implemented accordingly. In the LB models, the fundamental variables are the PDF, and therefore; the boundary conditions are based on the distribution functions [78, 83]:

- Constant concentration boundaries: It is applicable at the inflow/outflow boundaries of the analyzed domain. This kind of boundary condition is suitable when a concentration gradient is defined. The unknown directional concentrations are computed based on the weighting factors.
- Constant flux boundaries: These can be applied at the inflow/outflow boundaries of the domain, especially to represent any chemical reaction that can influence the concentrations at the boundaries.
- Bound-back boundaries: This type of boundaries plays an important role in the LB models where porous media are considered. They are applied at the fluid-solid interfaces, and it is assumed that PDFs hitting the solid surface are simply bounded back to where the particles came from.

- Periodic boundaries: Similar to the fluid flow LB model, the periodic boundaries are implemented at the sides perpendicular to the gradient concentration.

3.3 GDL Generation

During the last years, the interest of obtaining a more realistic model of porous media related to FCs has been increasing [87]. The pore-scale simulations where the morphological microstructure of the GDLs are used help to understand in detail the different transport phenomena occurring through the mentioned layer and can improve their properties. In addition, it can give insight to explore and investigate customized porous materials with enhanced properties and better performances [88].

The digital generation of the porous media representing the GDLs is one the most important issues in the study of the diffusion transport properties. Especially because in the description of the fluid flow behavior and the mass transport phenomena through the GDLs, the LBM requires specific information about the nature and position of each lattice node to be analyzed. Figure 3.4 shows an SEM image of a GDL in which the fiber and the pore space can be observed.

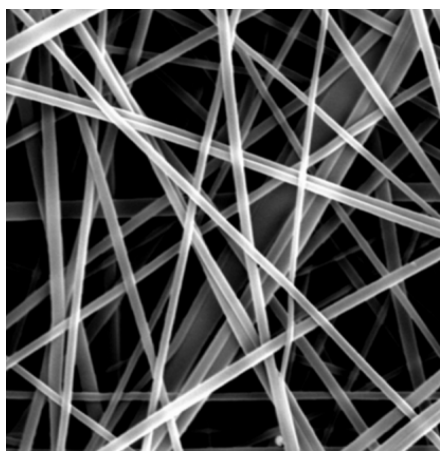

Figure 3.4 SEM image of a GDL in gray-scale colors
The in-plane view shows the microstructure of a selected GDL.

The SEM image presented in Fig. 3.4 can be digitally treated to obtain an image in which the solid and pore space can be represented. The digital conversion of grayscale image to a black-white image is shown in Figure 3.5.

Figure 3.5 Binary image showing an approximation of pore-solid structure
Black color regions represent the solid material while the withe color regions represent the pore-space.

In the digital generation of the GDLs, a phase function must be defined as follows:

$$\varphi(z) = \begin{cases} 0, & z \,\epsilon\, pore, white \\ 1, & z \,\epsilon\, solid, black \end{cases} \tag{3.18}$$

where z represents the position of the corresponding analyzed lattice element. In the current study, such a position is a 2D or 3D coordinate. When the LBM is applied to model a certain transport phenomena, if the phase function is 1 the bounce-back boundary conditions is employed. In addition, the mentioned function offers the opportunity to compute the porosity of the material by using Eq. (2.3).

The digitally created GDLs employed in the current study correspond to models in which the solid obstacles or fibers are placed stochastically into the domain. In the 2D models special care of the distance between the solid obstacles, representing the carbon fibers, should be considered. This is so because in the 2D models blockage of the fluid has to be avoided. Meanwhile, in the 3D models, the fibers are considered infinitely long and can intercept each other. For all the models, the fibers are undeformable under any circumstances, but they can be displaced in the study in which the compression effect is analyzed. More detailed information about the GDL generation is given in the following chapter together with main results obtained in the current investigation.

4 Main Results & Discussions

In this chapter, a brief description of the modeling conditions and the main results and discussions obtained in the appended papers are presented.

4.1 Paper I

In **Paper I**, a detailed revision of the FC modeling, possible transport parameters to be considered in the study, and the applicability of the LBM for describing the fluid behavior through complex geometries are presented. Figure 4.1 shows a simple graph relating the computational time, length scale and time scale modeling.

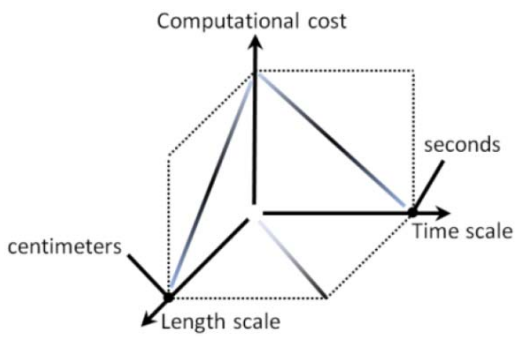

Figure 4.1 Simple relation between the scales and computational cost in FC modeling
Not to scale, and not necessarily straight lines. Figure from [89] by permission of ASME

Taken into account that the PEFC modeling at cell scale normally consider several assumptions and that having a more detailed information from smaller scales can give a more accurate PEFC model, it was decided to study the modeling at micro- and mesoscale.

However, a great variety of studies can be made at the mentioned levels, i.e., momentum transport, mass transport, heat transport and charge transport, etc. According to the literature review, two of the elements that were receiving most attention at micro- and mesoscale modeling are the GDLs and the CLs [90 - 92]. Both have complex geometries but with differences in the thickness and pore size diameter.

Considering the anisotropic and complex nature of the GDLs, a methodology that can deal with these complex microstructures is selected. The ability for describing phenomena at small scales, and its simple methodology makes the LBM a potential candidate to be used in the transport phenomena modeling. Because of all the advantages of the LBM, its applicability in FC modeling has been increasing during the last years as shown in Figure 4.2.

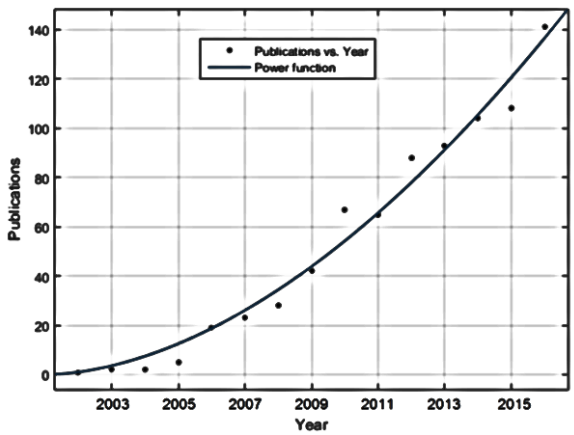

Figure 4.2 Number of publications with "Lattice Boltzmann Method" AND "Fuel Cell" as search topic.
The period corresponds between 2002 – 2016. The searchable database is Scopus©

The number of publications during the last years has been increasing in a sustained way, showing that LBM is a powerful tool to be employed in FC modeling. The solid blue line represents a growth in a power function fashion. In addition, a review of the possible research topics a pore-scale level was effected, and it was concluded that the most commonly applied schemes for PEFC modeling were D2Q9 and D3Q19 for two- and three dimensional models, respectively.

4.2 Paper II

In **Paper II**, a 2D model was created to evaluate different diffusion transport properties of digitally created GDLs as they are subjected to compression. The fluid behavior in the normal thickness and in the compressed thickness was analyzed. The impact of the compression over the porosity, gas-phase tortuosity and permeability was studied. The permeability of the GDLs was computed by using previous correlations as a function of the porosity and the fiber thickness.

The GDL is assumed to be an arrangement of solid materials stochastically placed on a two-dimensional domain representing the carbon fibers. Because this study is carried out in 2D, special care should be taken when the fibers are placed in normal conditions and in compressed conditions to avoid any possible total blockage of the fluid flow throughout the simulated GDL.

After the GDL generation, the study follows the following steps:

- Simulation of the fluid behavior through the GDL by using the LBM. At the inlet boundary the velocity is given while at the outlet the second derivative approximation is used.
- Computation of the velocity field, porosity and gas-phase tortuosity. The fiber radius is computed which is constant in all the simulations.
- The permeability is computed by means of previous proposed relationships in which it is a function of the porosity, or porosity and radius.
- The compression is digitally effected in uniform steps until obtaining the maximum allowed compression.

Due to the computational nature of the study, the maximum compression rate can be ad infinitum; however, it was established at 66% of the initial thickness. This value falls in an acceptable range if compared to previous studies [93, 94]. Figure 4.3 shows the arrangement of the fibers representing the digitally created GDLs for the uncompressed and compressed thickness.

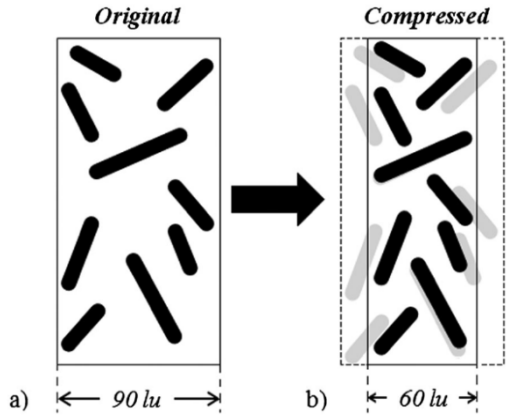

Figure 4.3 Two-dimensional arrange of the solid-like fiber representing the GDLs.
(a) GDL is not compressed, (b) GDL with maximum compression. Figure from [95] by permission of IJER

As mentioned, the fluid flow behavior through the GDLs at different compression rates is obtained by means of the LBM. For each value the GDL is compressed in steps of around 6.6% until the maximum compression rate is reached. The fluid flow behaviors for the initial layer thickness and the maximum compressed GDL are presented in Figure 4.4.

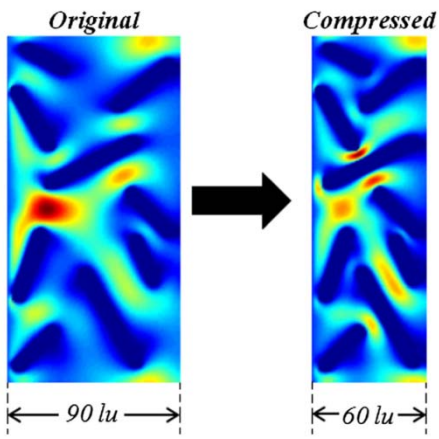

Figure 4.4 Fluid flow behavior through the original and compressed GDLs.
Higher velocities are represented by the red color regions, while lower velocities by the blue color regions.

As observed, the compression of the GDL modifies the fiber positions and therefore the fluid behavior through them is also affected. A comparison of the velocity profile computed in the original and compressed GDL is presented in Figure 4.5

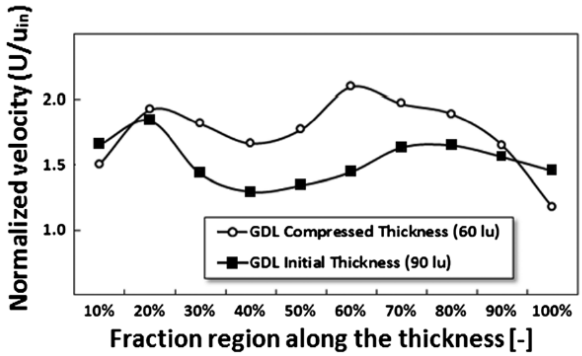

Figure 4.5 Fluid flow behavior through the original and compressed GDLs.
Higher velocities are represented by the red color regions, while lower velocities by the blue color regions.

Due to the compression, the velocity profile is modified having higher velocities when the fibers are closer. At the same time, the porosity of the layer is also affected. This study proposes a correlation between the porosity and the compression ratio. To this aim, the porosity is computed by each compression ratio and such values are depicted in Figure 4.6.

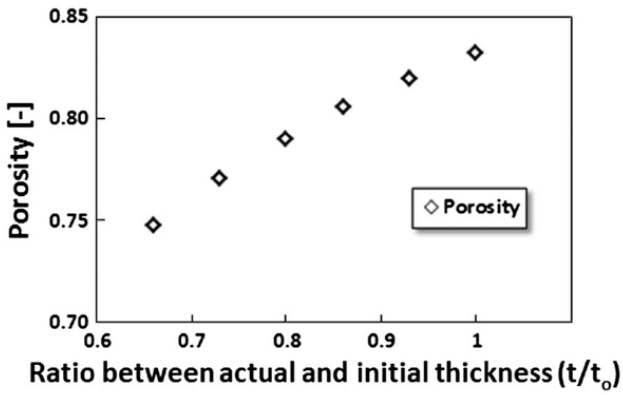

Figure 4.6 Porosity values for each compressed GDL.
Lower porosities are given when the layer is compressed in a high rate.

Considering the obtained results, a correlation between the porosity and the ratio of compression is proposed as follows:

$$\varepsilon_{2D}(\varsigma) = 0.3928 + 0.78 * \varsigma - 0.2893 * \varsigma^2 \quad (4.1)$$

where ς is the ratio between the actual and the initial thickness of the GDL. Based on the computed velocity field, the gas-phase tortuosity is also determined by each compression ratio as shown in Figure 4.7.

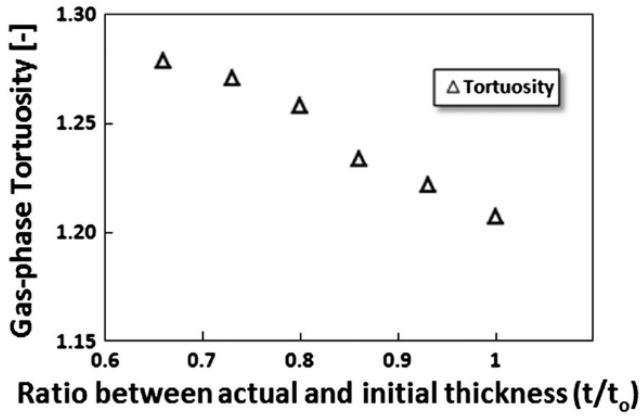

Figure 4.7 Gas-phase tortuosity values for each compressed GDL.
The gas-phase tortuosity increases when the compression rate increases.

The gas-phase tortuosity is also correlated to the compression rate by the following expression:

$$\tau(\varsigma) = 1.353 - 0.03343 * \varsigma - 0.1145 * \varsigma^2 \quad (4.2)$$

For both correlations, the fitted parameters were established based on the sums of squares due to error (SSE) and the root-mean-squared error (RMSE). The values fall in a range of 10^{-7} and 10^{-2}.

Finally, the permeability is computed for the GDL at each compression step. To compute the permeability, three different previous correlations were used. These require either the porosity or the porosity and fiber radius (2 of them). More detailed descriptions about the correlations are given in **Paper II** appended in this thesis. The computed values are compared with experimental values and a very good agreement is found, see Figure 4.8.

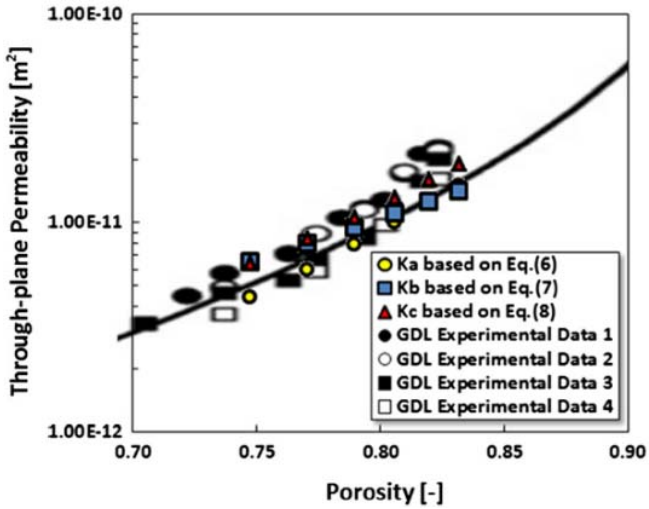

Figure 4.8 Comparison between the computed permeabilities and the experimental from a previous study. The computed permeabilities show a good agreement with experimental values from [56].

In general, this 2D model can easily explain the behavior of the porosity and gas-phase tortuosity as a function of the compression rate. In addition, the permeability is computed taking into account three previous correlations which consider only physical parameters of the porous media such as porosity and fiber radius.

4.3 Paper III

In **Paper III**, microstructural morphological considerations are taken into account to analyze their impact on the diffusion transport properties. In this study, the 2D model allows description of the fluid behavior and computation of parameters such as porosity, gas-phase tortuosity, permeability, diffusibility (often called obstruction factor [96, 97]) and inertial coefficient. In contrast to **Paper II**, the permeability is not computed by using previous relationships based on porosity, but by using the Darcy's law. Then it is possible to propose correlations based on the obtained results.

The results obtained in this study are based on a GDL assumed to be an arrangement of fibers placed in a 3D domain. However, only the 2D through plane direction is considered in the analysis. The fibers are considered as undeformable cylinders infinitely long. Again, due to the 2D nature of the model, it is important to be aware of any possible blockage of the fluid flowing through the generated GDLs. Figure 4.9 shows a section of the digital approximation for the GDLs employed in the current study.

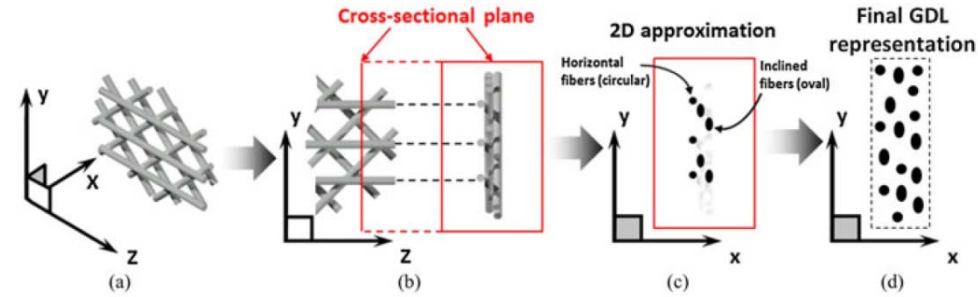

Figure 4.9 GDL generation approximation from 3D to a 2D model
(a) First 3D approximation of the GDLs, (b) In-plane and through-plane view. (c) 2D approximation. (d) Selected region of the final GDL representation. Figure from [98] by permission of IJER.

The analysis is carried out varying the percentage of inclined fibers from 0% to 100% in steps of 12.5%. For each configuration, the porosity is computed and the fluid behavior is described with the LBM. The inclination of the fibers is 45º, and the fiber diameter is varied from 4.00 to 6.00 μm. To represent an inclined rod in the 2D GDL, an oval shape is placed in the 2D domain. Figure 4.10 shows the fluid behavior through nine selected representative GDL regions. In the upside of the GDLs there is a nomenclature GDLa(#), where a represents the fiber diameter and # is the percentage of inclined fibers. The number of fibers per unit area is maintained at a constant value.

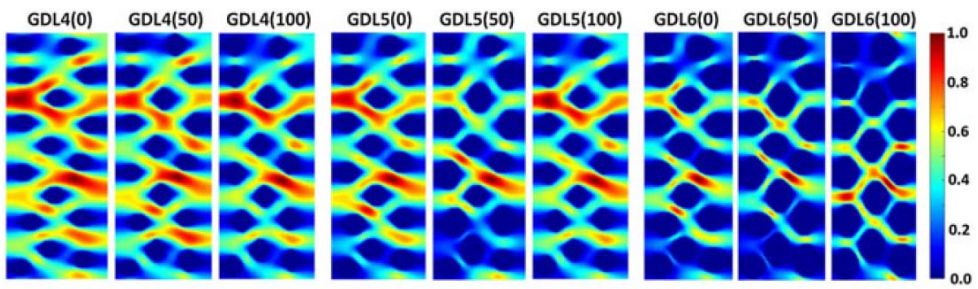

Figure 4.10 Fluid flow behavior for nine representative GDL samples.
Red color regions represent higher velocities, whereas blue color region represents low velocities. As expected, the velocity is zero where the fibers are placed.

The porosity is computed for all the samples and grouped by the fiber diameters in order to find correlations between the porosity and the percentage of inclined fibers. The porosity of all the samples falls in the range of 0.83 to 0.51, decreasing as the percentage of inclined fibers increases. Figure 4.11 shows the porosity behavior related to the percentage of the inclined fibers.

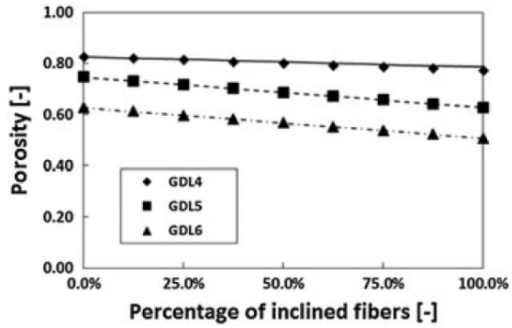

Figure 4.11 Porosity data computed from the GDL models.
As expected the thinner the fibers, the higher the porosity. The porosity values decrease with the increment of the percentage of inclined fibers.

Considering the computed porosity values and the percentage of inclined fibers, the correlations can be presented for each fiber diameter:

$$\varepsilon_{GDL4}(\delta) = -0.0004 * \delta + 0.8267 \tag{4.3}$$

$$\varepsilon_{GDL5}(\delta) = -0.0012 * \delta + 0.7467 \tag{4.4}$$

$$\varepsilon_{GDL6}(\delta) = -0.0012 * \delta + 0.6267 \tag{4.5}$$

where δ represents the percentage of inclined fibers present in the model; i.e., for 25% of inclined fibers, 25 should be replaced in the correlations. The gas-phase tortuosity is also computed, and a correlation for each fiber diameter and the percentage of inclined fibers was established. Figure 4.12 shows the gas-phase tortuosity values which fall in the range of 1.067 – 1.163.

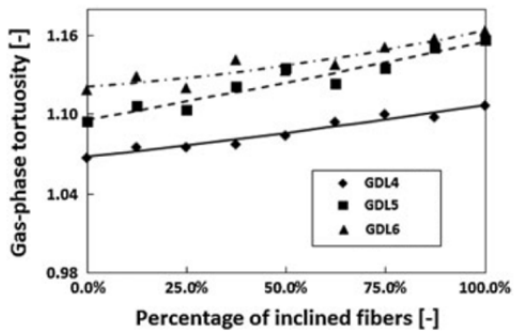

Figure 4.12 Gas-phase tortuosity data computed from the GDL models.
The gas-phase tortuosity increases with the increment of the percentage of inclined fibers.

It was demonstrated, based on the proposed models, that the gas-phase tortuosity increases with the percentage of inclined fibers. Thus, a correlation to predict the gas-phase tortuosity for each fiber diameter as a function of the percentage of inclined fibers is proposed:

$$\tau_{GDL4}(\delta) = 6.737x10^{-7} * \delta^2 + 3.252x10^{-4} * \delta + 1.068 \quad (4.6)$$

$$\tau_{GDL5}(\delta) = 5.290x10^{-7} * \delta^2 + 5.393x10^{-4} * \delta + 1.096 \quad (4.7)$$

$$\tau_{GDL6}(\delta) = 2.188x10^{-6} * \delta^2 + 2.089x10^{-4} * \delta + 1.121 \quad (4.8)$$

In addition to the correlations between the gas-phase tortuosity and the percentage of inclined fibers, the most common correlations in the open literature are relating the gas-phase tortuosity and porosity [39]. The computed values of the mentioned parameters are arranged and depicted in Figure 4.13. The trend is as expected, the lower the porosity the higher the gas-phase tortuosity. Three different empirical correlations are proposed, one is a rational function and the other two are power functions. However, the best choice is selected based on the SSE and the R-square, the lowest and the biggest, respectively.

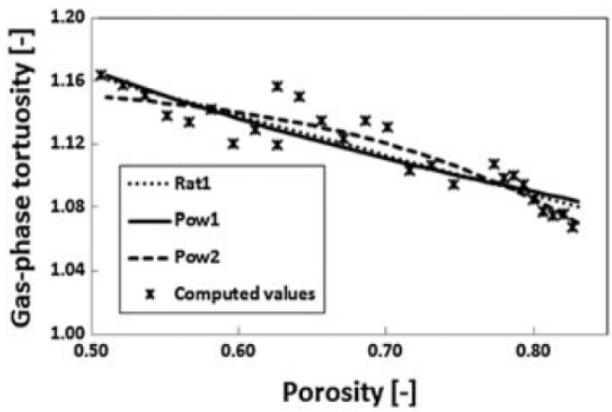

Figure 4.13 Gas-phase tortuosity vs. porosity.
Computed values from the simulated GDLs. Three best correlations are shown.

The correlations Rat1, Pow1 and Pow 2 have different goodness of fitting to the obtained date as presented in Table 4.1.

Table 4.1 Empirical correlations between the gas-phase tortuosity and porosity
For each correlation, the SSE and R-square is determined in order to choose the best option.

Name	Empirical relationship	SSE ($x10^{-3}$)	R-square
Rat1	$\frac{-211 * \varepsilon + 1086}{\varepsilon + 842.3}$	3.582	0.8259
Pow1	$1.042 * \varepsilon^{-0.175}$	2.846	0.8617
Pow2	$-0.2223 * \varepsilon^{5.057} + 1.157$	4.103	0.8007

As mentioned, considering the SSE and R-square values, the correlation named Pow1 is the most suitable to fit the obtained data. This correlation can be coupled to the Bruggeman correlation in which a scaling factor is included, similar to the study presented in [99]. It is important to notice that the proposed relationship predicts the gas-phase tortuosity for porosity values in the range of 0.51 – 0.83 based on the proposed simulated GDLs.

In the current study, the obstruction factor was evaluated as the ratio between the porosity and the gas-phase tortuosity. The impact of the presence of inclined fibers over this parameter was analyzed considering as reference GDL4(0). The computed obstruction factors decrease when the percentage of inclined fiber increases. The same trend is presented for each fiber diameter. Figure 4.14 shows the mentioned trend.

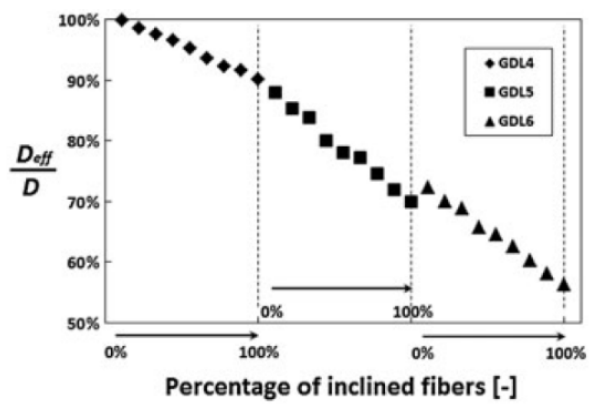

Figure 4.14 Obstruction factor variation for the simulated GDLs
GDL4 (0) is taken as a reference to evaluate the behavior of the obstruction factor.

Similar to the porosity and gas-phase tortuosity, the effects of the percentage of inclined fibers on the permeability are also evaluated. Figure 4.15 shows the computed values for permeability.

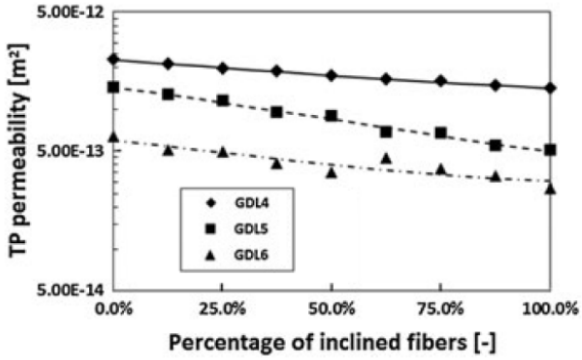

Figure 4.15 Permeability variation for the simulated GDLs
Collected data show that the permeability decrease when the percentage of inclined fibers increase.

Based on the obtained data, correlations between the permeability and the percentage of inclined fibers are proposed:

$$K_{GDL4}(\delta) = 3.619x10^{-17} * \delta^2 - 1.209x10^{-14} * \delta + 2.264x10^{-12} \quad (4.9)$$

$$K_{GDL5}(\delta) = 4.726x10^{-17} * \delta^2 - 1.415x10^{-14} * \delta + 1.439x10^{-12} \quad (4.10)$$

$$K_{GDL6}(\delta) = 2.084x10^{-17} * \delta^2 - 5.014x10^{-14} * \delta + 5.993x10^{-12} \quad (4.11)$$

In addition, the permeability is related to the porosity. The computed values of the mentioned parameters are arranged in Figure 4.16.

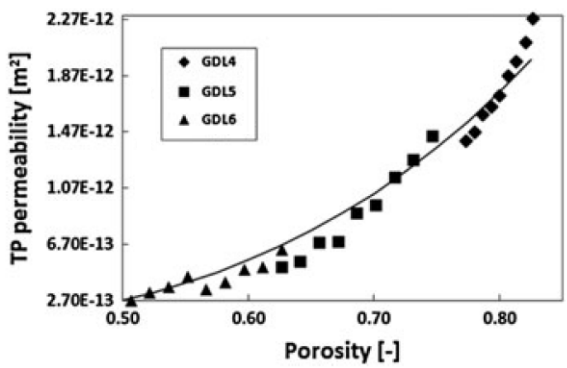

Figure 4.16 Permeability vs. porosity for the simulated GDLs
Collected data show that the permeability increases when porosity increases.

A proposed correlation between the permeability and porosity is expressed as:

$$K(\varepsilon) = 4.27x10^{-12} * \varepsilon^{3.988} \tag{4.12}$$

Finally, the effects on the inertial coefficient are analyzed. In this study, all the values involved in the relationship proposed by Liu et al. [54] are computed from the simulated GDLs. Figure 4.17 shows the obtained results compared with previous studies.

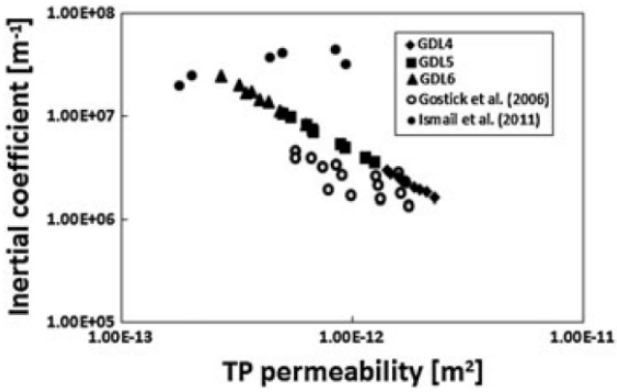

Figure 4.17 inertial coefficient vs. permeability for the simulated GDLs
Collected data compared to previous studies.

4.4 Paper IV

In **Paper IV**, a 3D model to simulate the fluid flow behavior through the GDLs is developed. This model allows to analyze the impact of considering the land/channel region on the gas-phase tortuosity and diffusibility. At the same time as the GDL model is obtained, the implemented boundary conditions are also developed and implemented.

Most of the previous studies of GDLs, including the studies from the author, consider the inflow to the GDL as having a uniform profile. However, in reality, the inflow, and therefore the flow of the gases through the GDLs, are affected by the presence or absence of the ribs in the flow plates as depicted in Figure 4.18.

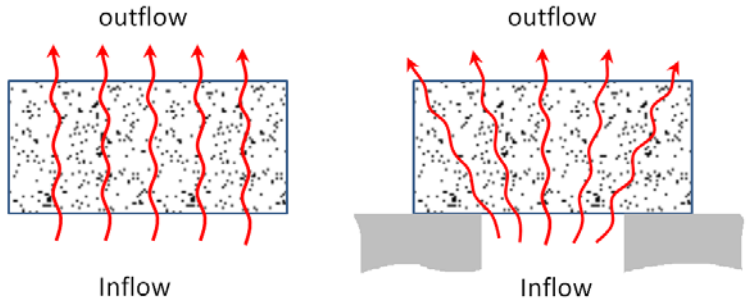

Figure 4.18 Through-plane view of the possible pathways followed by the gas through the GDLs
When the land/channel region is not considered (left) and when the land/channel region is considered in the model.

By considering the land/channel region during the simulation process, a variation in the gas-phase tortuosity computation is generated, and therefore; the diffusibility is also affected. The 3D GDL is modeled considering the porosity values found in the open literature and generated as follows:

- The fibers are randomly placed in a plane perpendicular to the main flow direction.
- The fibers are considered infinitely long and they are allowed to cross each other when they intercept.
- GDL fibers are assumed to be cylinder rods with constant diameter and non-deformable.
- The layers, composed of fibers in one layer, are stacked until getting the desirable GDL thickness.

The local porosity is computed for all the GDL samples, Figure 4.19 shows the local porosity for a selected GDL and its variation along the through-plane direction.

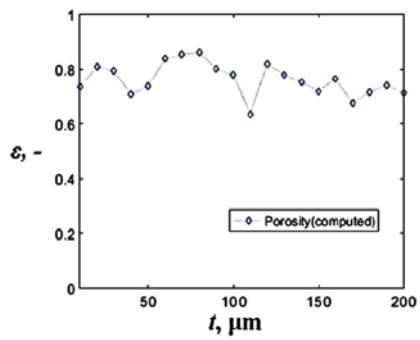

Figure 4.19 Local porosity computed in the through-plane direction of a selected GDL
Variation of the local porosity shows the stochastic nature of the model. Figure from [100] by permission of ECS.

In total, eleven GDL samples are digitally generated with an average porosity equal to 0.7555 and a standard deviation equal to 0.0139. The fluid flow behavior through the GDLs is obtained by means of the LBM. At the inlet boundary, the velocity is given allowing the Reynolds number smaller than 10^{-4} as found in real GDL applications. At the outlet boundary, i.e., CL interface, a second order derivative approximation is implemented. On the other four sides of the domain, periodic boundary conditions are applied. In presence of solid materials, i.e., carbon fibers, the simple bounce-back boundary condition is exerted. Figure 4.20 shows the fluid flow distribution at three different positions along the main flow direction when the land/channel region is not considered.

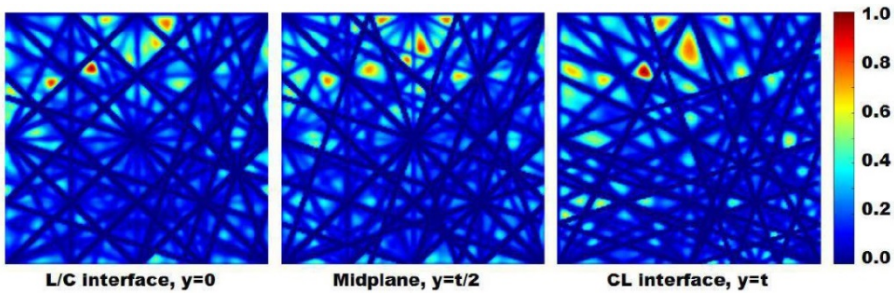

Figure 4.20 In-plane view of the fluid behavior at three different positions in the main flow direction (L/C=0)
Fluid behavior when the land/channel region is not considered.

To mimic the presence of the land/channel region, the inlet boundary conditions have to be modified. Thus, the inlet flow is set to zero in the regions corresponding to the ribs. This modification is implemented in steps of 0.1 until the land/channel ratio equal unity is reached. The fluid flow behavior at three different positions along the main flow direction considering the land/channel ratio equal 0.5 is shown in Figure 4.21.

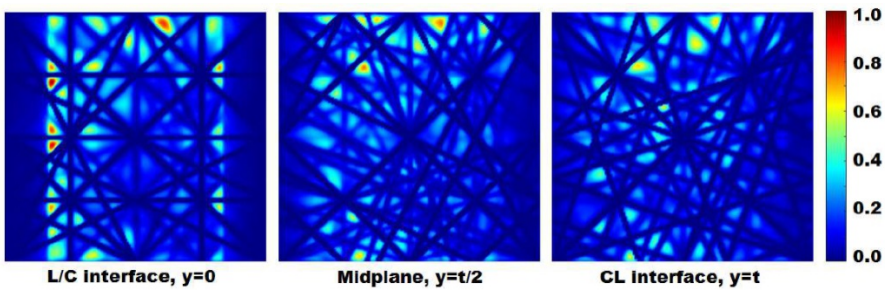

Figure 4.21 In-plane view of the fluid behavior at three different positions in the main flow direction (L/C=0.5)
Fluid behavior when the land/channel region is considered.

The land/channel region with a ratio equal to 0.5 affects the fluid behavior mainly in the region near to the flow plates. However, the impact is also appreciable in the region near the active sites. The variation in the fluid flow distribution affects the computation of the gas-phase tortuosity, and therefore the computation of diffusibility experience a change. Figure 4.22 shows the fluid flow behavior through the GDL when the land/channel ratio is equal to unity.

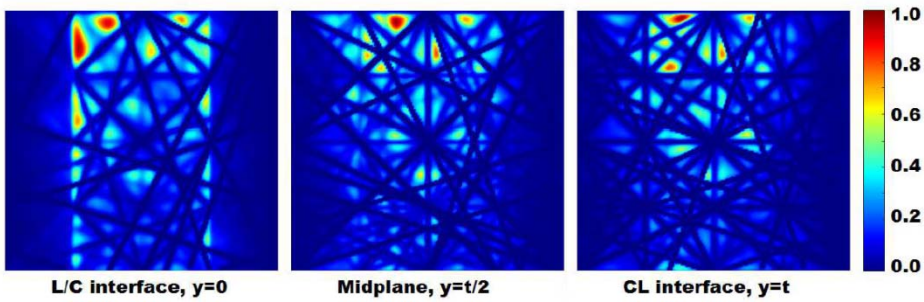

Figure 4.22 In-plane view of the fluid behavior at three different positions in the main flow direction (L/C=1.0)
Fluid behavior when the land/channel region is considered at the maximum ratio.

Comparing the results of the fluid flow behavior, the higher the land/channel ratio the fluid distribution in the CL region is less uniform. The gas-phase tortuosity is computed for land/channel ratios going from 0 to 1 in steps of 0.1. Figure 4.23 shows the computed gas-phase tortuosities.

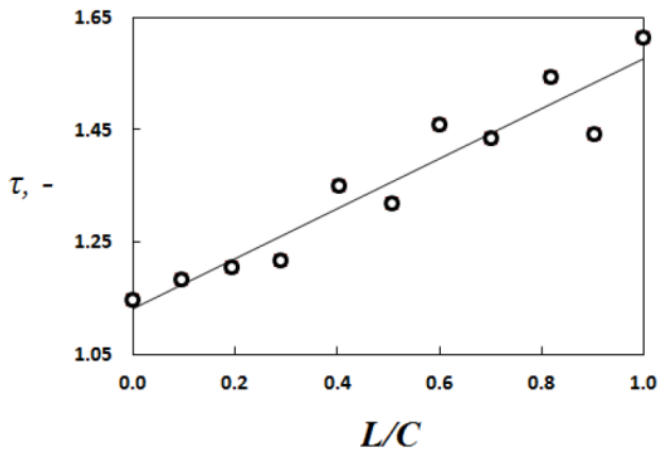

Figure 4.23 Computed gas-phase tortuosity vs. land/channel ratio
The gas-phase tortuosity increases while the land/channel ratio increases.

Based on the computed values of gas-phase tortuosity, a correlation can be determined as a function of the land/channel ratio. The correlation is expressed as follows:

$$\tau_{gas}(\vartheta) = \tau_o + 0.4496 * \vartheta \tag{4.13}$$

where ϑ is the land/channel ratio, and τ_o is the fitted value when the land/channel ratio is zero. With an R-square equal to 0.909, the τ_o is established in 1.1300. The diffusibility is computed as the ratio between the porosity and the gas-phase tortuosity. Figure 4.24 shows the trend of the computed diffusibility as a function of the land/channel ratio.

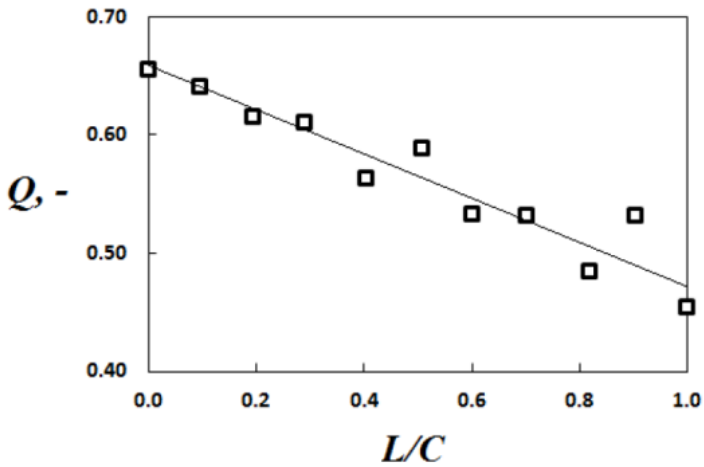

Figure 4.24 Computed diffusibility vs. land/channel ratio
The computed diffusibility decreases while the land/channel ratio increases.

Similar to the analysis of the gas-phase tortuosity, a correlation between the diffusibility and the land/channel ratio is proposed:

$$Q(\vartheta) = Q_o - 0.1839 * \vartheta \tag{4.14}$$

where the fitted value for Q_o is established in 0.6561, with a computed R-square equal to 0.905.

4.5 Paper V

In **Paper V**, the fluid flow LB and the mass transport LB model are implemented. The study is carried out in a 3D geometry, and the generation of the GDLs is based on the previous paper. A detailed comparative study of the most widely used correlations to determine the through-plane diffusibility in GDLs is accomplished.
A total of thirty-one GDLs are stochastically generated, all of them matching the porosity values found in the commercial ones, i.e., around 0.74. The fluid flow LB model allows to describe the fluid behavior through the GDLs and the computation of the gas-phase tortuosity. The diffusibility of each GDL sample is determined based on the obtained results from the mass transport LB model. Figure 4.25 shows the velocity field and the mass concentration of a selected GDL sample.

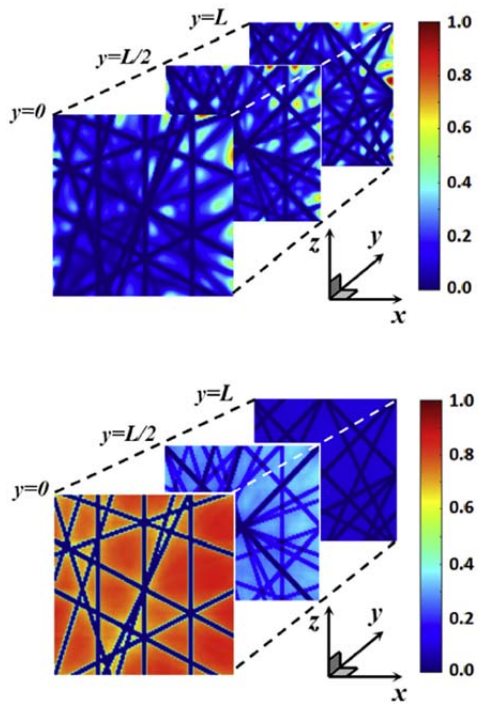

Figure 4.25 Velocity field (up) and Mass concentration (bottom) through a selected GDL sample
Red colored regions represent higher values, blue colored regions lower values. Figure from [101] by permission of IJHE.

The diffusibility for each sample, the cumulative mean and the cumulative standard deviation are presented in Figure 4.26.

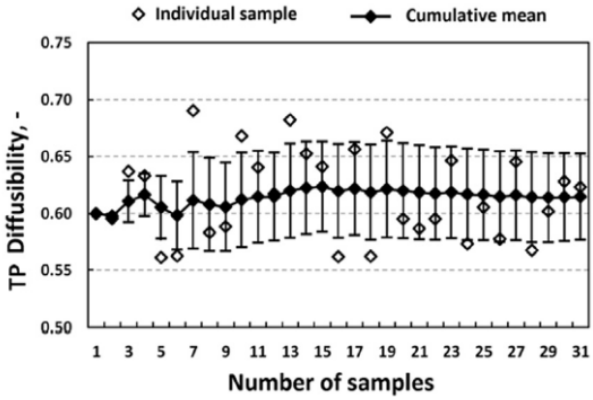

Figure 4.26 Computed diffusibility values for each GDL sample
Due to the stochastic nature of the GDL generation, the values fall between 0.55 and 0.70.

The computed diffusibility values using the mass transport LB model are compared to previous proposed diffusibility correlations. A comparison graph for all the GDL samples is depicted in Figure 4.27.

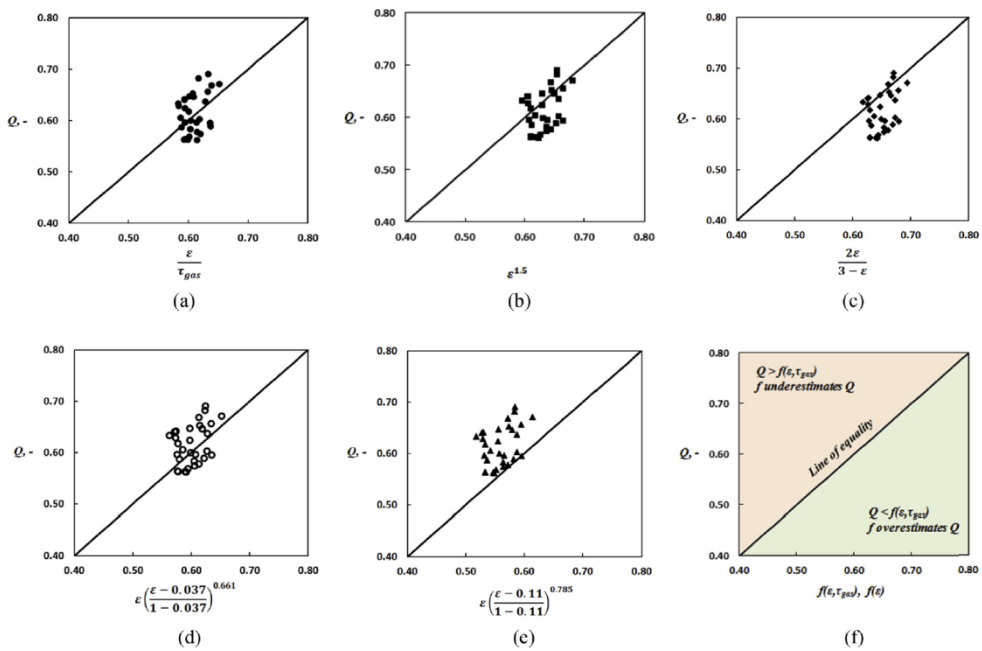

Figure 4.27 Comparison graph of the computed diffusibility values for all the GDL samples.
Vertical axis corresponds to the values computed using the mass transport LB model, whereas horizontal axis corresponds to the diffusibility values using previous proposed correlations.

Based on the obtained results, three different parameters were used to analyze the previous correlations: precision, accuracy and symmetry. The analysis was carried out considering the expected diffusibility the one computed using the mass transport LB model. Figure 4.28 shows the prediction rank of the analyzed correlations.

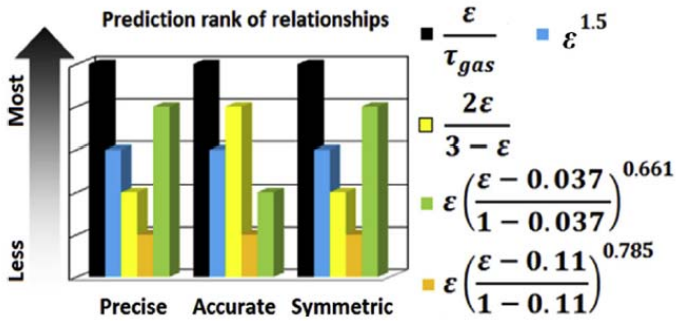

Figure 4.28 Ranking of the different correlations analyzed in the current study
They are ranked according to precision, accuracy and symmetry.

The most widely used correlation to predict the diffusibility, the Bruggeman approximation, blue color in Figure 4.28, is ranked third for all the characteristics considered.

5 Conclusions

The research presented in this thesis aimed to increase the understanding of the fluid flow behavior and mass transport phenomena through the GDLs from a pore-scale point of view. The different diffusion transport properties of the GDLs based on the digital generation of 2D and 3D geometries have been analyzed. The LBM has been applied for both, 2D and 3D GDLs, and the different boundary conditions have been implemented. Specifically, the scientific contributions can be summarized as:

- A 3D geometry representing the porous media found in realistic GDLs has been obtained to analyze diffusion transport properties taking into account microstructural and morphological considerations.

- Considering a 2D geometry, when a GDL is compressed up to 66% of its initial thickness, the porosity decrease around 10% and the gas-phase tortuosity increases approximately 6%. Under the same compression rate, the permeability is reduced by around 36% from the initial value.

- If the morphological variations are considered, i.e., percentage of inclined fibers, several correlations to predict the porosity, gas-phase tortuosity, permeability, obstruction factor and inertial coefficient, have been proposed. In addition, a correlation between the gas-phase tortuosity and porosity, as well as between the permeability and porosity have been proposed.

- Given that the land/channel region can affect the flow through the GDL, a 3D digitally generated GDL has been considered to analyze the mentioned

impact. Correlations for the gas-phase tortuosity and diffusibility related to the land/channel region have been proposed.

- A detailed pore-scale analysis of diffusibility correlations in GDLs, showed that the most accurate, precise and symmetry correlation is the one considering the porosity and gas-phase tortuosity in the estimation.

6 Future Work

Despite the increased pore-scale research in GDLs, there is a still a lot of questions to answer related to different properties of this important layer in the PEFC performance. In the current thesis, the diffusion transport parameters have been analyzed under certain circumstances, and therefore, a research considering the electronic transport and heat transport phenomena in the solid phase would be the next step. At the same time, the GDL geometry can be also improved getting a much more realistic configuration which allows one to obtain more accurate predictions. The LBM itself can be extended to analyze the multi-phase and multi-component phenomena. This can help us to improve, from a pore-scale point of view, the water management issue in the PEFCs, especially in the cathode side. More specifically, the following steps can be considered as a future work:

- Related to the GDL generation, consider the binder and PTFE material as part of the geometry. The fibers can be arranged not only as a stack of layers, but also with inclination between layers. The last mentioned issue will allow study of the real effect of compression and the consequences over the other related properties.

- In addition to the gas-phase analysis at the pore-scale level, the morphological configuration can be analyzed considering the solid-phase, i.e., the carbon fibers, with their corresponding properties such as ohmic and thermal resistance, electrical conductivity, etc. The heat and electric transport phenomena have to be included in the computational model.

- A multi-phase model have to be considered if a detailed multi-phenomena model is required. Water management can be studied to understand the

excess of water in the cathode side, and its incidence on the different transport properties of the GDLs.

- Similar to the consideration of the land/channel region, the complete flow plate can be also considered. The different diffusion transport parameters can be computed in a more accurate manner if more realistic path-flows followed by the fluid are taken into account.

Finally, if a more complete-detailed-accurate PEFC model in the whole range of length and time scales is the end-goal, the coupling between the pore-scale research with the cell-scale and molecular-level modeling is mandatory.

References

[1] Asif, M., & Muneer, T. (2007). Energy supply, its demand and security issues for developed and emerging economies. *Renewable and Sustainable Energy Reviews*, **11**(7), 1388–1413. doi:10.1016/j.rser.2005.12.004

[2] Schipper, L. (2009). Fuel economy, vehicle use and other factors affecting CO_2 emissions from transport. *Energy Policy*, **37**(10), 3711–3713. doi:10.1016/j.enpol.2009.07.028

[3] IEA – International Energy Agency (2016), CO_2 Emissions from Fuel Combustion 2016. doi:10.1787/co2_fuel-2016-en

[4] Amri, F. (2017). Intercourse across economic growth, trade and renewable energy consumption in developing and developed countries. *Renewable and Sustainable Energy Reviews*, **69**, 527–534. doi:10.1016/j.rser.2016.11.230

[5] He, Y., Xu, Y., Pang, Y., Tian, H., & Wu, R. (2016). A regulatory policy to promote renewable energy consumption in China: Review and future evolutionary path. *Renewable Energy*, **89**, 695–705. doi:10.1016/j.renene.2015.12.047

[6] Quaschning, V. (2016). *Understanding Renewable Energy Systems*. New York: Routledge. doi:10.4324/9781315769431

[7] E4Tech. (2016). The Fuel Cell Industry Review – 2016. Report retrieved from: www.FuelCellIndustryReview.com

[8] Larcher, D., & Tarascon, J.-M. (2014). Towards greener and more sustainable batteries for electrical energy storage. *Nature Chemistry*, **7**(1), 19–29. doi:10.1038/nchem.2085

[9] Sharaf, O. Z., & Orhan, M. F. (2014). An overview of fuel cell technology: Fundamentals and applications. *Renewable and Sustainable Energy Reviews*, **32**, 810–853. doi:10.1016/j.rser.2014.01.012

[10] Viggen, E. M. (2013). Acoustic multipole sources for the lattice Boltzmann method. *Physical Review E*, **87**(2). doi:10.1103/physreve.87.023306

[11] Hanasoge, S. M., Succi, S., & Orszag, S. A. (2011). Lattice Boltzmann method for electromagnetic wave propagation. *EPL (Europhysics Letters)*, **96**(1), 14002. doi:10.1209/0295-5075/96/14002

[12] Xiu-Ying, K., Da-He, L., Jing, Z., & Yong-Juan, J. (2005). Simulation of Blood Flow at Vessel Bifurcation by Lattice Boltzmann Method. *Chinese Physics Letters*, **22**(11), 2873–2876. doi:10.1088/0256-307x/22/11/041

[13] Papageorgopoulos D. (2010). DOE fuel cell technology program overview and introduction to the 2010 fuel cell pre-solicitation workshop in DOE fuel cell pre-solicitation workshop. Department of Energy, Lakewood, Colorado.

[14] Espinoza-Andaluz M. (2015). On Microstructural Analysis of Porous Media Existing in Fuel Cells Using the Lattice Boltzmann Method. Licentiate Dissertation, Division of Heat Transfer, Department of Energy Sciences, Lund University.

[15] Gittleman, C. D.M., Jorgensen, S., Waldecker, J., Hirano, S., & Mehall, M. (2010) Automotive fuel cell R&D needs. In: DOE fuel cell pre-solicitation workshop. Department of Energy, Lakewood, Colorado.

[16] Wang, Y., Chen, K. S., Mishler, J., Cho, S. C., & Adroher, X. C. (2011). A review of polymer electrolyte membrane fuel cells: Technology, applications, and needs on fundamental research. *Applied Energy*, **88**(4), 981–1007. doi:10.1016/j.apenergy.2010.09.030

[17] Geiger, S., & Copper, M.A.J. (2003). Fuel cell small stationary market survey. Fuel Cell Today 2003.

[18] James, B.D., & Kalinoski, J.A. (2007). Annual Progress Report, DOE Hydrogen Program, 700 – 704. Washington DC, U.S. Department of Energy.

[19] Reitz, W. (2007). Handbook of Fuel Cells: Fundamentals, Technology, and Applications, (Volume 2) W. Vielstich, A. Lamm, and H. A. Gasteiger (editors). *Materials and Manufacturing Processes*, **22**(6), 789–789. doi:10.1080/10426910701416336

[20] Larminie, J. and Dicks, A. (2003) Front Matter, in Fuel Cell Systems Explained, Second Edition, John Wiley & Sons Ltd., West Sussex, England. doi: 10.1002/9781118878330.fmatter

[21] Park, S., Lee, J.-W., & Popov, B. N. (2012). A review of gas diffusion layer in PEM fuel cells: Materials and designs. *International Journal of Hydrogen Energy*, **37**(7), 5850–5865. doi:10.1016/j.ijhydene.2011.12.148

[22] Burheim, O. S., Su, H., Hauge, H. H., Pasupathi, S., & Pollet, B. G. (2014). Study of thermal conductivity of PEM fuel cell catalyst layers. *International Journal of Hydrogen Energy*, **39**(17), 9397–9408. doi:10.1016/j.ijhydene.2014.03.206

[23] Bevers, D., Rogers, R., & von Bradke, M. (1996). Examination of the influence of PTFE coating on the properties of carbon paper in polymer electrolyte fuel cells. *Journal of Power Sources*, **63**(2), 193–201. doi:10.1016/s0378-7753(96)02465-2

[24] Yang, X.-G., Burke, N., Wang, C.-Y., Tajiri, K., & Shinohara, K. (2005). Simultaneous Measurements of Species and Current Distributions in a PEFC under Low-Humidity Operation. *Journal of The Electrochemical Society*, **152**(4), A759. doi:10.1149/1.1864492

[25] Lee, H.-K., Park, J.-H., Kim, D.-Y., & Lee, T.-H. (2004). A study on the characteristics of the diffusion layer thickness and porosity of the PEMFC. *Journal of Power Sources*, **131**(1-2), 200–206. doi:10.1016/j.jpowsour.2003.12.039

[26] Williams, M. V., Kunz, H. R., & Fenton, J. M. (2004). Operation of Nafion®-based PEM fuel cells with no external humidification: influence of operating conditions and gas diffusion layers. *Journal of Power Sources*, **135**(1-2), 122–134. doi:10.1016/j.jpowsour.2004.04.010

[27] Wang, Y., Wang, C.-Y., & Chen, K. S. (2007). Elucidating differences between carbon paper and carbon cloth in polymer electrolyte fuel cells. *Electrochimica Acta*, **52**(12), 3965–3975. doi:10.1016/j.electacta.2006.11.012

[28] Gas Diffusion Layer Comparison Table, FuelCellsEtc. Retrieved on 17-01-31 from: http://www.fuelcellsetc.com/store/DS/gas-diffusion-layer-properties.pdf

[29] Spiegel, C. (2008). Modeling the Gas Diffusion Layers. PEM Fuel Cell Modeling and Simulation Using Matlab, 197–241. doi:10.1016/b978-012374259-9.50009-4

[30] Frey, T., & Linardi, M. (2004). Effects of membrane electrode assembly preparation on the polymer electrolyte membrane fuel cell performance. *Electrochimica Acta*, **50**(1), 99–105. doi:10.1016/j.electacta.2004.07.017

[31] Wilkinson, D., Zhang, J., Hui, R., Fergus, J., & Li, X. (2010). Proton Exchange Membrane Fuel Cells: Materials Properties and Performance. First Edition, CRC Press, Boca Ratón, Florida, U.S. ISBN 9781439806647 - CAT# K10331

[32] Mathias, M. F., Roth, J., Fleming, J. and Lehnert, W. (2010). Diffusion media materials and characterisation. Handbook of Fuel Cells. doi:10.1002/9780470974001.f303046

[33] Giorgi, L., Antolini, E., Pozio, A., & Passalacqua, E. (1998). Influence of the PTFE content in the diffusion layer of low-Pt loading electrodes for polymer electrolyte fuel cells. *Electrochimica Acta*, **43**(24), 3675–3680. doi:10.1016/s0013-4686(98)00125-x

[34] Mortazavi, M., & Tajiri, K. (2014). Effect of the PTFE content in the gas diffusion layer on water transport in polymer electrolyte fuel cells (PEFCs). *Journal of Power Sources*, **245**, 236–244. doi:10.1016/j.jpowsour.2013.06.138

[35] Yu, G., Li, T. S., Xu, M., Andersson, M., Li, B., Tang, H., Parbey, J. & Shao, J. (2017). Fabrication of nickel-YSZ cermet nanofibers via electrospinning. *Journal of Alloys and Compounds*, **693**, 1214–1219. doi:10.1016/j.jallcom.2016.10.001

[36] Espinoza, M., Sunden, B., Andersson, M., & Yuan, J. (2015). Analysis of Porosity and Tortuosity in a 2D Selected Region of Solid Oxide Fuel Cell Cathode Using the Lattice Boltzmann Method. *ECS Transactions*, **65**(1), 59–73. doi:10.1149/06501.0059ecst

[37] Zhan, Z., Xiao, J., Li, D., Pan, M., & Yuan, R. (2006). Effects of porosity distribution variation on the liquid water flux through gas diffusion layers of PEM fuel cells. *Journal of Power Sources*, **160**(2), 1041–1048. doi:10.1016/j.jpowsour.2006.02.060

[38] Daino, M. M., & Kandlikar, S. G. (2012). 3D phase-differentiated GDL microstructure generation with binder and PTFE distributions. *International Journal of Hydrogen Energy*, **37**(6), 5180–5189. doi:10.1016/j.ijhydene.2011.12.050

[39] Shen, L., & Chen, Z. (2007). Critical review of the impact of tortuosity on diffusion. *Chemical Engineering Science*, **62**(14), 3748–3755. doi:10.1016/j.ces.2007.03.041

[40] Bruggeman, D. A. G. (1935). Berechnung verschiedener physikalischer Konstanten von heterogenen Substanzen. I. Dielektrizitätskonstanten und Leitfähigkeiten der Mischkörper aus isotropen Substanzen. *Annalen Der Physik*, **416**(7), 636–664. doi:10.1002/andp.19354160705

[41] Barrande, M., Bouchet, R., & Denoyel, R. (2007). Tortuosity of Porous Particles. *Analytical Chemistry*, **79**(23), 9115–9121. doi:10.1021/ac071377r

[42] Neale, G. H., & Nader, W. K. (1973). Prediction of transport processes within porous media: Diffusive flow processes within an homogeneous swarm of spherical particles. *AIChE Journal*, **19**(1), 112–119. doi:10.1002/aic.690190116

[43] Ghanbarian, B., & Cheng, P. (2016). Application of continuum percolation theory for modeling single- and two-phase characteristics of anisotropic carbon paper gas diffusion layers. *Journal of Power Sources*, **307**, 613–623. doi:10.1016/j.jpowsour.2015.12.142

[44] Koponen, A., Kataja, M., & Timonen, J. (1996). Tortuous flow in porous media. *Physical Review E*, **54**(1), 406–410. doi:10.1103/physreve.54.406

[45] Nabovati, A., Hinebaugh, J., Bazylak, A., & Amon, C. H. (2014). Effect of porosity heterogeneity on the permeability and tortuosity of gas diffusion layers in polymer electrolyte membrane fuel cells. *Journal of Power Sources*, **248**, 83–90. doi:10.1016/j.jpowsour.2013.09.061

[46] Hao, L., & Cheng, P. (2009). Lattice Boltzmann simulations of anisotropic permeabilities in carbon paper gas diffusion layers. *Journal of Power Sources*, **186**(1), 104–114. doi:10.1016/j.jpowsour.2008.09.086

[47] Van Doormaal, M. A., & Pharoah, J. G. (2009). Determination of permeability in fibrous porous media using the lattice Boltzmann method with application to

PEM fuel cells. *International Journal for Numerical Methods in Fluids*, **59**(1), 75–89. doi:10.1002/fld.1811

[48] Andersson, M., Beale, S. B., Espinoza, M., Wu, Z., & Lehnert, W. (2016). A review of cell-scale multiphase flow modeling, including water management, in polymer electrolyte fuel cells. *Applied Energy*, **180**, 757–778. doi:10.1016/j.apenergy.2016.08.010

[49] Froning, D., Gaiselmann, G., Reimer, U., Brinkmann, J., Schmidt, V., & Lehnert, W. (2014). Stochastic Aspects of Mass Transport in Gas Diffusion Layers. *Transport in Porous Media*, **103**(3), 469–495. doi:10.1007/s11242-014-0312-9

[50] Darcy, H. (1856). Les Fontaines Publiques de la Ville de Dijon. Victor Dalmont: Paris.

[51] Tamayol, A., McGregor, F., & Bahrami, M. (2012). Single phase through-plane permeability of carbon paper gas diffusion layers. *Journal of Power Sources*, **204**, 94–99. doi:10.1016/j.jpowsour.2011.11.084

[52] Fishman, Z., & Bazylak, A. (2011). Heterogeneous Through-Plane Distributions of Tortuosity, Effective Diffusivity, and Permeability for PEMFC GDLs. *Journal of The Electrochemical Society*, **158**(2), B247. doi:10.1149/1.3524284

[53] Forchheimer, P. (1914). Hydraulik; 1st Ed. Teubner, Leipzig and Berlin, Chap. 15. pp. 116-118.

[54] Liu, X., Civan, F., & Evans, R. D. (1995). Correlation of the Non-Darcy Flow Coefficient. *Journal of Canadian Petroleum Technology*, 34(10). doi:10.2118/95-10-05

[55] Ismail, M. S., Damjanovic, T., Ingham, D. B., Ma, L., & Pourkashanian, M. (2010). Effect of polytetrafluoroethylene-treatment and microporous layer-coating on the in-plane permeability of gas diffusion layers used in proton exchange membrane fuel cells. *Journal of Power Sources*, **195**(19), 6619–6628. doi:10.1016/j.jpowsour.2010.04.036

[56] Gostick, J. T., Fowler, M. W., Pritzker, M. D., Ioannidis, M. A., & Behra, L. M. (2006). In-plane and through-plane gas permeability of carbon fiber electrode backing layers. *Journal of Power Sources*, **162**(1), 228–238. doi:10.1016/j.jpowsour.2006.06.096

[57] Cunningham, R.E. (1980). Diffusion in gases and porous media. Plenum Press, New York, US.

[58] Yuan, J., & Sundén, B. (2014). On mechanisms and models of multi-component gas diffusion in porous structures of fuel cell electrodes. *International Journal of Heat and Mass Transfer*, **69**, 358–374. doi:10.1016/j.ijheatmasstransfer.2013.10.032

[59] Hoogschagen, J. (1955). Diffusion in Porous Catalysts and Adsorbents. *Industrial & Engineering Chemistry*, **47**(5), 906–912. doi:10.1021/ie50545a016

[60] Tomadakis, M. M., & Sotirchos, S. V. (1993). Ordinary and transition regime diffusion in random fiber structures. *AIChE Journal*, **39**(3), 397–412. doi:10.1002/aic.690390304

[61] Nam, J. H., & Kaviany, M. (2003). Effective diffusivity and water-saturation distribution in single- and two-layer PEMFC diffusion medium. *International Journal of Heat and Mass Transfer*, **46**(24), 4595–4611. doi:10.1016/s0017-9310(03)00305-3

[62] Das, P. K., Li, X., & Liu, Z.-S. (2010). Effective transport coefficients in PEM fuel cell catalyst and gas diffusion layers: Beyond Bruggeman approximation. *Applied Energy*, **87**(9), 2785–2796. doi:10.1016/j.apenergy.2009.05.006

[63] Andersson, M., Yuan, J., & Sundén, B. (2010). Review on modeling development for multiscale chemical reactions coupled transport phenomena in solid oxide fuel cells. *Applied Energy*, **87**(5), 1461–1476. doi:10.1016/j.apenergy.2009.11.013

[64] Grew, K. N., & Chiu, W. K. S. (2012). A review of modeling and simulation techniques across the length scales for the solid oxide fuel cell. *Journal of Power Sources*, **199**, 1–13. doi:10.1016/j.jpowsour.2011.10.010

[65] Succi, S. (2001). The lattice Boltzmann equation: for fluid dynamics and beyond. Oxford university press.

[66] Espinoza Andaluz, M., Sundén, B., & Andersson, M. (2014). Lattice Boltzmann Modeling From the Macro-to the Microscale-An Approximation to the Porous Media in Fuel Cells. *In REGenerative Energien und WAsserstofftechnologie-Symposium*, REGWA 2014.

[67] Espinoza-Andaluz, M., Andersson, M., & Sundén, B. (2016). Computational time and domain size analysis of porous media flows using the lattice Boltzmann method. *Computers & Mathematics with Applications*. doi:10.1016/j.camwa.2016.12.001

[68] Espinoza-Andaluz, M. (2015). On Microstructural Analysis of Porous Media Existing in Fuel Cells Using the Lattice Boltzmann Method. Licentiate dissertation, Division of Heat Transfer, Department of Energy Sciences, Lund University.

[69] Wang, M., Wang, J., Pan, N., & Chen, S. (2007). Mesoscopic predictions of the effective thermal conductivity for microscale random porous media. *Physical Review E*, **75**(3). doi:10.1103/physreve.75.036702

[70] Gebäck, T., & Heintz, A. (2014). A Lattice Boltzmann Method for the Advection-Diffusion Equation with Neumann Boundary Conditions. *Communications in Computational Physics*, **15**(02), 487–505. doi:10.4208/cicp.161112.230713a

[71] Razzaghian, M., Pourtousi, M., & Darus, A. N. (2012). Simulation of flow in lid driven cavity by MRT and SRT. In Thailand: *International Conference on Mechanical and Robotics Engineering*.

[72] Perumal, D. A., & Dass, A. K. (2013). Application of lattice Boltzmann method for incompressible viscous flows. *Applied Mathematical Modelling*, **37**(6), 4075–4092. doi:10.1016/j.apm.2012.09.028

[73] Bhatnagar, P. L., Gross, E. P., & Krook, M. (1954). A Model for Collision Processes in Gases. I. Small Amplitude Processes in Charged and Neutral One-Component Systems. *Physical Review*, **94**(3), 511–525. doi:10.1103/physrev.94.511

[74] Jinuntuya, F., Chen, R., Ostadi, H., Jiang, K., Gao, Y., & Zhang, X. (2014). The Impacts of Image Resolution on Permeability Simulation of Gas Diffusion Layer Using Lattice Boltzmann Method. *ECS Transactions*, **48**(1), 93–101. doi:10.1149/04801.0093ecst

[75] García-Salaberri, P. A., Hwang, G., Vera, M., Weber, A. Z., & Gostick, J. T. (2015). Effective diffusivity in partially-saturated carbon-fiber gas diffusion layers: Effect of through-plane saturation distribution. *International Journal of Heat and Mass Transfer*, **86**, 319–333. doi:10.1016/j.ijheatmasstransfer.2015.02.073

[76] Froning, D., Yu, J., Gaiselmann, G., Reimer, U., Manke, I., Schmidt, V., & Lehnert, W. (2016). Impact of compression on gas transport in non-woven gas diffusion layers of high temperature polymer electrolyte fuel cells. *Journal of Power Sources*, **318**, 26–34. doi:10.1016/j.jpowsour.2016.03.102

[77] Mohamad, A. (2011). Lattice Boltzmann method: fundamentals and engineering applications with computer codes. London: Springer. doi:10.1007/978-0-85729-455-5

[78] Sukop, M. C., & Thorne, D. T. (2007). Lattice Boltzmann modeling: an introduction for geoscientists and engineers. Berlin: Springer. doi:10.1007/978-3-540-27982-2

[79] Chen, S., Dawson, S. P., Doolen, G. D., Janecky, D. R., & Lawniczak, A. (1995). Lattice methods and their applications to reacting systems. *Computers & Chemical Engineering*, **19**(6-7), 617–646. doi:10.1016/0098-1354(94)00072-7

[80] Qian, Y. H., D'Humières, D., & Lallemand, P. (1992). Lattice BGK Models for Navier-Stokes Equation. *Europhysics Letters (EPL)*, **17**(6), 479–484. doi:10.1209/0295-5075/17/6/001

[81] Zou, Q., & He, X. (1997). On pressure and velocity boundary conditions for the lattice Boltzmann BGK model. *Physics of Fluids*, **9**(6), 1591–1598. doi:10.1063/1.869307

[82] Ponce Dawson, S., Chen, S., & Doolen, G. D. (1993). Lattice Boltzmann computations for reaction-diffusion equations. *The Journal of Chemical Physics*, **98**(2), 1514–1523. doi:10.1063/1.464316

[83] Yoshino, M., & Inamuro, T. (2003). Lattice Boltzmann simulations for flow and heat/mass transfer problems in a three-dimensional porous structure. *International Journal for Numerical Methods in Fluids*, **43**(2), 183–198. doi:10.1002/fld.607

[84] Zhang, L.-Z. (2014). A lattice Boltzmann simulation of mass transport through composite membranes. *AIChE Journal*, **60**(11), 3925–3938. doi:10.1002/aic.14564

[85] Guo, Z., Shi, B., & Zheng, C. (2002). A coupled lattice BGK model for the Boussinesq equations. *International Journal for Numerical Methods in Fluids*, **39**(4), 325–342. doi:10.1002/fld.337

[86] Wolf-Gladrow, D. (2004). Lattice-gas cellular automata and lattice Boltzmann models: an introduction. Berlin: Springer. doi:10.1007/b72010

[87] Shojaeefard, M. H., Molaeimanesh, G. R., Nazemian, M., & Moqaddari, M. R. (2016). A review on microstructure reconstruction of PEM fuel cells porous electrodes for pore scale simulation. *International Journal of Hydrogen Energy*, **41**(44), 20276–20293. doi:10.1016/j.ijhydene.2016.08.179

[88] El Hannach, M., Singh, R., Djilali, N., & Kjeang, E. (2015). Micro-porous layer stochastic reconstruction and transport parameter determination. *Journal of Power Sources*, **282**, 58–64. doi:10.1016/j.jpowsour.2015.02.034

[89] Espinoza, M., Sundén, B., & Andersson, M. (2014). Highlights of Fuel Cell Modeling From a Lattice Boltzmann Method Point of View. Volume 6A: Energy. doi:10.1115/imece2014-37010

[90] Salomov, U. R., Chiavazzo, E., & Asinari, P. (2014). Pore-scale modeling of fluid flow through gas diffusion and catalyst layers for high temperature proton exchange membrane (HT-PEM) fuel cells. *Computers & Mathematics with Applications*, **67**(2), 393–411. doi:10.1016/j.camwa.2013.08.006

[91] Chen, L., Feng, Y.-L., Song, C.-X., Chen, L., He, Y.-L., & Tao, W.-Q. (2013). Multi-scale modeling of proton exchange membrane fuel cell by coupling finite volume method and lattice Boltzmann method. *International Journal of Heat and Mass Transfer*, **63**, 268–283. doi:10.1016/j.ijheatmasstransfer.2013.03.048

[92] Gao, Y., Zhang, X., Rama, P., Chen, R., Ostadi, H., & Jiang, K. (2013). Lattice Boltzmann simulation of water and gas flow in porous gas diffusion layers in fuel cells reconstructed from micro-tomography. *Computers & Mathematics with Applications*, **65**(6), 891–900. doi:10.1016/j.camwa.2012.08.006

[93] Zhou, Y., Lin, G., Shih, A. J., & Hu, S. J. (2009). Multiphysics Modeling of Assembly Pressure Effects on Proton Exchange Membrane Fuel Cell Performance. *Journal of Fuel Cell Science and Technology*, **6**(4), 041005. doi:10.1115/1.3081426

[94] Ismail, M. S., Hughes, K. J., Ingham, D. B., Ma, L., & Pourkashanian, M. (2012). Effect of PTFE loading of gas diffusion layers on the performance of proton exchange membrane fuel cells running at high-efficiency operating conditions. *International Journal of Energy Research*, **37**(13), 1592–1599. doi:10.1002/er.2968

[95] Espinoza, M., Andersson, M., Yuan, J., & Sundén, B. (2015). Compress effects on porosity, gas-phase tortuosity, and gas permeability in a simulated PEM gas

diffusion layer. *International Journal of Energy Research*, **39**(11), 1528–1536. doi:10.1002/er.3348

[96] Cooper, S. J., Eastwood, D. S., Gelb, J., Damblanc, G., Brett, D. J. L., Bradley, R. S., … Shearing, P. R. (2014). Image based modelling of microstructural heterogeneity in LiFePO4 electrodes for Li-ion batteries. *Journal of Power Sources*, **247**, 1033–1039. doi:10.1016/j.jpowsour.2013.04.156

[97] Vallano, P. T., & Remcho, V. T. (2001). Assessment of Electroosmotic Perfusion in Capillary Chromatographic Columns Using Electrical Conductivity. *The Journal of Physical Chemistry B*, **105**(16), 3223–3228. doi:10.1021/jp003525m

[98] Espinoza, M., Andersson, M., & Sundén, B. (2016). Predicting transport parameters in PEFC gas diffusion layers considering micro-architectural variations using the Lattice Boltzmann method. *International Journal of Energy Research*. doi:10.1002/er.3661

[99] Thorat, I. V., Stephenson, D. E., Zacharias, N. A., Zaghib, K., Harb, J. N., & Wheeler, D. R. (2009). Quantifying tortuosity in porous Li-ion battery materials. *Journal of Power Sources*, **188**(2), 592–600. doi:10.1016/j.jpowsour.2008.12.032

[100] Espinoza, M., Sunden, B., & Andersson, M. (2016). Impact on Diffusion Parameters Computation in Gas Diffusion Layers, Considering the Land/Channel Region, Using the Lattice Boltzmann Method. *ECS Transactions*, **75**(14), 521–530. doi:10.1149/07514.0521ecst

[101] Espinoza-Andaluz, M., Andersson, M., & Sundén, B. (2017). Comparing through-plane diffusibility correlations in PEFC gas diffusion layers using the lattice Boltzmann method. *International Journal of Hydrogen Energy*. Article in Press. DOI: 10.1016/j.ijhydene.2017.02.096

Graphical model evolution

LBM?

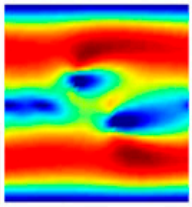

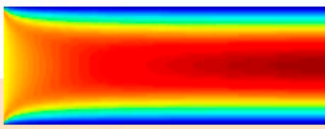

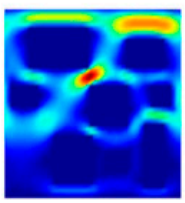

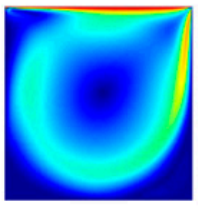

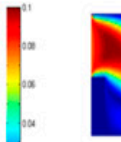

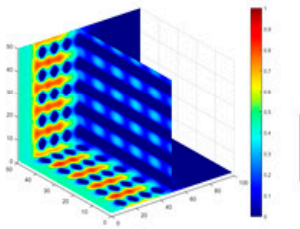

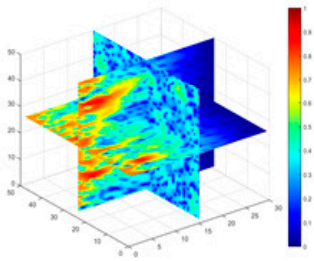

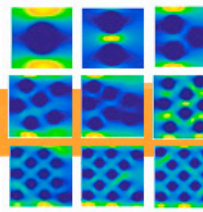

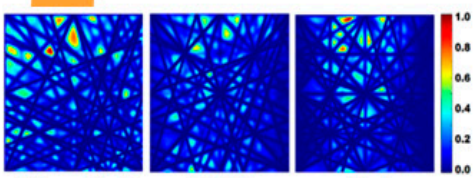

L/C no considered L/C = 0.5 L/C = 1

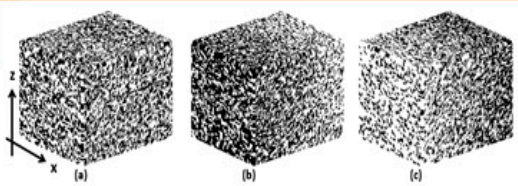

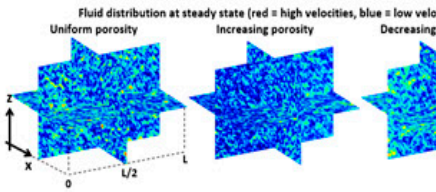

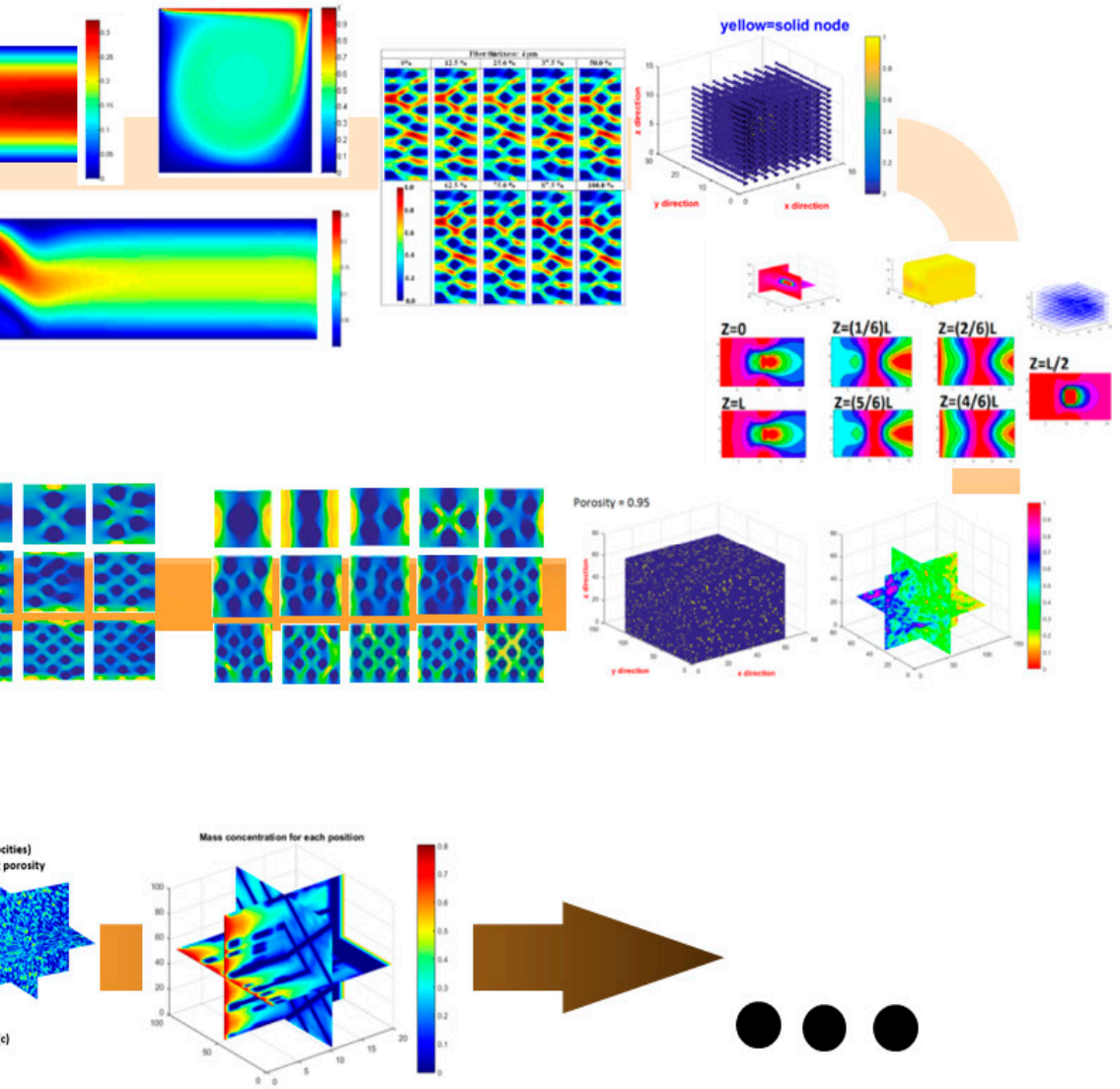
yellow=solid node
z direction
y direction
x direction
Z=0
Z=(1/6)L
Z=(2/6)L
Z=L/2
Z=L
Z=(5/6)L
Z=(4/6)L
Porosity = 0.95

Mass concentration for each position

Appended publications

Paper I

Proceedings of the ASME 2014 International Mechanical Engineering Congress & Exposition
IMECE2014
November 14-20, 2014, Montreal, Quebec, Canada

IMECE2014-37010

Highlights of Fuel Cell Modeling From a Lattice Boltzmann Method Point of View

Mayken Espinoza
Department of Energy Sciences
Lund University
Lund, Sweden

Bengt Sundén
Department of Energy Sciences
Lund University
Lund, Sweden

Martin Andersson
Department of Energy Sciences
Lund University
Lund, Sweden

ABSTRACT

Relative simplicity of use, no pollutions and high-efficiency are some of the advantages that will make fuel cells one of the best devices for getting electrical energy in the near future. Micro- and mesoscale modeling of fuel cells gives an important perspective about their efficiency and behavior during the energy conversion process. Due to the high cost of carrying out laboratory experiments related to different materials at the micro- and mesoscales, modeling and simulation of the different elements of the fuel cells are a useful approach and a point of departure for the experimental validation.

This paper describes fuel cell modeling starting with the fundamentals, including physical and chemical characteristics of fuel cells, moving to the current state of the study of modeling based on the Lattice Boltzmann Method (LBM). The principal characteristics and elements of the fuel cells are presented in general as well as the main differences between the Proton Exchange Membrane Fuel Cells (PEMFC) and Solid Oxide Fuel Cells (SOFC). Fuel cells have several parts that are modeled on the micro- and mesoscale level. These parts, conditions and governing equations for different transport phenomena are displayed in this manuscript. A detailed description of the main issues, advantages and recent advances related to Lattice Boltzmann Method as a method for modeling several physical processes that take place within fuel cells are presented.

INTRODUCTION

Nowadays, there are different models for studying the behavior and efficiency of renewable energy systems from different perspectives, i.e., one-dimensional, two-dimensional, three-dimensional, steady state, transient, type of system, etc.

Each renewable energy system has parts that can be modeled at different scale levels. Fuel cell (FC) is a promising element and an important device for a world free of fuel oil consumption. FC modeling and the analysis of different scales give a blueprint for improving the FC materials.

The selection of the scale for modeling depends on the characteristics that are analyzed, the length scale of the computational domain that is used and the time scale. The aim of FC modeling is to study and analyze the different chemical and physical processes that occur within the FC elements during the energy conversion process. The main overall objective is to improve the efficiency of FCs, decrease the cost of material compounds and have a tool for describing the different processes in order to predict the future behavior under different conditions.

A suitable model is a complete three-dimensional, transient one that describes all physical and chemical phenomena that occur along all the length scales, from the atomistic level to the system level. Currently, such a model is unattainable not only due to the computational power required, but also because it is necessary to establish the correct

boundary, initial conditions and couplings during the modeling process according to the real applications.

The purpose of this manuscript is to give detailed information about FC modeling on micro- and mesoscale based on the Lattice Boltzmann Method (LBM) and show some results from recent investigations related to this topic.

The first part gives the background information related to FCs in a general manner, such as the basic structure and the general electrochemical reaction. It describes the basic characteristics of PEMFCs and SOFCs, their advantages and disadvantages. FCs have several parts that can be modeled from the electrolyte until the current collectors. Each one of these parts assists in the FC performance during energy conversion process.

In recent years, though LBM has been applied to models related to FC modeling, the range of applications of LBM is not limited to the field of energy sciences. The LBM advantages will be presented along with the basics and principles of this method. Characteristics and issues related to this model applied to micro- and the mesoscale in FC modeling for different physical phenomena are displayed. Finally, some FC modeling results and conclusions related to the LBM applied to the downscale are also presented.

BACKGROUND OF FUEL CELLS

The growth in world population produces a rise in energy demands. A major part of the energy used in the world comes from fossil fuels [1]. The use of these fuels results in the emission of polluting gases that adversely affect nature, biodiversity and human life. Renewable energy appears to be one of the best choices to meet the future energy demand and reduce the polluting gases.

There are different systems based on renewable energy sources, e.g., wind energy, solar energy, hydrogen technologies, among others. The hydrogen technology system has an important device in its structure, namely, the fuel cell (FC). Basically, the principal function of the FC is to convert the chemical energy present in the fuel, i.e., hydrogen, methane, etc. into electrical and thermal energy. The conversion process occurs cleanly and silently and the residues generally are exhaust gases and water.

A single FC, in general, consists of basic elements common to all kinds of FCs, i.e., anode, cathode and electrolyte (Fig. 1). The electrolyte material, support material and the catalyst layer compound depend on the type of FC that is being used in the system. These basic elements have different properties depending on the power output and operating conditions. Some of these properties are studied at different scales in order to improve the behavior and efficiency of the FCs.

The electrochemical reactions that take place in FCs produce an electric potential difference between the anode and the cathode. During the electrochemical reaction, free electrons move towards an external circuit producing electrical power.

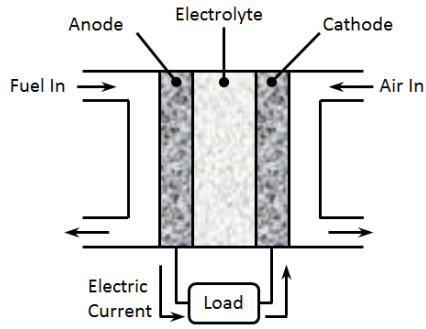

Figure 1. Simplified scheme of a single Fuel Cell

The overall cell reaction that occurs in a FC is given by [2]:

$$H_2 + \frac{1}{2} O_2 = H_2O \tag{1}$$

The electrical potential difference depends on the Gibbs free energy (ΔG) change associated with the electrochemical reaction. The relationship between the Gibbs free energy and the ideal voltage produced is given as follows [3]:

$$E_{ideal} = \frac{\Delta G}{z\,F} \tag{2}$$

where z is the number of electrons participating in the reaction and F is Faraday's constant (96485 C/mol).

Theoretically, the ideal open circuit voltage (OCV) is higher than 1.0 V, but the most common output voltage of a single FC is between 0.6 V ~ 0.85 V [4]. These voltages are low for real or industrial applications and it is always desirable and necessary to make interconnections between several single cells. The interconnection of several single cells is called an FC stack, which interconnected with other electrical and mechanical elements of balance in a combined plant can reach higher power rates. For example, one combined plant is able to produce up to 14.9 MW of electrical power [5].

Another important fact that makes the FC a promising device in the development of renewable energy fields is its electrical efficiency. The FC electrical efficiency is related to Gibbs free energy (ΔG) and enthalpy (ΔH) [3].

$$Fuel\ cell\ efficiency = \frac{\Delta G}{\Delta H} \tag{3}$$

The efficiency depends upon the kind of FC used and the operating conditions; the FC stack efficiency is around 40% ~ 75% [4].

PEMFC AND SOFC IN BRIEF

There are different types of FCs; the classification is related to the constitutive elements or characteristics present in the FC, i.e. type of electrolyte used, purity of fuel necessary for accurate performance, output power, work range temperature, portability, durability, size, etc.

The FC classification related to the electrolyte type, and the most researched is as follows:

- Polymer Electrolyte Membrane Fuel Cell (PEMFC)
- Direct Methanol Fuel Cell (DMFC)
- Phosphoric Acid Fuel Cell (PAFC)
- Solid Oxide Fuel Cell (SOFC)
- Molten Carbonate Fuel Cell (MCFC)
- Alkaline Fuel Cell (AFC)

This manuscript is focused on PEMFC and SOFC; their principles, structures and applications are presented in the next part.

PEMFC basics

It is an electrochemical device that converts the chemical energy present in the fuel into electrical energy. In order to obtain accurate performance, the fuel used in PEMFC must be pure hydrogen. The electrolyte is a thin polymer membrane that allows the passage of hydrogen ions only during the conversion process.

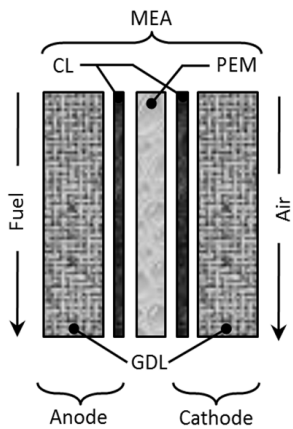

Figure 2. Single PEMFC basic structure

The basic structure of a PEMFC (Fig. 2) requires a membrane electron assembly (MEA) that consists of the proton exchange membrane (PEM), the catalyst layer (CL) and the gas diffusion layers (GDL). The electrochemical reactions occur at the anode and the cathode supported by the GDL and the CL. The free electrons in each electrode are able to produce an electrical current in an external circuit or load. The semi-electrochemical reactions involved are [6]:

$$Anode\ Reaction: H_2 = 2H^+ + 2e^- \quad (4)$$

$$Cathode\ Reaction: \frac{1}{2}O_2 + 2H^+ + 2e^- = H_2O \quad (5)$$

SOFC basics

This electrochemical device converts the chemical energy present in the fuel, i.e., methane, hydrogen, carbon monoxide (CO), hydrocarbons, or a combination of these [7], into electrical and thermal energy. The electrolyte is a ceramic material that allows the transport of oxygen ions during the energy conversion process. The basic structure of an SOFC (Fig. 3) requires anode/cathode support and active layers in order to produce the necessary reforming equations.

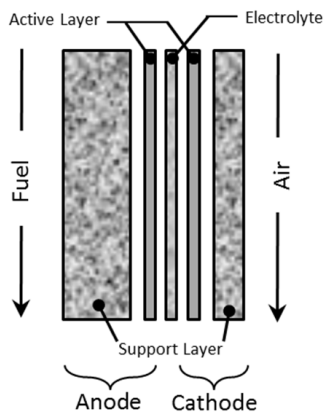

Figure 3. Single anode supported SOFC basic structure

The electrochemical reactions that occur within the SOFC depend on the element compounds present in the support and

active layers. The semi-electrochemical reactions involved during the energy conversion process are given by [6]:

$$Anode\ Reaction: H_2 + O^{2-} = H_2O + 2e^- \quad (6)$$

$$Cathode\ Reaction: \frac{1}{2}O_2 + 2e^- = O^{2-} \quad (7)$$

Comparison between PEMFC and SOFC

The operating temperature range, general applications and the mobile ion related to both FCs can be seen in Table I [8].

Table I. PEMFC and SOFC comparison

	Fuel cell types	
	PEMFC	**SOFC**
Mobile ion	H^+	O^{2-}
Operating temperature	30 - 100° C	500 - 1000° C
Applications	Vehicles and mobile applications, and for lower power CHP systems	Suitable for all sizes of CHP systems, 2 kW to multi-MW

The FCs present some disadvantages. One disadvantage of PEMFC is that it requires pure hydrogen and the use of expensive catalysts, but has a fast start-up due to the low temperature range. On the other hand, although the start-up is longer in SOFC due to the high temperature range, it is possible to achieve higher output power and electrical efficiency.

FUEL CELL MODELING

To date, no FC computational model has been able to simulate the complete physical and chemical phenomena that occur in a single FC or FC stack over the full scale range. There are different limitations in the modeling process that increase the difficulty of getting a description of the whole system, such as, see [9], inclusion of the complete physical and chemical phenomena, knowledge of transport parameters, computational power and proper validation.

It is necessary to define the scale for the modeling process. This scale is related to the length of the computational domain. The length scale, the time scale and the computational cost are related. Figure 4 shows that the computational cost increases while the time scale decreases. Similar relation occurs between the computational cost and the length scale, whereas if the length scale increases the time scale also increases.

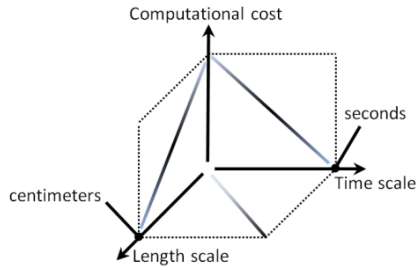

Figure 4. Simple relation among the variables in FC modeling (not to scale, and not necessarily straight lines)

Micro- and mesoscale

The scale level of FC modeling varies from the molecular to the system level. Different physical and chemical phenomena are studied at each scale level and this scale level is defined based on the length scale. There are different definitions about the range that corresponds to the region of micro- and mesoscale length. Considering reference [10], the range corresponds to values higher than ~ 1 nm and lower than ~ 10 µm. This range is similar to the one in reference [11], but the higher limit is considered up to ~ 100 µm and the division between the micro and mesoscale occurs around 10 µm. According to reference [12], there is no defined region for microscale; instead, only nanoscale, mesoscale and macroscale are defined with the mesoscale region overlapping the other two regions. In conclusion, without being exhaustive, the micro- and mesoscale region can be considered between the nanometer and hundreths of micrometer.

Fundamental FC parts previously described, i.e., the electrolyte, catalyst layer, gas diffusion layer and electrode support are the regions where the different physical and chemical processes occur. The behavior of material compounds in these layers during the energy conversion process influence the FC performance. Micro- and mesoscale regions cover the range of thickness of each layer mentioned above as is shown in Table II.

Table II. Layer thickness of PEMFC [13, 37] and anode supported SOFC [10, 14]

PEMFC	
Proton exchange membrane	50 ~ 180 µm
Catalyst layer	5 ~ 30 µm
Gas diffusion layer	17 ~ 400 µm
SOFC	
Electrolyte	10 ~ 20 µm
Active layer	7 ~ 12 µm
Support layer	200 ~ 500 µm

Important phenomena that occur in these layers are known as homogeneous transport, i.e., mass, charge and heat transfer. The most important parameters needed for modeling charge, mass and heat transport phenomena in a FC at the micro- and mesoscale levels are listed in Table III.

Table III. List of transport parameters needed for single FC performance models. Adapted from [9].

Charge transport
Ionic conductivity of the electrolyte Electrolyte electrical conductivity (transference number, SOFCs) Kinetic relationship for reaction Ionic conductivity in the electrode Electrical conductivity in the electrode
Mass transport
Gas-phase diffusivities - Adjustment for porous media Liquid-phase transport (Low-temperature fuel cells): - Saturation versus capillary pressure relationship for porous media - Liquid- and gas-phase permeability as a function of saturation Mass transport relationships in electrolyte besides charge transport (e.g., diffusion or permeation of water, reactant crossover, impurities, etc.)
Heat transport
Specific heat and thermal diffusivity of all materials (transient simulation only) Thermal conductivity of all materials Latent heat (multi-phase simulations only)

In PEM- and SOFCs, some other processes can occur at micro- and mesoscale levels, e.g., poisoning, coking, passivation, microfracture, defects, residual strains, sintering, redox cycling and aging [15]. Each of these phenomena occurs approximately in the same length region, but at different time scales and furthermore, the computational cost is different.

LATTICE BOLTZMANN METHOD

Lattice Boltzmann Method (LBM) is not only applied in FC modeling, but as well in several research fields. The number of publications related to LBM has been increasing during the last decade. The next figure shows the number of publications of investigations in which Lattice Boltzmann Method has been applied. The number of publications has been grouped in periods of two years during the last ten years, and tells about an increment of 175% relative to the first period.

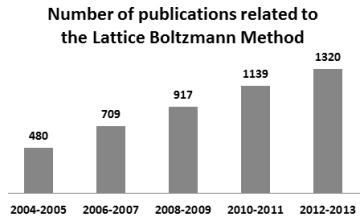

Figure 5. Number of publications related to LBM (i.e., not only for FCs). Year period 2004-2013. Searched words: Lattice Boltzmann Method. Source: Scopus.

LBM principles

LBM is based originally from lattice gas automata (LGA). This method examines its own states and the states of some of its neighbors [16]. The principal idea of LBM is to study the behavior of a collection of particles instead of a single sub-atomic particle like in molecular dynamics (MD). Knowing the average characteristics of this collection of particles it is possible to make approximations with considerable accuracy of the physical phenomena, not only at the microscale, but also at macroscale level [17].

The analysis of the movement of millions of atomic particles is simplified using the particle distribution function (PDF). PDF gives a statistical description of the collection of particles and in consequence, the principal characteristics of the fluid behavior.

The domain that will be solved has to be divided into lattice points. Each lattice point has velocity connections with its neighborhood. The common way to represent the lattice arrangement is *DmQn* where *m* represents the dimension of the problem to be solved (1-D, 2-D or 3-D) and *n* determines the number of connections with the other lattice nodes.

Each velocity connection has a corresponding weighting factor that depends on the total number of connections between the nodes. The total sum of the weighting factors must always be unity. The schemes of LBM often used are D2Q9 and D3Q19, and are represented in Fig. 6.

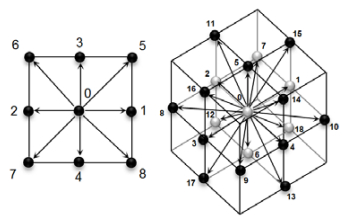

Figure 6. Most common lattice arrangements applied in LBM. D2Q9 (left) and D3Q19 (right).

The backbone of LBM is the Boltzmann transport equation, which is based on the distribution function. The distribution function corresponds to the number of particles in a determined region within a range of velocities at one specific time. The distribution function remains the same if there is no collision between the molecules (streaming); otherwise, it will have a net change in the distribution function (collision). A simplified form of the Boltzmann equation can be expressed as:

$$\frac{\partial f(r,t)}{\partial t} + c.\nabla f(r,t) = \Omega \tag{8}$$

where f is the particle distribution function that depends on position, velocity c and time. Ω is the collision operator that is a function of f.

To solve the Boltzmann equation, one approximation is used for replacing Ω; this approximation is called the Bhatnagar, Gross, and Krook (BGK) approximation. Then, Eq. (8) can be expressed as:

$$\frac{\partial f_i(r,t)}{\partial t} + c_i \nabla f_i(r,t) = \frac{1}{\tau}\left[f_i^{eq}(r,t) - f_i(r,t)\right] \tag{9}$$

where f_i(r,t) is the particle distribution function at position r and time t; f_i^{eq}(r,t) is the equilibrium particle distribution function and τ is the relaxation time, c is the velocity in the corresponding i- direction.

To solve Eq. (9), it is necessary to define the equilibrium particle distribution function (f_i^{eq}) in a different way for each problem to be solved. LBM can solve the diffusion, advection-diffusion, momentum, and energy equations. The equilibrium particle distribution function comes from a Taylor polynomial approximation and Maxwell's distribution function, and can be written as [17]:

$$f_i^{eq} = \phi\, w_i \left[A + B\, c_i.u + C\, (c_i.u)^2 + D\, u^2\right] \tag{10}$$

where u is the macroscopic velocity vector, w_i is the weighting factor, and A, B, C and D have to be defined based on the conservation equation that is applied; for more detailed information about the definitions of these values (A, B, C and D) the reader is referred to Mohamed [17]. Φ is a scalar parameter that often refers to density, temperature or species concentration.

Once Eq. (9) is solved, it is possible to recover macroscopic parameters such as density, velocity and momentum by the equations below.

$$\rho = \sum_{i=0}^{n-1} f_i \tag{11}$$

$$u = \frac{1}{\rho}\sum_{i=0}^{n-1} f_i\, c_i \tag{12}$$

LBM advantages

LBM presents many advantages in the modeling of different processes in several research fields. LBM can be used to solve problems related to single and multiphase flows, unsteady flows, and heat transport [16]. Comparing Navier-Stokes equation and Boltzmann equation, the first one is a second - order differential equation where it is necessary to treat the non-linear convective term; the Boltzmann equation, however, is a first - order differential equation and avoids the convective term [17].

This method is useful in predicting and visualizing physical processes in microstructures [11]. LBM is a suitable candidate for efficient parallel computations due to the algorithm used in solving the problems [18]. LBM is a useful tool for mesoscale modeling of single-phase and multiphase flow [19], e.g., two-phase flow in mixing layers, electro-osmotic flow, and viscous fingering phenomena. LBM is computationally more efficient than the finite difference method for the same grid size [20].

The results of investigations show that LBM is a viable alternative solution method to traditional numerical methods for solving flow problems in heterogeneous porous media [21]. The study of porous media is of vital importance in FCs. The next figure shows the porous structure of an SOFC electrode.

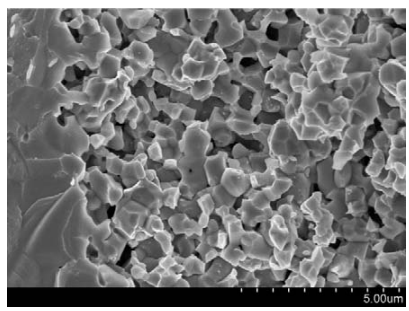

Figure 7. SEM micrograph shows the porous structure of a SOFC cathode. Credits: Ningbo Institute of Materials Technology & Engineering (NIMTE).

LBM APPLIED TO FC MODELING

LBM is a useful tool to model different parts and phenomena in PEMFCs and SOFCs. In PEMFCs, the CL and GDL are frequently modeled, and in SOFCs, the anode is the part more researched.

One of the most recent investigations of PEMFC using LBM is related to GDL. Akbari and Molaeimanesh [22] investigated the effects of GDL microstructure on species and current density distributions.

Using D3Q19, Akbari and Molaeimanesh studied the behavior of different parameters when the orientation of the carbon fibers (Fig. 8) in the GDL anode was changed.

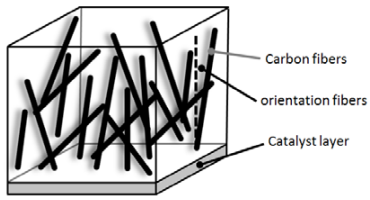

Figure 8. Carbon fibers representation in GDL used by Akbari and Molaeimanesh, [22].

The investigation considered the variation of a factor called anisotropic parameter β. Depending of the β values the fibers have different orientations. If β is around 0.01 the fibers are more normal oriented to the material plane. Three GDL were reconstructed with the same lattice size, porosity and fiber diameter but with a different anisotropic parameter. The fibers were considered cylindrical and infinitely long. Figure 9 shows the mole fraction distribution of the two reconstructed GDLs.

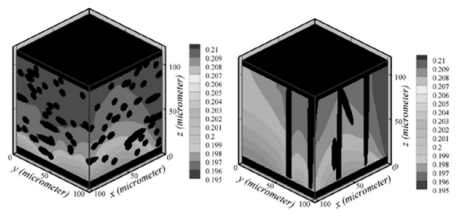

Figure 9. Oxygen mole fraction distribution of two reconstructed GDLs by Akbari and Molaimanesh [22].

The results of the Akbari and Molaimanesh investigation showed that when the carbon fibers are mostly perpendicular to the catalyst layer, i.e., β = 0.01 (Fig. 9 right side) the oxygen density boundary layer is thicker.

Several studies have been made using LBM such as flow simulations in GDL and pore-scale transport phenomena in CL. The following table shows other applications of LBM in modeling of PEMFC and the corresponding schemes used.

Table IV. Characteristics or part of PEMFC research using LBM

Characteristic/part researched	Scheme
Pore-scale simulations of the fluid flow for the direct numerical calculation of the permeability [23].	D3Q19
Pore-scale transport phenomena in the GDL and CL as well as proton conduction in the CL [24].	D2Q9
To perform pore-level flow simulations in the reconstructed GDL samples [25].	D3Q-
To obtain effective material properties - permeability and tortuosity - of paper type GDLs [26].	D3Q19
To examine the interfacial phenomena in liquid water transport in porous materials [27].	D2Q-
To investigate water flow in the GDLs using a combination of the LBM and X-ray computed tomography at the micron scale [28].	D3Q19
To obtain the velocity field in the porous media through the 3D void space of segmented GDL [29].	D3Q27

LBM is applied to model of several parameters in microstructures and porous media in the SOFC anodes. Paradis [11] developed a microscale model to resemble an SOFC anode. Momentum transport was implemented in a D3Q19 scheme and D3Q7 was used for heat, mass and charge transport. Paradis [11] used LBM to model the transport processes in a porous medium in 2D and 3D. The 3D geometry is constituted of spheres of different sizes to represent the two materials, i.e., Ni and YSZ. The next figure shows some characteristics of the computational domain used in the model.

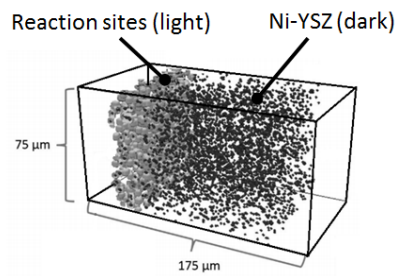

Figure 10. Schematic domain of the SOFC anode used by Paradis [11]

The velocity distribution in the porous domain and the concentration distribution of hydrogen were modeled in the schematic domain previously described. Figure 11 shows the concentration distribution of H_2.

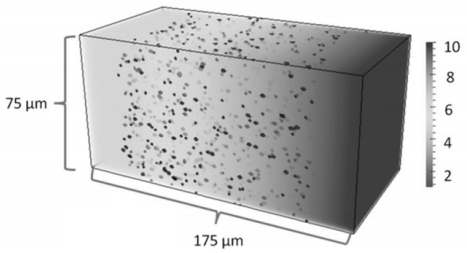

Figure 11. Concentration distribution of H_2 [mol/m^3] in the modeled porous domain by Paradis [11].

LBM is applied to study heat and mass transfer in microstructures, to solve gaseous, ionic and electronic transport equations and to describe the diffusion process in complex pore structures. Some characteristics and properties investigated in different SOFC models from other authors are presented in Table V.

Table V. Characteristics or part of SOFC research using LBM

Characteristic/part researched	Scheme
To evaluate the numerical simulation method for cell anode polarization using Ni–YSZ microstructures reconstructed [30].	D3Q6
To predict the overpotential of three-dimensional microstructure of mixed ionic and electronic conducting cathode [31].	D3Q6
Examination of the transport processes in the heterogeneous electrode structure [32].	D3Q19
To solve gaseous, ionic, and electronic transport equations with electrochemical reactions at the three phase boundary (TPB) [33].	D3Q19
To describe the diffusion process in complex pore structures [34].	D2Q-
Evaluation of tortuosity factors in a three dimensional reconstructed anode [35].	D3Q6
To model multicomponent diffusion trough the pore space [36].	D3Q19

CONCLUSIONS

Knowing and understanding the behavior of different elements and transport phenomena that occur in FCs is possible to reach better efficiencies during the energy conversion process. FC modeling appears to be a helpful tool for getting several descriptions about processes that happen within the FC. To obtain a complete description along the complete range of scales, the study of micro- and mesoscale represents a fundamental issue to be researched.

LBM is a connection between the continuum and discrete approaches. This method presents several advantages for modeling processes in FCs such as solving problems in complex geometries, multiphase problems, and porous media. An overview of different applications of LBM in FC modeling applied to PEMFC and SOFC was given.

Modeling and simulation of several phenomena that occur in FCs provide a detailed description of the physical and chemical phenomena involved. Furthermore, it helps to improve FC efficiency and reduces material cost.

Nomenclature

c	lattice velocity connection
ΔG	Gibbs free energy (J mol^{-1})
ΔH	enthalpy change of reaction (J mol^{-1})
E	voltage (J C^{-1})
F	Faraday's constant (C mol^{-1})
r	position
t	time
u	macroscopic velocity
w	weighting factor in f^{eq}
z	number of electrons in the reaction (-)

Abbreviations

AFC	alkaline fuel cell
BGK	Bhatnagar, Gross and Krook
CHP	cogeneration or combined heat and power
CL	catalyst layer
DMFC	direct methanol fuel cell
FC	fuel cell
GDL	gas diffusion layer
LBM	lattice Boltzmann method
LGA	lattice gas automata
MCFC	molten carbonate fuel cell
MD	molecular dynamics
MEA	membrane electron assembly
OCV	open circuit voltage
PAFC	phosphoric acid fuel cell
PDF	particle distribution function
PEM	proton exchange membrane
PEMFC	polymer electrolyte membrane fuel cell
SOFC	solid oxide fuel cell
TPB	three phase boundary

Chemical

CO	carbon monoxide
e^-	electron
H^+	hydrogen ion
H_2	hydrogen
H_2O	water
Ni	nickel
O_2	oxygen
O^{2-}	oxygen ion
YSZ	yttria-stabilized zirconia

Greek symbols

β	anisotropic parameter
ρ	density
τ	relaxation time
ϕ	scalar parameter in f^{eq}
Ω	collision operator

ACKNOWLEDGEMENTS

The present study is financially supported by the National Secretary of Higher Education Science, Technology and Innovation – Ecuador (Senescyt) which is gratefully acknowledged. Additional financial support was received from ERC project MMFCs 226238.

REFERENCES

[1] BP, 2013, "BP Statistical Review of World Energy June 2013", 1 St James's Square, London SW1Y 4PD UK, Eds., pp. 42. http://www.bp.com/content/dam/bp/pdf/statistical-review/statistical_review_of_world_energy_2013.pdf

[2] Brandon, N., Hart, D., 1999, "An Introduction to Fuel Cell Technology and Economics", Published by the Centre for Energy Policy and Technology, Imperial College, London SW7 2PE

[3] Birnbaum, K. U., Linssen, J., Leifeld, P., 2008, "Reduction of Residential Carbon Dioxide Emissions through the Use of small Cogeneration Fuel Cell Systems". IEA Greenhouse R&D Programme, Orchard Business Centre, Stoke Orchard, Cheltenham Glos. GL52 7RZ. UK

[4] Saxe, M. , 2008, "Bringing Fuel Cells to Reality and Reality to Fuel Cells", Doctoral Thesis, Department of Chemical Sciences and Engineering, Royal Institute of Technology, ISBN 9789174151984, Sweden.

[5] Carter, D., Wing, J., 2013, "The Fuel Cell Industrial Review", Fuel Cell Today, Gate 2, HQ Building, Orchard Road, Royston, Herts SG8 5HE, UK

[6] Khuvendra, Y., Vivek, K., Rupesh, K., Aaditya S., Prayag T., 2013, "Design and Development of Fuel Cell Technology", IJRMET **3** (2), pp. 241.

[7] Zhu, H., Kee R., Janardhanan, V., Deutschmann, O., and Goodwin, D., 2005, "Modeling Elementary Heterogeneous Chemistry and Electrochemistry in Solid-Oxide Fuel Cells", Journal of The Electrochemical Society, **152** (12) pp. A2427.

[8] Larminie, J., Dicks, A., 2003, *Fuel Cell Systems Explained*, John Wiley & Sons Ltd, The Atrium, Southern Gate, Chichester, West Sussex PO19 8SQ, England, pp. 15, Chap. 1.

[9] Mench, M., 2010, "Advanced Modeling in Fuel Cell Systems: a Review of Modeling Approaches", *Hydrogen and Fuel Cells – Fundamentals, Technologies and Applications*, ed Detlef Stolten, WILEY-VCH Verlag GmbH & Co. KGaA, Weinheim, pp. 92.

[10] Andersson, M., 2011, "Solid Oxide Fuel Cell Modelling at the Cell Scale - Focusing on Species, Heat, Charge and Momentum Transport as well as the Reaction Kinetics and Effects", Ph.D. thesis. Department of Energy Sciences, Lund University. Lund, Sweden. http://lup.lub.lu.se/luur/download?func=downloadFile&recordOId=2202607&fileOId=2203668

[11] Paradis, H., 2013, "Micro- and Macroscale Modeling of Transport Processes in Solid Oxide Fuel Cells", Ph.D. thesis. Lund University, Department of Energy Sciences, Lund University. Lund, Sweden.

[12] Ryan, E., Khaleel, M., 2012, *Fuel Cell Science and Engineering: Materials, Processes, Systems and Technology*, eds Detlef Stolten and Bernd Emonts, Wiley-VCH Verlag GmbH & Co. KGaA, Bochstr. 12, 69469 Weinheim, Germany. pp. 734.

[13] Spiegel, C., 2008, *PEM Fuel Cell Modeling and Simulation Using Matlab*, Academic Press, Elsevier Inc., pp. 168, Chap. 7, pp. 243, Chap. 9, pp. 199, Chap. 8.

[14] Elcogen, 2013, Fuel Cell Technology, SOFC Single Cells, http://www.elcogen.com/images/Elcogen_brochure_2013_eng.pdf

[15] Grew, K., and Chiu, W., 2011, "A review of modeling and simulation techniques across the length scales for the solid oxide fuel cell", Journal of Power Sources, **199** (2012), pp. 1 - 13.

[16] Sukop, M., Thorne, D., 2006, *Lattice Boltzmann Modeling – And Introduction for Geoscientists and Engineers*, Springer-Verlag Berlin Heidelberg, Germany, pp. 13, chap 2.

[17] Mohamed, A., 2011, *Lattice Boltzmann Method Fundamentals and Engineering Applications with Computer Codes*, Springer-Verlag London, UK, pp. 3, chap 1., pp. 19, chap 2.

[18] Dhiraj, P., Kannan, P., Sanjoy, B., 2014, "Multigrid lattice Boltzmann method for accelerated solution of elliptic equations", Journal of Computational Physics, **265** (2014), pp. 172–194.

[19] Yan, Y., Zu, Y., Dong, B., 2011, "LBM, a useful tool for mesoscale modeling of single-phase and multiphase flow", Applied Thermal Engineering **31** (2011), pp. 649-655.

[20] Seta, T., Takegoshi, E., Okui, K., 2006, "Lattice Boltzmann simulation of natural convection in porous media", Mathematics and Computers in Simulation **72** (2006), pp. 195–200.

[21] Spaid, M., Phelan F., 1997, "Lattice Boltzmann methods for modeling microscale flow in fibrous porous media", Phys. Fluids **9** (9), pp. 2468 – 2474.
[22] Molaeimanesh, G., Akbari, M., 2014, "A three-dimensional pore-scale model of the cathode electrode in polymer-electrolyte membrane fuel cell by lattice Boltzmann method", Journal of Power Sources **258** (2014), pp. 89-97.
[23] Uktam, S., Eliodoro, C., Pietro, A., 2014, "Pore-scale modeling of fluid flow through gas diffusion and catalyst layers for high temperature proton exchange membrane (HT-PEM) fuel cells", Computers and Mathematics with Applications **67** (2014), pp. 393–411.
[24] Li, C., Yong-Liang, F., Chen-Xi, S., Lei, C., Ya-Ling, H., Wen-Quan, T., 2013, "Multi-scale modeling of proton exchange membrane fuel cell by coupling finite volume method and lattice Boltzmann method", International Journal of Heat and Mass Transfer **63** (2013), pp. 268–283.
[25] Nabovati, A., Hinebaugh, J., Bazylak, A., Amon, C., 2014, "Effect of porosity heterogeneity on the permeability and tortuosity of gas diffusion layers in polymer electrolyte membrane fuel cells", Journal of Power Sources **248** (2014), pp. 83-90.
[26] Froninga, D. Brinkmann, J., Reimer, U., Schmidt, V., Lehnert, W., Stolten, D., 2013, "3D analysis, modeling and simulation of transport processes in compressed fibrous microstructures, using the Lattice Boltzmann method", Electrochimica Acta **110** (2013), pp. 325–334.
[27] Han, B., Meng, H., 2013, "Numerical studies of interfacial phenomena in liquid water transport in polymer electrolyte membrane fuel cells using the lattice Boltzmann method", International J. Hydrogen Energy **38** (2013), pp. 5053-5059.
[28] Gaoa, Y., Zhang, X., Rama, P., Chen, R., Ostadi, H., Jiang , K., 2013, "Lattice Boltzmann simulation of water and gas flow in porous gas diffusion layers in fuel cells reconstructed from micro-tomography", Computers and Mathematics with Applications **65** (2013), pp. 891–900.
[29] Rosen, T., Eller, J., Kang, K., Prasianakis, N., Mantzaras, J., Buchi, F., 2012, "Saturation Dependent Effective Transport Properties of PEFC Gas Diffusion Layers", Journal of The Electrochemical Society, **159** (9), pp. F536-F544.
[30] Kanno, D., Shikazono, N., Takagia, N., Matsuzaki, K., Kasagi, N., 2011, "Evaluation of SOFC anode polarization simulation using three-dimensional microstructures reconstructed by FIB tomography", Electrochimica Acta **56** (2011), pp. 4015–4021.
[31] Matsuzaki, K., Shikazono, N., Kasagi, N., 2011, "Three-dimensional numerical analysis of mixed ionic and electronicconducting cathode reconstructed by focused ion beam scanning electron microscope", Journal of Power Sources **196** (2011), pp. 3073–3082.
[32] Grew, K., Peracchio, A., Chiu, W., 2010, "Characterization and analysis methods for the examination of the heterogeneous Solid oxide fuel cell electrode microstructure: Part 2. Quantitative measurement of the microstructure and contributions to transport losses", Journal of Power Sources **195** (2010), pp. 7943–7958.
[33] Shikazono, N., Kanno, D., Matsuzaki, K., Teshima, H., Sumino, S., Kasagi, N., 2010, "Numerical Assessment of SOFC Anode Polarization Based on Three-Dimensional Model Microstructure Reconstructed from FIB-SEM Images", Journal of The Electrochemical Society, **157** (5), pp. B665-B672.
[34] Grew, K., Joshi, A., Peracchio, A., Chiu, W., 2010, "Pore-scale investigation of mass transport and electrochemistry in a solid oxide fuel cell anode", Journal of Power Sources **195** (2010), pp. 2331–2345.
[35] Iwai, H., Shikazono, N., Matsui, T., Teshima, H., Kishimoto, M., Kishida, R., Hayashi, D., Matsuzaki, K., Kanno, D., Saito, M., Muroyama, H., Eguchi, K., Kasagi, N., Yoshida,H., 2010, "Quantification of SOFC anode microstructure based on dual beam FIB-SEM technique", Journal of Power Sources **195** (2010), pp. 955–961.
[36] Joshi, A., Grew, K., Izzo, J., Peracchio, A., Chiu, W., 2010, "Lattice Boltzmann Modeling of Three-Dimensional, Multicomponent Mass Diffusion in a Solid Oxide Fuel Cell Anode", Journal of Fuel Cell Science and Technology, Vol. 7, pp. 011006-1 - 011006-8.
[37] Gu, W., Yu., P., Carter, R., Makharia, R., Gasteiger, H., 2010, "Modeling of Membrane-Electrode-Assembly Degradation in Proton-Exchange-Membrane Fuel Cells – Local H2 Starvation and Start–Stop Induced Carbon-Support Corrosion", *Modeling and Diagnostics of Polymer Electrolyte Fuel Cells, Modern Aspects of Electrochemistry 49*, U. Pasaogullari, C.-Y. Wang (eds.), DOI 10.1007/978-0-387-98068-3_2, Springer Science+Business Media, LLC 2010, pp: 54.

Paper II

International Journal of Energy Research

INTERNATIONAL JOURNAL OF ENERGY RESEARCH
Int. J. Energy Res. 2015; **39**:1528–1536
Published online 18 June 2015 in Wiley Online Library (wileyonlinelibrary.com). DOI: 10.1002/er.3348

Compress effects on porosity, gas-phase tortuosity, and gas permeability in a simulated PEM gas diffusion layer

Mayken Espinoza*,†, Martin Andersson, Jinliang Yuan and Bengt Sundén

Department of Energy Sciences, Lund University, PO Box 118, 22100 Lund, Sweden

SUMMARY

Among the parameters to take into account in the design of a proton exchange membrane fuel cell (PEMFC), the energy conversion efficiency and material cost are very important. Understanding in deep the behavior and properties of functional layers at the microscale is helpful for improving the performance of the system and find alternative materials. The functional layers of the PEMFC, i.e., the gas diffusion layer (GDL) and catalyst layer, are typically porous materials. This characteristic allows the transport of fluids and charges, which is needed for the energy conversion process. Specifically, in the GDL, structural parameters such as porosity, tortuosity, and permeability should be optimized and predicted under certain conditions. These parameters have effects on the performance of PEMFCs, and they can be modified when the assembly compression is effected.

In this paper, the porosity, gas-phase tortuosity, and through-plane permeability are calculated. These variables change when the digitally created GDL is under compression conditions. The compression effects on the variables are studied until the thickness is 66% of the initial value. Because of the feasibility to handle problems in the porous media, the fluid flow behavior is evaluated using the lattice Boltzmann method. Our results show that when the GDL is compressed, the porosity and through-plane permeability decrease, while the gas-phase tortuosity increases, i.e., increase the gas-phase transport resistance. Copyright © 2015 John Wiley & Sons, Ltd.

KEY WORDS

gas diffusion layer; porosity; gas-phase tortuosity; through-plane permeability; lattice Boltzmann method; proton exchange membrane fuel cell

Correspondence

*Mayken Espinoza, Department of Energy Sciences, Lund University, PO Box 118, 22100 Lund, Sweden.
†E-mail: mayken.espinoza_andaluz@energy.lth.se

Received 19 January 2015; Revised 24 February 2015; Accepted 14 April 2015

1. INTRODUCTION

Fuel cell (FC) appears as one of the most propitious devices to reduce fossil fuel consumption and therefore the reduction in emissions of polluting gases such as carbon dioxide and sulfur dioxide. This electrochemical device directly converts the chemical energy present in the fuel, i.e., chemical compounds with hydrogen as constitutive element, into electrical energy and water. Their conversion efficiency is considerably high in comparison with the other kinds of energy systems [1], i.e., combustion engines and turbines, especially if small-scale power plant is considered.

There are different types of FCs, and they are classified depending on the electrolyte employed in the energy conversion process, operating temperature, or applicability. Two of the most widely investigated FCs are proton exchange membrane (PEMFC) and solid oxide fuel cell. PEMFC has low working temperature and fast start-up, but pure hydrogen as fuel is required, whereas solid oxide fuel cell because of high-temperature operation can work with a variety of fuels [2].

For portable applications, because of the previously mentioned characteristics, PEMFCs are more suitable. Reducing cost and increasing performance represent the topics to be focused on this type of FCs to solve part of the energetic demand in the near future and compete with the traditional energy sources. Knowing in deep, the behavior of the fluids (hydrogen, oxygen, and water) inside the PEMFC allows us to improve the functional components. Such components present in the electrodes, i.e., gas diffusion layer (GDL) and catalyst layer, are often porous media [3] and permit the fluid and charge transport for energy conversion.

Studies concerning to thermal–hydraulic characteristics and effects over the behavior in PEMFCs have been

carried out [4,5]. Additionally, some experimental measurements and analytical studies related to the GDL structures and performance have been realized [6–8]. However, there are still some characteristics of the fluid flow behavior through the GDLs to be studied, especially considering properties at the microscale, such as porosity, gas-phase tortuosity, and through-plane permeability.

The aim of this work is to study the behavior of gas phase flow through a porous domain and to calculate the porosity, gas-phase tortuosity, and through-plane permeability in a 2D artificially generated GDL under different compression conditions. These variables were computed together with the velocity field at steady state, by the lattice Boltzmann method (LBM). This method is considered because of its feasibility for solving problems in complex geometries, such as in porous structures.

The rest of the paper is divided as follows: the second part focuses on reconstruction of GDL, domain characteristics, and the variables studied in this work. The third section is related to LBM, governing equations, boundary conditions implemented, and applied methodology. Section four is dedicated to the results and discussions, and finally the conclusions are presented.

2. GAS DIFFUSION LAYER—BACKGROUND INFORMATION

GDL plays an important role in the distribution of the reactant gases on the catalyst layers in each side of PEMFCs. The porous characteristics allows the flow of the gases and liquid phase. Figure 1 shows the image of one GDL obtained by scanning electron microscopy. Typical thickness of the GDL is around 250–350 μm with a typical porosity between 60 and 90% [9].

There are two types of permeabilities analyzed in GDLs. One type is considered when the flow goes in parallel direction relative the layer (in-plane permeability) and the other type when the flow is normal to the plane (through-plane permeability). This work is focused on the variations of porosity, gas-phase tortuosity, and through-plane permeability when the GDL is compressed. These properties are computed for six different thicknesses of the modeled domain during the digital compression process.

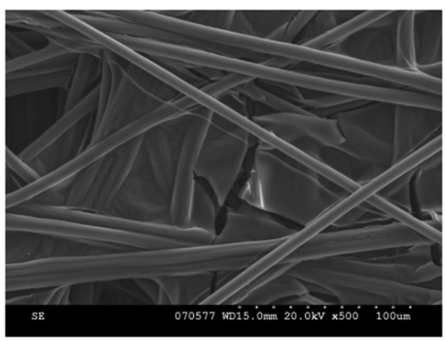

Figure 1. SEM image of carbon paper without teflon treatment. Scanning electron microscopy (SEM) image of a GDL from Zamel [10] allows us to observe the microstructure of the layer and permit to have an idea for the model implemented in this work. Image used with permission of the author.

2.1. Domain characteristics

Based on the image showed in Figure 1, and considering the model studied by Nakajima [11], the modeled domain can be considered as an aleatory arrow of thin carbon fibers place in different directions. Figure 2 shows the 2D approximation of the GDL implemented in this work. Our studied domain is a 90×180 μm rectangle region.

In reality, i.e., in the 3D case, the pathways for the fluid flow are connected in and out the plane implemented in our model. Thus, while constructing the model, it is necessary to avoid overlapped fibers in order to ensure continued pathways through the porous domain.

2.2. Variables computed

2.2.1. Porosity

As mentioned, the anode and cathode of PEMFCs are considered porous media achieving multi-functions of facilitating the flow of gases and liquids, as well as charges. Porosity is defined as the ratio between the void space and the total volume. General expression to calculate this variable is as follows:

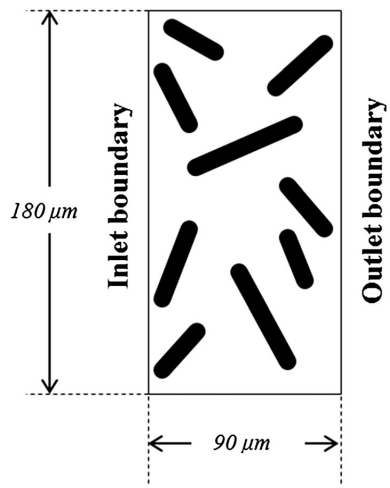

Figure 2. Artificially generated porous domain that represents a GDL. Digital representation of the porous domain used in this work. The fibers are placed in arbitrary positions and directions over the rectangular domain. In order to have a continuous path flow, no overlapped fibers in the model are used. This restriction could be avoided in a 3D representation.

$$\varphi = \frac{\text{Void Volume}}{\text{Total Volume}} \tag{1}$$

Because the physical domain analyzed in this work is a two-dimensional case, the previous equation is modified to calculate the porosity in the modeled GDL,

$$\varphi_{2D} = \frac{\text{Void Area}}{\text{Total Area}} = \frac{A_{air}}{A_{air} + A_{solid}} \tag{2}$$

where A_{air} is the part of the domain occupied by the voids, whereas A_{solid} is the region of the domain covered by the solid material, i.e., carbon fibers. According to the definition, the porosity is dimensionless and can only reach values between 0 and 1.

2.2.2. Gas-phase tortuosity

In the porous domain, where the flow path is not straight, it is important to define a variable that allows us to describe this phenomenon. There are three main kinds of tortuosity to analyze in PEMFCs, i.e., hydraulic, ionic, and electrical. In this study, we are studying only the gas phase, and therefore, the hydraulic tortuosity is determined. The hydraulic tortuosity values are helpful to describe the diffusion of species as mentioned in Zhang and Jia [3]. Therefore, this variable plays an important role in the microstructural analysis when the GDL is compressed. Hydraulic tortuosity as well is called as gas-phase tortuosity and is defined as the ratio between the actual length and the shortest length followed by the fluid. Based on this definition, the expression for computing the gas-phase tortuosity can be expressed as

$$\tau_{gas} = \frac{L_{actual}}{L_{shortest}} \tag{3}$$

Measuring the actual and the shortest length of the complete group of particles is not an easy task. Therefore, an equivalent expression to Eqn (3) is based on the fluid velocity and is expressed as follows [12]:

$$\tau_{gas} = \frac{\sum_{i,j} u_{mag}(i,j)}{\sum_{i,j} |u_x(i,j)|} \tag{4}$$

where u_{mag} represents the velocity magnitude at position (i,j) and u_x corresponds to the velocity in the main flow direction of the fluid. The velocity magnitude at the position (i,j) can be calculated with the following expression:

$$u_{mag}(i,j) = \sqrt{u_x(i,j)^2 + u_y(i,j)^2} \tag{5}$$

Based on the definition, the gas-phase tortuosity is a dimensionless quantity and bigger than 1 if obstacles are included in the domain.

2.2.3. Permeability

The physical property that allows the fluid, i.e., gas or liquid, flow through the material is called permeability. There are different ways to calculate the permeability, and several studies have been performed to determine this variable [13,14].

Depending on the porosity, direction of the flow through the material, and fiber radius, some expressions have been proposed. One expression for anisotropic permeabilities in carbon paper GDLs was presented by Hao and Cheng [15]. They determined a relationship to calculate the permeability as function of the porosity of the material. This expression is based on simulation results and written as follows:

$$K = C \frac{\varphi^3}{(\ln\varphi)^2} \tag{6}$$

where φ is the porosity of the material and $C = 8.9504 \times 10^{-13}\,\text{m}^2$.

In a previous study about permeability in fibrous porous media with applications to PEMFCs presented by Van Doormall and Pharoah [16], the permeability was related not only to the porosity but also with the fiber radius. The expression is as follows:

$$K = 0.26 \frac{\varphi^{3.6}}{1-\varphi} r^2 \tag{7}$$

where φ is the porosity of the material and r is the fiber radius.

Another relation to calculate the permeability of random fiber structures is proposed by Tomadakis and Robertson [17]. This equation, similar to previously mentioned, was related to porosity and fiber radius, but in a more complex relation, and it depends on other characteristic constants:

$$K = \frac{\varphi}{8\,(\ln\varphi)^2} \frac{\left(\varphi - \varphi_p\right)^{\alpha+2}}{\left(1-\varphi_p\right)^{\alpha}\left[(\alpha+1)\varphi - \varphi_p\right]^2} r^2 \tag{8}$$

where variables φ_p and α depend on the dimension of the analyzed case and the direction of the flow, i.e., parallel or normal to the fibers. In this study, the permeability is determined using $\varphi_p = 0.11$ and $\alpha = 0.521$.

3. METHODOLOGY

A simulated GDL was created to analyze the effects on the porosity, gas-phase tortuosity, and through-plane permeability when the thickness is decreased by a digital compression. The model corresponds to an arrow of thin fibers placed in a rectangular domain. The fluid motion through the porous domain is captured for each case. Because of the feasibility to handle flows in porous media, the LBM is applied for getting the velocity field.

The backbone equation of the LBM is the Boltzmann equation that is based on the particle distribution function. The Boltzmann equation is expressed as follows [15]:

$$\frac{\partial f(r,t)}{\partial t} + c.\nabla f(r,t) = \Omega \tag{9}$$

where f is the particle distribution function that depends on position r, velocity c, and time t. The Ω is the so-called collision operator.

Int. J. Energy Res. 2015; **39**:1528–1536 © 2015 John Wiley & Sons, Ltd.
DOI: 10.1002/er

Commonly, the collision operator is replaced with the Bhatnagar, Gross, and Krook approximation. Therefore, Eqn (9) can be expressed as

$$\frac{\partial f_i(r,t)}{\partial t} + c_i \nabla f_i(r,t) = \frac{1}{\tau_1}[f_i^{\mathrm{eq}}(r,t) - f_i(r,t)] \qquad (10)$$

where $f_i^{\mathrm{eq}}(r,t)$ is the equilibrium particle distribution function, τ_1 corresponds to the relaxation time, and c is the velocity in the corresponding i direction.

After solving Eqn (10), the macroscopic variables such as density and velocity field can be recovered using the following expressions:

$$\rho = \sum_{i=0}^{n-1} f_i \qquad (11)$$

$$u = \frac{1}{\rho}\sum_{i=0}^{n-1} f_i c_i \qquad (12)$$

In Eqns (11) and (12), n corresponds to the number of linked directions that the group of particles has with its neighborhood. This value is defined according to the LBM scheme used. The problem investigated in this paper is a 2D case, and the scheme applied is D2Q9.

3.1. Algorithm and solution method

Initial GDL thickness is defined as 90 lu; the momentum equation is solved in order to evaluate the velocity field. Based on the velocity field, and using Eqn (4), the gas-phase tortuosity is computed. From the digital domain, the fiber thickness is determined and the porosity is calculated using Eqn (2). With the results obtained (porosity and fiber radius), the through-plane permeability is computed using three different relationships (Eqns (6–8)). After this process, the thickness is reduced by 3 lu in each side. This process is repeated until the final thickness, i.e., 60 lu.

In general, the solution steps for calculating the variables in this work is presented in Figure 3.

3.2. Boundary conditions

Boundary conditions are implemented in each side of the domain. The flow direction is from the left to the right; the top and bottom boundaries are considered periodic. Over the inlet boundary (the left side), Von Neumann boundary condition was applied based on Zou and He [18]. On the outlet boundary, because the model is one section of the complete GDL, second derivative approximation was implemented as proposed by Mohamed [19].

The domain where the boundary conditions were applied is shown in Figure 4. Figure 4a shows the case under initial conditions, i.e., the thickness is 90 lu, while Figure 4b presents the final case with a thickness of 60 lu. There are four other cases (not shown) between them. By each thickness, the boundary conditions are applied in the same manner. To match the real problem to the lattice domain, 1 μm was considered to be equivalent to 1 lu.

Because its digital nature, the domain implemented in this work can be compressed continuously to a lower thickness; but to get a realistic solution, the digital compression process should not be followed ad infinitum. In this model, the final thickness after several compression steps was established in 66% of the initial thickness. This value falls approximately in acceptable compression ratios according some experimental and numerical studies previously performed [20,21]. It is important to notice that every GDL will have different rate of compression depending on its microstructure and the assembly pressure. For example, the maximum compression ratio presented in this study, i.e., 66% of the initial thickness, can be reached with around 15 MPa according to [20].

4. RESULTS AND DISCUSSIONS

As mentioned, the velocity field was calculated using LBM for six different thicknesses. In Figure 5, the normalized

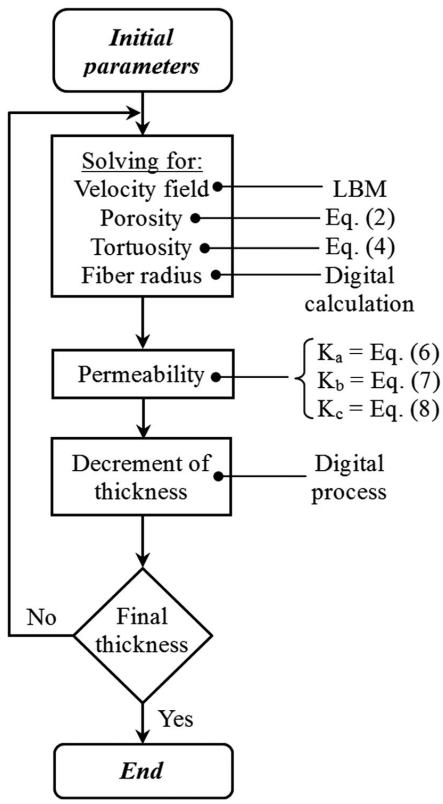

Figure 3. Solution steps followed during the calculation procedure. The diagram shows the different steps followed to compute the properties involved in this work until to get the final compressed thickness.

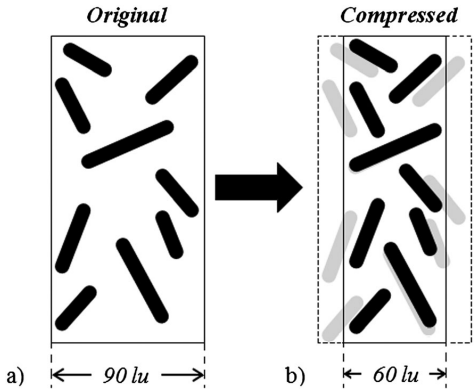

Figure 4. Fiber position and comparison between the initial and final thickness conditions. During the digital compression, no significant rotation of the fibers is assumed. The fiber thickness is not changed between the initial thickness and the last thickness. The thickness of the layer was digitally compressed to 66% of the original value.

velocity (related to the inlet velocity) for initial thickness (t_o) and the final compressed thickness are presented.

The predictions demonstrate that the velocity values are higher when the thickness is lower, i.e., low porosity. These higher velocity values in the compressed thickness are presented in the 80% of the modeled domain. The regions close to the inlet and outlet boundaries, i.e., the first and final 10% of the total length, are not in concordance with this behavior because of the major presence of obstacles close to the boundaries reduces the velocity values and therefore the gain is reduced.

To present the results in Figure 5, normalized average velocity was considered for the relative length to the total length. The values in horizontal axis represent the fraction of the thickness, each 10% of the total length.

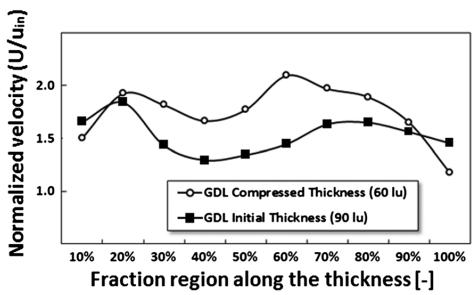

Figure 5. The computed normalized average velocity show that the higher values are obtained in the compressed GDL. The figure represents the average velocity in nine different positions along the thickness direction. The average velocity is normalized with the inlet velocity. If compressed thickness is studied, the fibers are closer, and under the same flow conditions, the velocities are higher.

To better understand the behavior of the fluid, the 2D velocity field is presented in Figure 6. Note that where the place is occupied by fibers (the solid and impermeable obstacles), the velocity must be zero. The zero velocity is represented by blue color, and the higher velocities are shown in red color.

4.1. Porosity results

Compression of the GDL turns into a reduction in the void space between the fibers. If the void space between the fibers is reduced, the porosity must decrease. The following figure shows the porosity calculated for five different thicknesses obtained after the compression. The horizontal axis in Figure 7 corresponds to the fraction of the thickness relative to the initial thickness (t_o), and the vertical axis represents the porosity calculated from the model.

The results confirm that the porosity decreases when the GDL is compressed. In this work, no deformation of the fibers was considered during the compression process. The deformation of the domain is assumed only in x direction. This assumption does not produce an impact on the results because the compression is considered as the decrement of void spaces. The position of the fibers placed in the center of the domain is assumed not

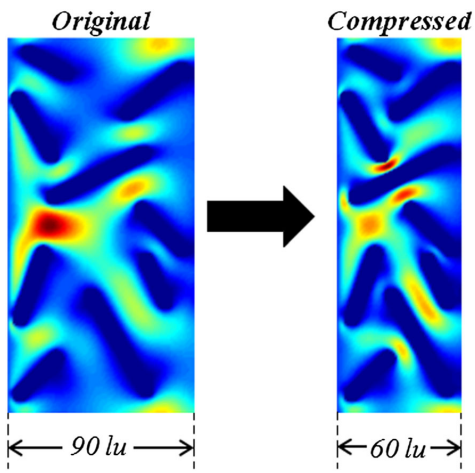

Figure 6. Normalized velocity distribution showing higher velocities when the fibers are closer to each other. Blue color represents zero velocity regions, and red color region is representing the higher velocity value. The velocity field is normalized with respect to the inlet velocity in the model. When fibers are closer, the velocities are higher (red color zones), and in the presence of obstacles, velocity field must be zero. In the left hand side case (90 lu), the maximum velocity is 0.0075 lu/ts, whereas in the right hand case, this value is higher, i.e., 0.0089 lu/ts.

Int. J. Energy Res. 2015; **39**:1528–1536 © 2015 John Wiley & Sons, Ltd.
DOI: 10.1002/er

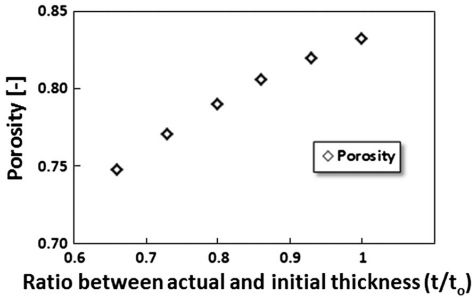

Figure 7. Calculated porosity shows that the porosity values decrease while the thickness decreases. The trend between the porosity and the decrement of thickness because of the compression are clear. The porosity values are computed using the model. GDL subject to compression decreases its thickness and the void spaces, and therefore, the porosity decreases.

affected by the digital compression, and the other fibers are approached in a uniform way in x direction. Taking into account these considerations, the predicted porosity results corroborate the equation proposed in Gostick *et al.* [7], that is expressed as

$$\varphi_c = 1 - \frac{1-\varphi}{\frac{t}{t_o}} \tag{13}$$

where φ_c is the porosity of the GDL after the compression, whereas that φ, t and t_o are the known values of porosity, actual thickness and initial thickness, respectively.

Considering the porosity results obtained, and using the fitting curve, the following expression can be used to establish a relationship between the porosity and the ratio of compression ($\zeta = t/t_o$). Note that the following expression is valid for the specific thickness and compression range presented in this work.

$$\varphi(\zeta) = 0.3928 + 0.728(\zeta) - 0.2893(\zeta)^2 \tag{14}$$

where ζ is the ratio between the actual and the initial thickness of the GDL. The fitting parameters were chosen using the sum of squares due to error (SSE) and root-mean-squared error (RMSE) criteria. Considering the SSE, the estimated is 9.407e-07, and by the RMSE, the error is 5.6e-04.

4.2. Gas-phase tortuosity results

As presented in the previous section, if compressing the thickness of the GDL, the porosity is expected to decrease, i.e., also the gas-phase tortuosity changes. The gas-phase tortuosity values are calculated after the velocity field is obtained using the LBM. Once the velocity field is found for each lattice node, Eqn (4) is used to calculate the gas-phase tortuosity values.

Following the same analysis that in the previous section, one curve can be approximated to express the relation between the gas-phase tortuosity and compression. One expression for fitting these results in a better way is a second-order polynomial function, which reads as follows:

$$\tau_{\text{gas}}(\zeta) = 1.353 - 0.03343(\zeta) - 0.1145(\zeta)^2 \tag{15}$$

where ζ corresponds to the ratio between the actual and the initial thickness of the GDL. The SSE and RMSE errors are 9.479e-05 and 4.868e-02, respectively.

Figure 8 shows the gas-phase tortuosity values for each compressed GDL. Reducing the thickness of the GDL results in increased gas-phase tortuosity.

Several general studies have been performed to find a relationship between the porosity and gas-phase tortuosity [12,22] in porous media. If we compare the gas-phase tortuosity values found in this work, and the gas-phase tortuosity calculated using the previous studies mentioned in the preceding texts, the deviation error is lower than 8%. The comparison between the gas-phase tortuosity calculated in this work and

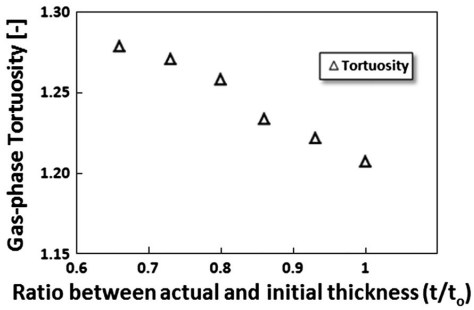

Figure 8. Gas-phase tortuosity results show that the tortuosity increases while the thickness decreases. The results reveal the relation between the gas-phase tortuosity and the compression of the GDL thickness. If we relate these calculated gas-phase tortuosity with the porosity values shown in Figure 7, the porosity decreases when the thickness decreases; as a result, the gas-phase tortuosity must increase.

Table I. Deviation between the calculated porosity and gas-phase tortuosity with other relations in literature.

Values calculated from the model in this work		Deviation compared to previous $\varphi - \tau_{\text{gas}}$ relationships	
Porosity (φ)	Gas-phase tortuosity (τ)	Ref. 22	Ref. 12
0.8315	1.2073	6.01%	5.09%
0.8195	1.2216	6.32%	5.44%
0.8056	1.2337	6.34%	5.51%
0.7894	1.2582	7.13%	6.38%
0.7703	1.2707	6.84%	6.18%
0.7473	1.2787	5.99%	5.46%

The porosity–tortuosity relationships found in the referred previous work were obtained analyzing the fluid flow through a 2D porous domain. All gas-phase tortuosity values computed in this work are larger than the tortuosity values in the referred literature.

the one calculated in the literature as a function of the porosity is presented in the next table (Table I).

Note that the first column of the table corresponds to the porosity values calculated from the model for the different compressed thickness and the second column presents the values of gas-phase tortuosity computed using LBM for each different compression thickness. The third and fourth columns correspond to the comparison between the gas-phase tortuosity obtained in this work with the tortuosity calculated (based on porosity values in column 1) using the mentioned relationships.

4.3. Through-plane permeability results

Once the porosity and gas-phase tortuosity have been computed, the permeability is the variable to be analyzed. Using the porosity calculated in the model and the fiber radius computed, the through-plane permeability was determined using Eqns (6–8). It was found that the permeability decreases when the GDL is compressed. $K_a - K_c$ were assigned to the Eqns (6–8), respectively. The through-plane permeability for each compressed thickness is shown in the following figure (Figure 9).

Although the computed values differ in each compressed thickness, the behavior of the through-plane permeability presents similar trend. The results obtained in this work are compared with the experimental data from [7]. Figure 10 shows the comparison mentioned, different to the previous figures, horizontal axis correspond to the porosity (calculated by each thickness), and the vertical axis represents the through-plane permeability.

As shown in Figure 10, our simulated results are consistent with the experimental data reported in previous work.

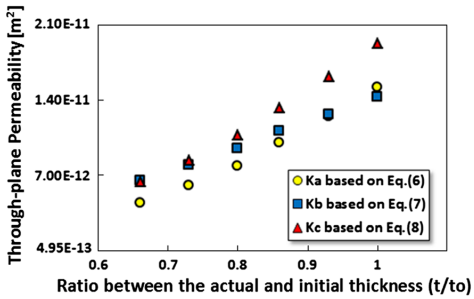

Figure 9. The computed values show that the through-plane permeability decreases while the GDL thickness decreases. The input variables in the relations presented (Eqns (6–8)) are porosity and fiber radius. It is seen that the relationship 'K_b' agrees well with 'K_a' when the ratio of compression (t/t_o) is close to 1 and agrees in good manner with 'K_c' when the ratio of compression is close to 0.7.

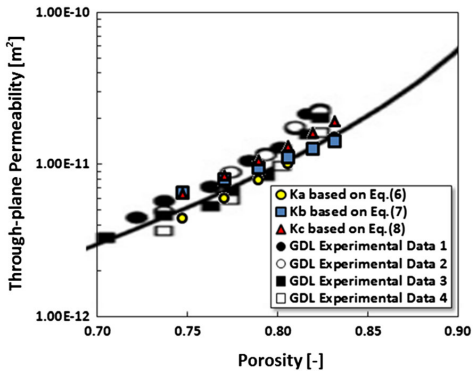

Figure 10. Permeability increases with the porosity, and calculated values agree well with the previous measured data. The figure presents the behavior of the through-plane permeability values versus porosity values. Because in this work the porosities calculated are within 0.7 and 0.9, some experimental data were selected from Gostick *et al.* [7] to contrast them. It is seen that the values obtained in this work agree with the referred data.

5. CONCLUSIONS

To sum up, we have obtained the values of porosity, gas-phase tortuosity, and through-plane permeability for an artificially generated GDL. Computations were carried out to different thickness simulating the mechanical compression of the thickness. The LBM for solving the velocity field inside the porous media was applied. In a GDL, porosity and through-plane permeability decrease with the compression, whereas the gas-phase tortuosity increases.

According to our results, if the thickness of the GDL is reduced to 66% of the initial value, the porosity decreases with around 10%, and the gas-phase tortuosity increases approximately 6%, whereas that the through-plane permeability is reduced, in average, to a 36% of the initial value calculated. The current study was limited to 2D, but according to the results obtained, can be considered a good approximation for a more realistic model. The computed variables are in good agreement with the previous theoretical and experimental measurements. Future work will include the calculation of the inertial coefficient and the analysis of the in-plane permeability. In order to get a better approximation of the reality, the presence or absence of ribs of the flow plates in the FC scheme can be considered.

NOMENCLATURE

BGK	= Bhatnagar, Gross, and Krook
CL	= catalyst layer
r	= fiber radius
FC	= fuel cell
GDL	= gas diffusion layer

Int. J. Energy Res. 2015; **39**:1528–1536 © 2015 John Wiley & Sons, Ltd.
DOI: 10.1002/er

LBM	= lattice Boltzmann method
lu	= lattice unit (LBM length)
m	= meter
PDF	= particle distribution function
f	= particle distribution function, Eqn (9)
K	= permeability
r	= position
PEMFC	= proton exchange membrane FC
RSME	= root-mean-squared error
SEM	= scanning electron microscopy
SOFC	= solid oxide fuel cell
SSE	= squares due the error
t	= thickness
ts	= time step (LBM time)
u	= velocity
i	= x position
j	= y position

Greek symbols

α	= constant value, Eqn (8)
φ	= porosity
μ	= micro
ρ	= density distribution
τ	= gas-phase tortuosity
τ_1	= relaxation time
Ω	= collision operator

Subscripts

p	= constant porosity value, Eqn (8)
o	= initial
in	= inlet (boundary condition)
mag	= magnitude
x	= x direction
y	= y direction
solid	= solid material, Eqn (2)
air	= void space, Eqn (2)
gas	= gas phase
2D	= two-dimensional case, Eqn (2)

Superscripts

eq	= equilibrium state

ACKNOWLEDGEMENTS

The financial support for this research comes from the National Secretary of Higher Education Science, Technology and Innovation - Senescyt Ecuador—which is very grateful.

REFERENCES

1. Farooque M, Maru HC. Fuel cells-the clean and efficient power generators. *Proceedings of the IEEE* 2001; **89**(12):1819–1829.
2. Zhu H, Kee R, Janardhanan V, Deutschmann O, Goodwin D. Modeling elementary heterogeneous chemistry and electrochemistry in solid-oxide fuel cells. *Journal of the Electrochemical Society* 2005; **152**(12):A2427.
3. Zhang Z, Jia L. Parametric study of the porous cathode in the PEM fuel cell. *International Journal of Energy Research* 2009; **33**:52–61. doi:10.1002/er.1471.
4. Ferng YM, Sun CC, Su A. Numerical simulation of thermal–hydraulic characteristics in a proton exchange membrane fuel cell. *International Journal of Energy Research* 2003; **27**:495–511. doi:10.1002/er.891.
5. Ferng YM, Su A, Lu SM. Experiment and simulation investigations for effects of flow channel patterns on the PEMFC performance. *International Journal of Energy Research* 2008; **32**:12–23. doi:10.1002/er.1320.
6. Nikooee E, Karimi G, Li X. Determination of the effective thermal conductivity of gas diffusion layers in polymer electrolyte membrane fuel cells: a comprehensive fractal approach. *International Journal of Energy Research* 2011; **35**:1351–1359. doi:10.1002/er.1896.
7. Gostick JT, Fowler MW, Pritzker MD, Ioannidis MA, Behra LM. In-plane and through-plane gas permeability of carbon fiber electrode backing layers. *Journal of Power Sources* 2006; **162**(1):228–238.
8. Feser JP, Prasad AK, Advani SG. Experimental characterization of In-plane permeability of gas diffusion layers. *Journal of Power Sources* 2006; **162**(2):1226–1231.
9. Spiegel C. *PEM Fuel Cell Modeling and Simulation Using Matlab* (1st edition). Elsevier Inc: Oxford, UK., 2008 Book.
10. Zamel N. Transport properties of the gas diffusion layer of PEM fuel cells. Ph.D. Thesis, University of Waterloo. 2011.
11. Nakajima H. Lattice Boltzmann modeling of the gas diffusion layer of the polymer electrolyte fuel cell with the aid of air permeability measurements. *Mass Transfer - Advances in Sustainable Energy and Environment Oriented Numerical Modeling*, Dr. Nakajima H (ed). 2013. ISBN: 978–953–51–1170–2, InTech, DOI: 10.5772/56363
12. Nabovati A, Sousa M. Fluid flow simulation in random porous media at pore level using the lattice Boltzmann method. *Journal of Engineering Science and Technology* 2007; **2**(3):226–237.
13. Wilde PM, Maendle M, Murata M, Berg N. Structural and physical properties of GDL and GDL/BPP combinations and their influence on PEMFC performance. *Fuel Cells* 2004; **4**(3):180–184.
14. Froning D, Gaiselmann G, Reimer U, Brinkmann J, Schmidt V, Lehnert W. Stochastic aspects of mass

transport in gas diffusion layers. *Transport in Porous Media* 2014; **103**(3):469–495.
15. Hao L, Cheng P. Lattice Boltzmann simulations of anisotropic permeabilities in carbon paper gas diffusion layers. *Journal of Power Sources* 2009; **186**(1):104–114.
16. Van Doormaal MA, Pharoah JG. Determination of permeability in fibrous porous media using the lattice Boltzmann method with application to PEM fuel cells. *International Journal for Numerical Methods in Fluids* 2009; **59**(1):75–89.
17. Tomadakis MM, Robertson TJ. Viscous permeability of random fiber structures: comparison of electrical and diffusional estimates with experimental and analytical results. *Journal of Composite Materials* 2005; **39**(2):163–188.
18. Zou Q, He X. On pressure and velocity boundary conditions for the lattice Boltzmann BGK model. *Physics of Fluids* 1997; **9**(6):1591–1598.
19. Mohamed A. *Lattice Boltzmann Method Fundamentals and Engineering Applications with Computer Codes*. Springer-Verlag London: UK, 2011.
20. Zhou Y, Lin G, Shih AJ, Hu SJ. Multiphysics modeling of assembly pressure effects on proton exchange membrane fuel cell performance. *Journal of Fuel Cell Science and Technology* 2009; **6** / 041005-1.
21. Ismail MS, Hughes KJ, Ingham DB, Ma L, Pourkashanian M. Effect of PTFE loading of gas diffusion layers on the performance of proton exchange membrane fuel cells running at high-efficiency operating conditions. *International Journal of Energy Research* 2013; **37**(13):1592–1599. doi:10.1002/er.2968.
22. Koponen A, Kataja M, Timonen J. Tortuos flow in porous media. *Physical Review E* 1996; **54**(1): 406–410.

Paper III

International Journal of Energy Research

INTERNATIONAL JOURNAL OF ENERGY RESEARCH
Int. J. Energy Res. 2017; **41**:565–578
Published online 7 October 2016 in Wiley Online Library (wileyonlinelibrary.com). DOI: 10.1002/er.3661

Predicting transport parameters in PEFC gas diffusion layers considering micro-architectural variations using the Lattice Boltzmann method

Mayken Espinoza*,†, Martin Andersson and Bengt Sundén

Department of Energy Sciences, Lund University, PO Box 118, 22100 Lund, Sweden

SUMMARY

A deep understanding of the behavior of microstructural parameters in proton exchange fuel cells (PEFCs) will help to reduce the material cost and to predict the performance of the device at cell scale. Changes in morphological configuration, that is, fiber diameter and fiber orientation, of the gas diffusion layers (GDLs) result in variations of fluid behavior throughout the layer, and therefore, the microstructural parameters are affected. The aim of this study is to analyze, for three selected fiber diameters and different percentage presence of inclined fibers, the behavior of the different microstructural parameters of the GDLs.

This study is carried out over digitally created two-dimensional GDL models, in which the fluid behavior is obtained by means of the lattice Boltzmann method. Once the fluid behavior is determined, the microstructural parameters, that is, the porosity, gas-phase tortuosity, obstruction factor, through-plane permeability, and inertial coefficient, are computed. Several relationships are found to predict the behavior of such parameters as function of the fiber diameter, presence of inclined rods, or porosity. The results presented in this work are compared and validated by previous theoretical and experimental studies found in the literature. Copyright © 2016 John Wiley & Sons, Ltd.

KEY WORDS

gas diffusion layer; proton exchange fuel cell; lattice Boltzmann method; transport parameters; micro-architecture

Correspondence

*Mayken Espinoza, Department of Energy Sciences, Lund University, PO Box 118, 22100 Lund, Sweden.

†E-mail: mayken.espinoza_andaluz@energy.lth.se

Received 10 May 2016; Revised 10 August 2016; Accepted 31 August 2016

1. INTRODUCTION

A fuel cell (FC) is an electrochemical device that converts the chemical energy present in the fuel (commonly hydrogen or some chemical compound with hydrogen as constitutive) into electrical energy and water. This device has been pointed as one of the most promising devices to produce electrical energy as during the energy conversion process, it provides no production of noise, emission reduction of pollution gases, and high efficiency [1]. There are different types of FCs, and they can be grouped according to different aspects such as operating temperature, electrolyte, application, or output power generation.

When a fast start-up is required because the FC system takes part of a mobile application, the polymer electrolyte membrane fuel cell (PEFC) is commonly used. A PEFC is formed, additional to the current collectors, by several functional layers such as gas diffusion layer (GDL), catalyst layer (CL), and a thin polymer electrolyte membrane. Figure 1 shows a simplified scheme of a typical PEFC. All the layers together form the so-called membrane electrode assembly (MEA).

As shown in Figure 1, GDLs are placed on both sides of a PEFC, that is anode and cathode, and play an important role during the energy conversion process. Through this functional layer, electronic and fluid transport processes occur. The anode side is crossed by the hydrogen flow (H_2), whereas on the cathode side, the oxygen (O_2) flows. The GDLs act as an interface between the CLs and the flow plates; therefore, they have to offer a good electrical and thermal conductivity and to give mechanical support to the MEA [2]. Because of the importance of the GDLs, several parameters of this multifunctional layer are studied in this paper under different morphological conditions that will be detailed in the corresponding sections.

Reducing material cost and improving efficiency of the FC systems have been the aim during the last years in order to increase the presence of the FCs in the world market. Modeling research appears as a helpful tool to give detailed information to reduce manufacturing cost of

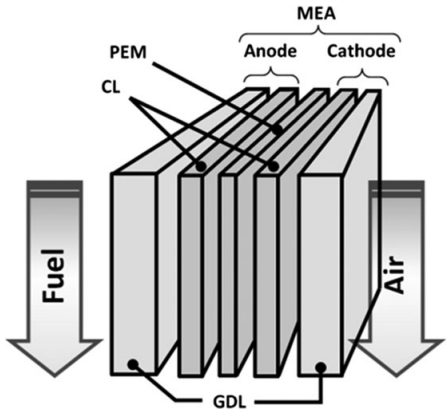

Figure 1. Simplified scheme of a PEFC showing the different functional layers. GDLs are placed between the flow plates and the CLs.

materials, decrease aging effects, and improve the FC efficiency. Cell or system scale models often require several input parameters, frequently assumed, that can be obtained from microscale analysis. Due to the complex geometries found in GDLs, pore-scale modeling provides exclusive conditions to understand the fluid behavior throughout this functional layer considering the microstructures of the medium. Among the different methodologies applied to describe the GDLs can be mentioned: the fine-scale computational fluid dynamics (CFD), molecular dynamics, and lattice Boltzmann method (LBM) [3]. The ultimate mentioned method is applied in this study because it has been proved to be a powerful tool for solving different transport phenomena at microscale in complex geometries as found in the GDLs [4–6].

During the last years, numerical and experimental studies have been carried out on GDLs and their microstructural parameters. From an experimental point of view, different effects on PEFC performance related to the fabrication processes of GDL are presented in Ref. [7], and parameters as porosity and permeability have been measured in Ref. [8]. On the other hand, the effect of the permeability on water and thermal management using CFD is presented in Ref. [9] as a modeling study. However, there is no research works presented to evaluate the transport parameters like the thickness, orientation of fibers, and the percentage of inclined fibers. The aim of this study is to predict the behavior of different microstructural parameters appearing in the GDLs and in particular to consider thinner fiber diameters and various percentages of inclined fibers. LBM is applied for solving the fluid flow through the two-dimensional digitally created GDLs. The parameters calculated in this work are porosity, gas-phase tortuosity, obstruction factor, through-plane (TP) permeability, and inertial coefficient. The presented results in this work help to predict the behavior of the GDL parameters, and based on these findings, the FC performance can be described. The results obtained offer relevant and insightful information that can be applied in the 3D microprinting of FCs, following the manufacturing process of microbatteries as presented in Ref. [10].

The rest of the paper is divided as follows: Section 2 is dedicated to the description of the microstructural parameters computed in this work and their definitions. Section 3 presents the methodology applied and characteristics of the solved domain. Section 4 is mainly aimed to the obtained results and discussions. Finally, the conclusions are given in Section 5.

2. MICROSTRUCTURAL PARAMETERS

The GDLs are crucial in the charge and fluid transport during the energy conversion process. They do not only distribute the reactant gases from the channel to the CLs but also transport the free electrons from the CLs to the current collectors. Additionally, they help to remove water to the catalyst in order to prevent flooding and provide mechanical strength to the MEA. The microstructural parameters have influence over the mentioned GDL transport properties. The following sub-sections are aimed to define the parameters studied in this paper and their characteristics.

2.1. Porosity

The porosity is one of the essential parameters measured in the GDLs and represents the availability for the fluid to occupy a certain volume. This is a dimensionless parameter and can be computed according to the following equation:

$$\varepsilon = \frac{Void\ volume}{Total\ volume} \tag{1}$$

According to the definition, this parameter can reach values between 0 and 1 and frequently is represented as a percentage. Considering the two-dimensional characteristics of this study, the porosity is determined as follows:

$$\varepsilon_{2D} = \frac{Void\ area}{Total\ area} = \frac{A_{Fluid}}{A_{Fluid} + A_{Solid}} \tag{2}$$

where A_{Fluid} and A_{Solid} are the 2D regions in which the fluid can flow and the solid material occupies, respectively. A digitally created image representing the cross-sectional view of a material with porosity 0.5 is shown in Figure 2.

2.2. Gas-phase tortuosity

To describe the microstructural morphology of the porous media, gas-phase tortuosity is one of the proper parameters. The gas-phase tortuosity is a measure of the complexity of the pathways the fluid has to follow through the material. There have been several studies showing that this

Int. J. Energy Res. 2017; **41**:565–578 © 2016 John Wiley & Sons, Ltd.
DOI: 10.1002/er

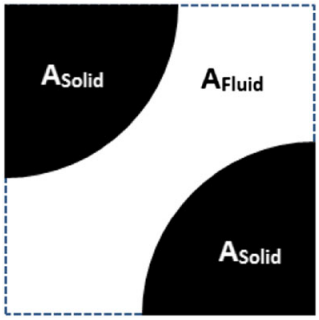

Figure 2. A digitally created domain with porosity equal to 50%. The black color regions represent solid material, and the white color region represents a void space. [Colour figure can be viewed at wileyonlinelibrary.com]

parameter has a considerable impact on the gas diffusion process [11,12].

When a cell scale model is developed, the gas-phase tortuosity value is generally approximated or assumed. These approximations are carried out by using theoretical or empirical relationships, mainly as a function of the porosity [13,14]. In order to avoid these assumptions, the gas-phase tortuosity can be determined as the ratio between the actual path length and the shortest path length trajectory followed by the fluid. According to the definition, this parameter can be stated as follows:

$$\tau_{gas} = \frac{L_{actual}}{L_{shortest}} \tag{3}$$

Based on Eqn (3), the gas-phase tortuosity is a dimensionless parameter. The values obtained are always greater than unity, with the lowest case being unity when the porosity is 100%; that is, the fluid is moving in a medium with no obstacles. Figure 3 shows a simplified representation of the pathways of the fluid.

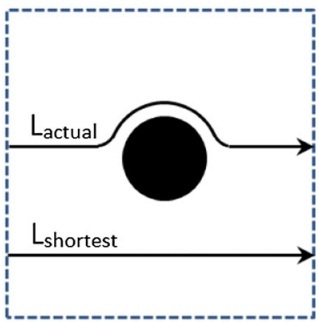

Figure 3. Digital representation of the actual and shortest length paths. Fluid avoiding the obstacle results in actual length increment. For this graph, tortuosity is approximately 1.12. [Colour figure can be viewed at wileyonlinelibrary.com]

To measure this parameter, the velocity field through the porous media is used as proposed in Ref. [15]. Considering the x positive axis as the main flow direction, the gas-phase tortuosity can be determined as:

$$\tau_{gas} = \frac{\sum_{i,j} u_{mag}(i,j)}{\sum_{i,j} |u_x(i,j)|} \tag{4}$$

where $u_{mag}(i,j)$ corresponds to the velocity magnitude at position (i,j) and $u_x(i,j)$ is the velocity vector in the main flow direction through the porous media. Considering Eqn (4), the calculation of the gas-phase tortuosity values differ if another main flow direction is considered.

2.3. Obstruction factor

When the diffusion takes place through a porous medium, the effective diffusion parameter has to be determined. Mason *et al.* [16] showed that the effective diffusion coefficient (D_{eff}) is smaller than the diffusion coefficient (D) according to the following equation:

$$D_{eff} = \frac{\varepsilon}{\tau} D \tag{5}$$

where the ratio (ε/τ) is the so-called obstruction factor, and therefore highly dependent on the morphological properties of the porous media analyzed. In the study performed by Van Brakel *et al.*, [17] the ratio D_{eff}/D is introduced as the diffusibility (Q), and they found a very high dependence of this parameter on the porosity and gas-phase tortuosity. However, they added a parameter called constrictivity, which is not considered in the current study. Constrictivity is not considered in our study because the uniformity of fiber distribution gives a ratio between maximum and minimum cross-section less than two, and according to data presented by Van Brakel *et al.*, the constrictivity is approximately unity. In analysis of transport phenomena, as the percolation and constrictivity are considered, the ratio defined in this subsection receives the name of the M-factor. More detailed information can be found in Ref. [18]. Given the characteristics of the proposed model, the computation of obstruction factor by using Eqn (5) is an approximation in which the porosity and tortuosity are considered.

2.4. Through-plane permeability

Permeability is a measure of the ability of a porous medium to allow the flow of a fluid. Considering the very low Reynolds numbers present in the different layers of the FCs [3,19], to describe such flows through the porous media the Darcy's law can be applied. According to the Darcy experiment [20] and reordering the original expression, the permeability can be evaluated by using the following relationship:

$$K = q\mu \frac{\Delta X}{\Delta P} \tag{6}$$

where q is the Darcy flux ($m\,s^{-1}$), μ is the dynamic viscosity (Pa s), ΔX is the thickness of the analyzed material (m), and ΔP is the pressure drop across the layer (Pa). Using appropriately the corresponding units, the permeability is obtained in m^2.

Because the pressure drop is applied in a perpendicular direction relative to the plane, the TP permeability is analyzed. Notice that the permeability can be measured in different directions for the same material depending on where the pressure drop is applied.

2.5. Inertial coefficient

Reordering the terms and using the gradient definition, Eqn (6) can be stated as

$$-\nabla P = \frac{\mu}{K} q \tag{7}$$

Because of the low velocities, in Eqn (7), only viscous effects are considered. However, at higher velocities, the relationship between the Darcy flux and the pressure gradient is not linear. Under the mentioned conditions, the Forchheimer term [21], a second-order polynomial Darcy flux term, has to be added to the right-hand side of the equation as follows:

$$-\nabla P = \frac{\mu}{K} q + \beta \rho q^2 \tag{8}$$

where β is the inertial coefficient often called the non-Darcy coefficient (m^{-1}) and ρ is the fluid density ($kg\,m^{-3}$). Although high velocities are not expected in normal operating conditions in FCs, it can occur exceptionally, that is an unexpected high flow rate of reactants, and therefore affect the overall performance of the FC system. Considering such situations, some studies determining the value of the inertial coefficient in GDLs have been carried out [8,22].

3. METHODOLOGY

The two-dimensional models artificially generated in this work, consider the microstructural characteristics of the GDLs. Due to the transport phenomena involved during the energy conversion process, these layers are constructed as porous media. To solve the fluid flow behavior through the porous media, the LBM is applied.

There are two main types of GDLs, carbon paper and carbon cloth. The building up of the model is based on the model of a carbon paper type, in which the fiber thickness and percentage of inclined fibers can be controlled during the manufacturing process. These variables can be controlled given the accuracy which the microprinters are generating to the different elements present in energy conversion systems [10]. Taking into account the physical characteristics of the GDL type, that is, typical dimensions and average size, the porous media are digitally generated to describe the importance of not only the fiber diameters but also the presence of a specified percentage of inclined fibers in the domain, on the microstructural parameters mentioned in Section 2. More detailed information related to the model characteristics and methodology applied is presented in the following sub-sections.

3.1. Lattice Boltzmann method

Lattice Boltzmann method has been widely applied for solving different transport phenomena in the different FC functional layers [4,23]. The basic idea of LBM is to consider the fluid as a group of particles distributed throughout a lattice. Each group of particles receives the name of particle distribution function (PDF), and they interact with other groups of particles of the same or different nature, that is fluid–solid or fluid–fluid. The backbone of LBM is the Boltzmann equation, which can be expressed as follows [24]:

$$\frac{\partial f(r,t)}{\partial t} + c \cdot \nabla f(r,t) = \Omega \tag{9}$$

where f is the PDF, which depends on the position r, bulk velocity c, and time t. The right-hand side of Eqn 9 represents the collision operator, which is often replaced, in the simplest way, by the approximation proposed by Bhatnagar *et al.* [25]. Replacing the Bhatnagar, Gross, and Krook approximation in Eqn (9) and discretizing the lattice Boltzmann equation is obtained:

$$\frac{\partial f_k(r,t)}{\partial t} + c_k \nabla f_k(r,t) = \frac{1}{\tau'} \left[f_k^{eq}(r,t) - f_k(r,t) \right] \tag{10}$$

where τ' is the relaxation parameter and f_k^{eq} represents the equilibrium particle distribution. The subscript k represents the number of linked velocities that each analyzed lattice element has with its neighborhood. The linked velocities allow the momentum transfer between the lattice elements in the domain when LBM is applied. To recover the total density for each lattice node, the sum of the PDFs in all directions should be effected. The velocity field is determined by using the following equation:

$$u(r,t) = \frac{\sum_k f_k \, c_k(r,t)}{\rho(r,t)} \tag{11}$$

where k is, as mentioned, given for the number of linked velocities. As the models in this study are solved in 2D lattice systems, each lattice element transfers the physical properties to its eight lattice neighbors, that is one for each cardinal direction and one for each intercardinal direction, and additionally, its own velocity is considered giving a total of nine linked velocities. This solution scheme is called

D2Q9. More information about the scheme can be found in Ref. [24].

One of the critical things to be taken into account for obtaining an accurate model and avoiding instability is the selection of the right boundary conditions. Figure 4 shows a schematic of the boundary conditions implemented over the domain.

The porous media generated for this study is represented by a rectangular domain (more details are given in the next sub-section), in which periodic boundary conditions at the bottom and top are implemented. On the left and right boundaries, the pressure-driven boundary based on the Zou and He [27] procedure is applied. When fluid–solid lattice nodes meet, bounce-back boundary conditions are applied.

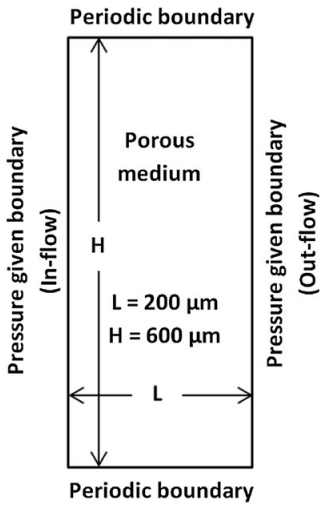

Figure 4. Rectangular domain where the pore domain is generated. Periodic boundaries at the bottom and top, and pressure given at left and right boundaries are implemented. The thickness of the GDLs is defined as an average value from commercial products and previous studies [4,6,26]

3.2. Domain characteristics

A typical GDL can be described as an array of carbon fibers grouped in several layers. In practice, carbon fibers can be oriented at different angles with respect to the z axis, but for this study, the inclination is assumed to be 45°. Figure 5 shows the manner in which the approximation of the model is carried out. The pressure drop is given along the x axis direction and, given the pressure conditions, from the cross sectional view, that is, x–y plane, the fluid is moving from the left to the right. Given the characteristics of the model, that is, a rectangular domain with constant dimensions, orientations different than 45° are not considered because it may result in a partial or total blockage of the flow through the layer. To reconstruct the GDLs, fibers belonging to the same layer are distributed on a semi-random manner into the domain. Such specific conditions can be achieved by using microprinters, which allow obtaining micrometer-scale devices [28].

The 2D approach, as presented in Figure 5, is selected to perform this study considering that the computational demand of a 2D approximation is lower compared with a 3D approach as already has been pointed out and demonstrated in various previous studies [29,30]. On the other hand, the study of the fluid behavior in the x–y plane is of great importance because one of the variables to analyze is the TP permeability, that is permeability computed when the gas flows in the normal direction to the layers. In addition, this mentioned plane allows recognition of the fluid flow behavior from the channel flow plates to the active sites in the FCs.

Three different fiber diameters are considered, that is 4.00, 5.00, and 6.00 µm. These values were selected to determine the effects of fiber diameter lower than the values found in the literature [8,22]. This is because of the trend of reducing the physical size of the FCs [31,32] by decreasing the GDL thickness. Furthermore, the GDL thickness is important because the reactant concentration at the

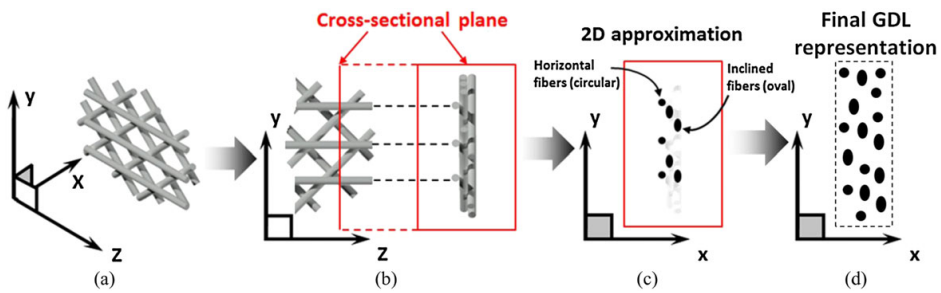

Figure 5. First 3D approximation of a GDL (a). In-plane and through-plane view of the GDL (b). Rectangular domain where the pore domain is generated in the through-plane view (c). Final digital GDL representation showing 50% of inclined fibers in (d). [Colour figure can be viewed at wileyonlinelibrary.com]

GDL/CL interface is less than the reactant concentration in the flow channels. Accordingly, decreasing the GDL thickness will decrease the concentration losses. Additionally, the percentage of presence of the inclined rod sections, represented by oval-shape obstacles, for each pore domain is a variable taken into account. For each fiber diameter, the percentage of inclined fiber varies from 0 to 100% in steps of 12.5% is considered. Subsequently, a total number of 27 digitally created GDLs are considered.

Although the inclined fibers are placed in the domain in an aleatory way for all the GDLs, the number of cross-sectional fibers does not change; that is, the number of rods per area is maintained at a constant value. This condition is considered to evaluate the incidence of the micro-architectural variations without changing the amount of material during the manufacturing process of the GDLs. After the porous media have been digitally generated, the fluid flow behavior is solved by using LBM in order to analyze the different variables mentioned in Section 2. In every model, some assumptions are needed. To implement the models in the current work, the following assumptions are made: the fluid is treated as incompressible and the process is isothermal, the porosity is considered as the effective porosity; that is, all the void spaces can be occupied by the fluid in the model, and no overlapping of cross-sectional fibers is enforced. From a cell scale point of view, the land/channel region effects are neglected. All the fibers are assumed to be rigid and undeformed rods with circular cross section (Figure 5). Physical fluid characteristics to match the Reynolds number in GDL are defined according to Froning *et al.* [19].

Based on the simulation domain size presented in Figure 4, computations of the variables considering a range of ±30% of the domain size variations were carried out. The magnitude of error for the computed variables falls in a range of 10^{-3} and 10^{-2}, which means that the selected domain size generates acceptable results.

4. RESULTS AND DISCUSSIONS

Once the steady state is reached, that is once the sum of residual velocities at all lattice nodes fall below 10^{-6}, the iterative process is terminated and the velocity field is presented. A representative sample region of nine (from a total of 27) GDLs is presented in Figure 6. The red color represents high velocities, and the blue color regions correspond to zero velocities. To specify the results obtained for a certain GDL fiber thickness, they are adequately named. GDL with fiber diameter equal 4.00 µm is titled GDL4. If 5.00 µm is the diameter, it is named GDL5, and the one corresponding to 6.00 µm is entitled GDL6. To identify the percentage of inclined rods, whenever needed, GDL and the number followed in a parenthesis with such a percentage are presented. For instance, GDL4(25) corresponds to the GDL with fiber diameter 4.00 µm, and 25% of the fibers are inclined. Results obtained, discussions, and validation by comparison with previous theoretical and experimental works are presented in the following sections.

4.1. Effects on porosity

It is important to notice that the obtained porosity results are based on a 2D approximation of the GDLs. This 2D porosity, for a given configuration, that is fiber thickness and percentage of inclined fibers, does not change in function of the z-coordinate (Figure 5) because the cross-sectional material is obtained from the same amount of fibers. In other words, changing the z-coordinate where the cross-sectional material is obtained, produces a change in the position of the circular and oval shapes, but no variation in the amount of solid material involved in the simulations.

Using Eqn (2), the porosity for each GDL is computed. Results show that the porosity for GDL4, GDL5, and GDL6 falls between 0.83–0.77, 0.75–0.63, and 0.63–0.51, respectively. Notice that for different fiber thicknesses, it is possible to have the same porosity depending on the percentage of inclined rods. An example of the mentioned situation is that the porosities of GDL5 (100) and GDL6(0) have the same value. From GDL4(0) to GDL6(100), the porosity decreases about 38.55%. Figure 7 shows the results of the computed porosity for the GDLs.

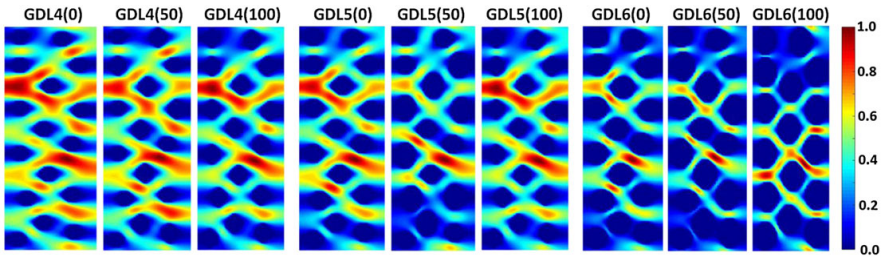

Figure 6. Fluid behavior for nine representative GDL samples are presented so readers can observe the incidence of the fiber thickness and inclination. The red color represents high velocities, whereas the blue color represents low velocities. Fiber diameter is increasing from the left to the right. At top of figures, fiber diameter and percentage of inclined fibers are labeled as previously explained. [Colour figure can be viewed at wileyonlinelibrary.com]

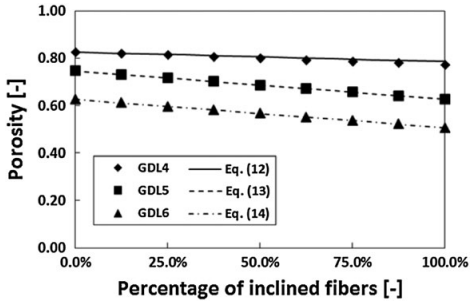

Figure 7. Porosity data collected for each GDL. Minimum and maximum computed values are 0.51 and 0.83, respectively. Fitted curves are presented together with the data.

For a given fiber thickness, the porosity varies linearly as a function of the percentage of inclined rods. This is shown by fitting the curves by using the values computed. The coefficient of determination (so-called R-square), which represents the percentage of the data that can be predicted with the fitted curve, is unity, and the sum of squares due to error is extremely low, that is an order of magnitude -32, for each fitted relationship. The expressions that relate the porosity and the percentage of inclined fiber for a corresponding fiber diameter in the modeled GDLs are as follows:

$$\varepsilon_{GDL4}(\delta) = -0.0004*\delta + 0.8267 \tag{12}$$

$$\varepsilon_{GDL5}(\delta) = -0.0012*\delta + 0.7467 \tag{13}$$

$$\varepsilon_{GDL6}(\delta) = -0.0012*\delta + 0.6267 \tag{14}$$

where δ represents the percentage of inclined rods as a percentage value; that is, if 20% is the value of the inclined fiber present, then δ should be replaced by 20. Porosity results agree with the values found in manufacturer data sheet and in previous studies related to GDLs [26,33].

4.2. Effects on gas-phase tortuosity

Gas-phase tortuosity is another variable to take into account when the microstructure is analyzed. As mentioned in Section 2, in porous media, the tortuosity always is greater than unity, and it can be determined by using Eqn (4). As a precedent step, the velocity field is solved by using LBM. Depending on the complexity of the geometry, the fluid through the porous domain follows different pathways as depicted in Figure 8.

The complexity of the porous media gives the fluid different pathways to flow and therefore influences the gas-phase tortuosity computation. The values found in this work grouped according to the fiber diameter, that is GDL4, GDL5, and GDL6, are presented in Figure 9.

Although the gas-phase tortuosity values found do not follow a uniform or linear behavior, the trend is clear: a larger fiber diameter implies a larger gas-phase tortuosity. Considering the gas-phase tortuosity values for a given fiber diameter, a relationship for the tortuosity as a function of the percentage of inclined rods is established. These relationships are as follows:

$$\tau_{GDL4}(\delta) = 6.737 \times 10^{-7}*\delta^2 + 3.252 \times 10^{-4}*\delta + 1.068 \tag{15}$$

$$\tau_{GDL5}(\delta) = 5.290 \times 10^{-7}*\delta^2 + 5.393 \times 10^{-4}*\delta + 1.096 \tag{16}$$

$$\tau_{GDL6}(\delta) = 2.188 \times 10^{-6}*\delta^2 + 2.089 \times 10^{-4}*\delta + 1.121 \tag{17}$$

where δ represents the percentage of inclined fiber as a percentage value. All the gas-phase tortuosity values obtained in this work can be predicted by using Eqns 15–17 in a percentage of 96%, 92%, and 89%, respectively. The

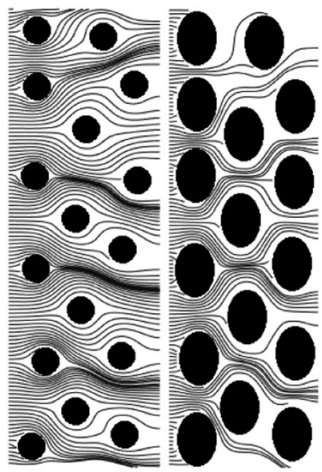

Figure 8. Flow pathways for two selected representative GDL samples. GDL4(0) and GDL6(100) are presented on the left and right sides of the figure, respectively.

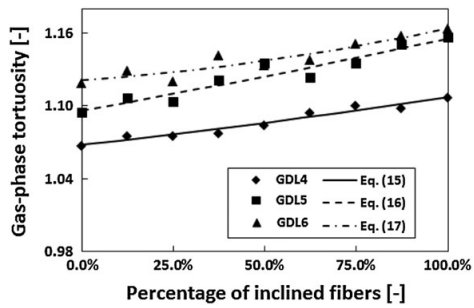

Figure 9. Gas-phase tortuosity values found for the modeled GDLs. The values found are disperse and fall between 1.067 and 1.163. Fitted curves are presented together with the data.

last mentioned percentages correspond to the coefficient of determination between the variables involved, that is tortuosity and percentage of inclined fibers.

There are several studies showing relationships, both theoretical and experimental, between porosity and gas-phase tortuosity in porous media [34]. Considering the values found in this work, a relation between the gas-phase tortuosity and porosity is proposed. Figure 10 shows the data found in this work for each corresponding porosity previously computed. It is possible to observe the approach of the gas-phase tortuosity to unity when the porosity approaches the same value.

Three different ways to fit the curves are applied to find a relationship describing the values found. One is based on a rational function, and the other two are considering the gas-phase tortuosity as a power function of the porosity. Such relationships are entitled as Rat1, Pow1, and Pow2. The mentioned relationships are evaluated for a range of porosity values and are depicted in Figure 11.

Table I shows the relationship for the obtained curves, depicted in Figure 11, with their corresponding parameters to evaluate the goodness of fit.

Considering the smallest sum of squares due to error and biggest R-square, that is, 2.846×10^{-3} and 0.8617, respectively. The most useful curve for prediction is the labeled as Pow1, and it is expressed as follows:

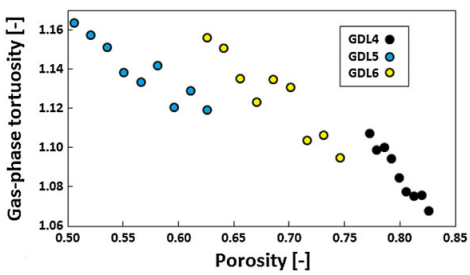

Figure 10. Gas-phase tortuosity versus porosity values found for the modeled 27 GDLs. [Colour figure can be viewed at wileyonlinelibrary.com]

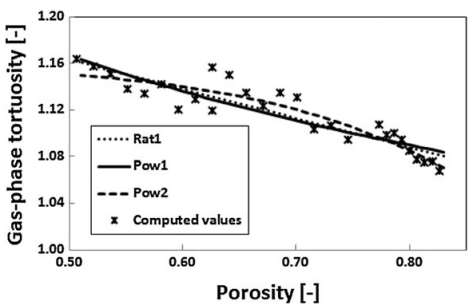

Figure 11. Fitting curve for data obtained in the current work. Three proposed curve fits are applied.

$$\tau_{gas-phase} = 1.042 * \varepsilon^{-0.175} \quad (18)$$

Notice that the proposed relationship is expected to predict values of the gas-phase tortuosity as a function of the porosity in the specified range of porosities in this study, that is 0.51–0.83. To validate the results, the computed porosity–tortuosity values are compared with previous studies in Figure 12.

In addition to Figure 12, the tortuosity values found in this work compared with the previously mentioned references show deviation errors falling in acceptable range, that is around 10%.

4.3. Effects on obstruction factor

Diffusion of gases is affected by the obstruction factor as shown in Eqn (5), and therefore, the performance of the FCs is affected. Taking into account the porosity and gas-phase tortuosity values found in the current work, the obstruction factor is computed as mentioned in Section 2. This value helps to determine the variation of the effective diffusion coefficient for the different GDLs. The computed obstruction factors are presented in Figure 13, where GDL4(0) is the reference to analyze the behavior.

Comparing GDL4(0) and GDL6(100), there is a difference of 44% in the factor to determine the effective diffusion. Considering Eqns (5) and (18), the effective diffusion coefficient can be estimated, as a function of

Table I. Empirical relationships for tortuosity values as a function of porosity with their corresponding SSE and *R*-square values.

Name	Empirical relationship	SSE ($\times 10^{-3}$)	*R*-square
Rat1	$\frac{-211\ \varepsilon + 1086}{\varepsilon + 842.3}$	3.582	0.8259
Pow1	$1.042\ \varepsilon^{-0.175}$	2.846	0.8617
Pow2	$-0.2223\ \varepsilon^{5.057} + 1.157$	4.103	0.8007

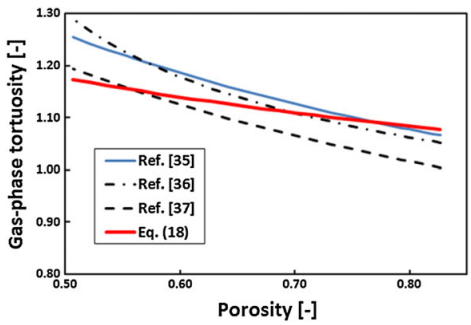

Figure 12. Gas-phase tortuosity vs. porosity. Relationships found in literature data [35–37] and relationship found in the present work. [Colour figure can be viewed at wileyonlinelibrary.com]

the porosity and diffusion coefficient, using the following expression:

$$D_{eff} = 0.9597 * \varepsilon^{1.175} D \tag{19}$$

where ε is the porosity, which can be evaluated in the range proposed in this work.

4.4. Effects on through-plane permeability

In order to apply the Darcy's law, to calculate the permeability, it has to be demonstrated that the pressure difference has no influence on the computed permeability. In other words, the permeability is a constant value independent of the pressure drop applied over a specific porous media domain. To demonstrate this, the permeability was calculated for GDL4(0), GDL5(0), and GDL6(0) subject to different pressure gradients. Computed permeability values are shown in Figure 14.

It is shown that the permeability is independent of pressure. TP permeabilities for all the modeled GDLs are determined. The minimum and maximum values of the TP permeability obtained are $2.72 \times 10^{-13}\,\mathrm{m}^2$ and $2.28 \times 10^{-12}\,\mathrm{m}^2$, respectively. These values correspond to an acceptable range if compared with previous studies [8,22]. Figure 15 presents the TP permeability found in the current work grouped for each selected fiber diameter.

Considering the values shown in Figure 15, and representing such values as a function of the inclined fibers in the model, expressions relating the TP permeability and the percentage of inclined rods can be proposed:

$$K_{GDL4}(\delta) = 3.619\ \times 10^{-17} * \delta^2 - 1.209\ \times 10^{-14} * \delta + 2.264\ \times 10^{-12}\ \left[\mathrm{m}^2\right] \tag{20}$$

$$K_{GDL5}(\delta) = 4.726\ \times 10^{-17} * \delta^2 - 1.415\ \times 10^{-14} * \delta + 1.439\ \times 10^{-12}\ \left[\mathrm{m}^2\right] \tag{21}$$

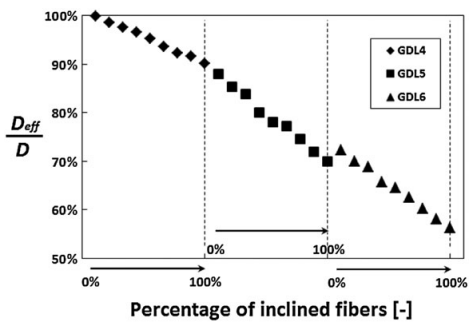

Figure 13. Obstruction factor variation for the different GDLs modeled in this work considering GDL4(0) as a reference value. For each GDL label, the percentage of inclined fiber goes from 0 to 100%.

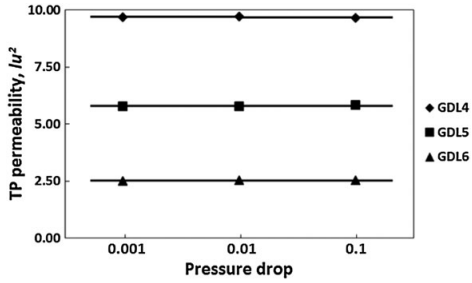

Figure 14. Permeability values obtained have no significant variation for different pressure gradients.

$$K_{GDL6}(\delta) = 2.084\ \times 10^{-17} * \delta^2 - 5.014 \times 10^{-15} * \delta + 5.993\ \times 10^{-13}\ \left[\mathrm{m}^2\right] \tag{22}$$

where δ represents the percentage of inclined rods as a percentage value. All the TP permeability values can be predicted using Eqns 20–23 in a percentage of 99%, 99%, and 86%, respectively.

The obtained TP permeability values are presented as a function of the porosity in Figure 16. It is clear that the relationship between these two variables is not linear.

To find an expression of the TP permeability values as a function of the porosity, fitting tools are applied. The best fit is given by a power function as follows:

$$K_{TP}(\varepsilon) = 4.27 \times 10^{-12} * \varepsilon^{3.988} \tag{23}$$

where ε is the porosity and the TP permeability is expressed in m^2.

There are several theoretical, numerical, and experimental studies to describe the relationship between the permeability and porosity. The most common expression to relate these two variables is the so-called Kozeny–Carman (KC) equation. The KC equation can be adapted according to the characteristics of the medium being

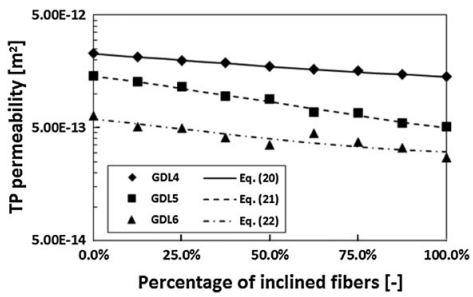

Figure 15. TP permeability values found in the current work. Notice that the vertical axis is in logarithmic scale. Fitted curves are presented together with the data.

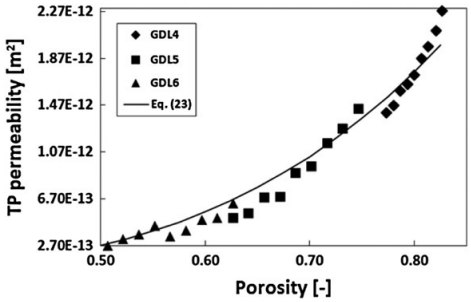

Figure 16. TP permeability increases in a non-linear fashion as a function of the porosity. Fitted curve is presented as a continuous line.

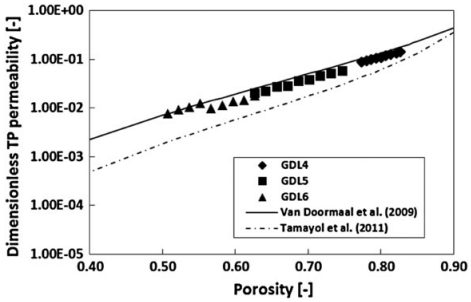

Figure 17. Dimensionless TP permeability as a function of the porosity compared with previous results.

described [38,39], and generally, some fitting parameters are determined. The adaptation of KC equation proposed by McGregor [40] relates the porosity, permeability, and the fiber diameter. This equation is expressed as follows:

$$K = \frac{{d_f}^2 \varepsilon^3}{16\, k_{\mathrm{KC}}\, (1-\varepsilon)^2} \tag{24}$$

where d_f represents the fiber diameter, ε is the porosity, and k_{KC} is the KC coefficient. Based on the values obtained in the current work, the KC coefficient was determined and presented in Table II. The KC coefficients computed in the current work fall in the range found in the experimental work performed by Gostick *et al.* [8]

The values of porosity and permeability were grouped with respect to the fiber diameter, and the KC coefficients were determined by using Eqn (24). The average and standard deviations for each group of data are presented in the last column in Table II.

The validation of the obtained results can be carried out by using the dimensionless TP permeability, that is the computed values of the TP permeability divided by the square of the fiber diameter. Figure 17 shows the values together with results from previous studies.

The results obtained in this study agree well with the results presented in Ref. [41,42] as depicted in Figure 17. To finalize the TP permeability section results, Figure 18 is presented. As an attempt to relate the computed variables, that is porosity, gas-phase tortuosity, and TP permeability,

Table II. KC coefficient based on the porosity, diameter, and permeability computed in this work.

Diameter [μm]	Porosity [−]	Permeability [$\times 10^{-12}$ m^2]	k_{KC}
4.00	0.83–0.77	2.28–1.41	7.33 ± 0.64
5.00	0.75–0.63	1.43–0.50	6.18 ± 0.51
6.00	0.63–0.51	0.64–0.27	5.41 ± 0.99

the two first variables are matched in the x–y plane, whereas the TP permeability is represented as a function by using a color scale. The dark red color represents high permeability values, while the dark blue color represents low TP permeabilities.

4.5. Effects on inertial coefficient

At low flow rates, the inertial effects are not considered, but if the flow rate values reach high levels, such effects have to be taken into account. Several studies related to the inertial coefficient in GDLs have been carried out [8,43] calculating this parameter by using the relationship proposed by Liu *et al.* [44]. It is expressed as follows:

$$\beta = 2.88 \times 10^{-6}\, \frac{\tau}{\varepsilon K} \tag{25}$$

where the constant (2.88×10^{-6}) is in length units. Although the mentioned studies use Eqn (25), they estimate the tortuosity values by the theoretical well-known Bruggeman equation. Such an estimation is not

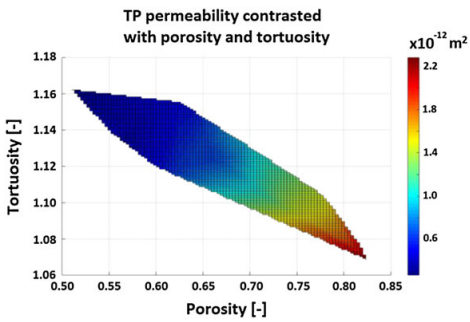

Figure 18. Porosity and gas-phase tortuosity depicted in the x–y plane. The TP permeability is represented by a color scale. [Colour figure can be viewed at wileyonlinelibrary.com]

Int. J. Energy Res. 2017; **41**:565–578 © 2016 John Wiley & Sons, Ltd.
DOI: 10.1002/er

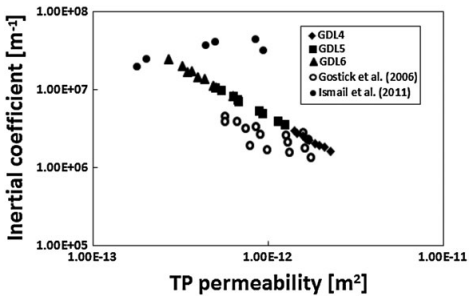

Figure 19. Inertial coefficient versus TP permeability compared with previous studies.

considered in the current work because all the involved parameters in Eqn (25) are computed from the proposed models. The inertial coefficient values versus the TP permeability are depicted in Figure 19.

According to Figure 19, the values computed agree with several values presented in Ref. [8,22]. In the previously mentioned works, the permeability values are determined experimentally from real GDLs. More investigations related to the inertial coefficient have to be carried out to reveal its importance in the PEFCs behavior.

5. CONCLUSIONS

A detailed analysis of porosity, gas-phase tortuosity, obstruction factor, TP permeability, and inertial factor for 27 different two-dimensional models of GDLs was carried out. For each GDL model, all the variables were computed after the fluid behavior through the porous media had been obtained by using the LBM.

To predict the porosity values as a function of the percentage of inclined rods in the porous medium, three different relationships were presented for a given fiber diameter. In a similar way, three equations relating gas-phase tortuosity values and inclined rods were proposed. The obtained values of porosity and gas-phase tortuosity agree well with previous studies, that is fall in a range of 10% of deviation error considering the minimum and maximum deviation. Additionally, an expression for the gas-phase tortuosity and porosity was addressed.

Porosity and gas-phase tortuosity have influence over the diffusion parameters. According to the definition of the obstruction factor, it was found that the ratio of the effective diffusion coefficient and the bulk diffusion coefficient may decrease until about 55% due to the porosity and gas-phase tortuosity variation given by the morphological changes in the microstructures.

Darcy's law was applied to determine the TP permeability in all the GDL models. Previously, it was assured the independence of the permeability of the pressure drop. Equations relating the TP permeability and the percentage of inclined rods for a given diameter were presented. As part of this study, an expression for determining the TP permeability values as a function of the porosity was given. Also, based on the KC equation, the KC coefficient was determined for a given fiber diameter. The computed TP permeabilities agree well in comparison with previous theoretical and experimental studies.

Finally, results related to the inertial coefficients were presented. Although the results showed similar behavior as previous studies, more studies related to this variable are as its incidence in PEFCs is not yet determined.

In our study, the inclination of the fibers during the modeling was established in 45°. This condition is a convenient choice due to the constant rectangular dimensions of our 2D domain. The incidence of the inclination different from 45° will be addressed in further studies as a 3D model is considered. In such conditions, the percentage of inclined fiber and diameter will not be the only variables to be considered, but the angle of inclination needs to be considered as well. This will allow carrying out comparisons between the different transport parameters in a wide range of fiber inclinations.

In general, for all the analyzed variables, the simplified assumptions presented in this work have shown good agreement with the behavior of the parameters in actual real GDLs. This study proposed several relationships which can be useful for future manufacturers using microprinting techniques and modeling researchers in predicting the different microstructural parameters according to the morphological conditions employed during the build up of the GDLs.

NOMENCLATURE

A	= area [L^2]
BGK	= Bhatnagar, Gross, and Krook
c	= bulk velocity
CFD	= computational fluid dynamics
CL	= catalyst layer
d	= diameter [L]
f	= particle distribution function
FC	= fuel cell
GDL	= gas diffusion layer
H	= height [L]
K	= Permeability [L^2]
KC	= Kozeny–Carman
L	= length [L]
LBE	= lattice Boltzmann equation
LBM	= lattice Boltzmann method
MD	= molecular dynamics
MEA	= membrane electrode assembly
P	= pressure [$ML^{-1}T^{-2}$]
PDF	= particle distribution function
PEFC	= proton exchange membrane fuel cell
q	= Darcy flux [LT^{-1}]
r	= position vector
t	= time

TP = through-plane
X = thickness of the material [L]

Chemicals

D = diffusion coefficient [$L^2 T^{-1}$]
D_{eff} = effective diffusion coefficient [$L^2 T^{-1}$]
H_2 = hydrogen
O_2 = oxygen
Q = diffusibility

Greek symbols

β = inertial coefficient [L^{-1}]
Δ = change of a property or variable
δ = percentage of inclined rods
ε = porosity [−]
μ = dynamic viscosity [$ML^{-1} T^{-1}$]
ρ = density [ML^{-3}]
Σ = summatory
τ = tortuosity [−]
τ' = relaxation parameter for LBE
φ = diameter [L]
Ω = collision operator in Eqn (9)
∇ = gradient symbol

Subscripts

KC = Kozeny–Carman constant
2D = two-dimensional case
Fluid = refer to a fluid component
Solid = refer to a solid component
actual = refer to the actual distance
shortest = refer to the shortest distance
i = refer to the ith x position
j = refer to the jth y position
k = refer to the number of linked velocities in Eqn (9)
mag = refer to the magnitude vector
x = refer to the x direction
y = refer to the y direction
z = refer to the z direction
f = to define the fiber diameter

Superscripts

eq = refer to equilibrium particle distribution

ACKNOWLEDGEMENTS

Financial support for this work comes from Senescyt and Espol (Ecuador), which is very grateful. Also, the authors want to thank to VINNOVA (2015-01485) and the National Natural Science Foundation of China (Grant no. 51550110238).

REFERENCES

1. Hörmandinger G, Lucas NJ. An evaluation of the economics of fuel cells in urban buses. *International Journal of Energy Research* 1997; **21**(6):495–525.
2. Mehta V, Cooper JS. Review and analysis of PEM fuel cell design and manufacturing. *Journal of PowerSources* 2003; **114**(1):32–53.
3. Mukherjee PP, Wang CY. Polymer electrolyte fuel cell modeling–a pore-scale perspective. *Progress in Green Energy* 2011; 181–221.
4. Espinoza, M., Sundén, B., & Andersson, M. (2014). Highlights of fuel cell modeling from a lattice Boltzmann method point of view. In ASME 2014 International Mechanical Engineering Congress and Exposition (pp. V06AT07A058-V06AT07A058). American Society of Mechanical Engineers.
5. Espinoza M, Andersson M, Yuan J, Sundén B. Compress effects on porosity, gas-phase tortuosity, and gas permeability in a simulated PEM gas diffusion layer. *International Journal of Energy Research* 2015; **39**(11):1528–1536.
6. Froning D, Yu J, Gaiselmann G, Reimer U, Manke I, Schmidt V, Lehnert W. Impact of compression on gas transport in non-woven gas diffusion layers of high temperature polymer electrolyte fuel cells. *Journal of Power Sources* 2016; **318**:26–34.
7. Bresciani F, Casalegno A, Varisco G, Marchesi R. Water transport into PEFC gas diffusion layer: experimental characterization of diffusion and permeation. *International Journal of Energy Research* 2014; **38**(5):602–613.
8. Gostick JT, Fowler MW, Pritzker MD, Ioannidis MA, Behra LM. In-plane and through-plane gas permeability of carbon fiber electrode backing layers. *Journal of Power Sources* 2006; **162**(1):228–238.
9. Ahmed DH, Sung HJ, Bae J. Effect of GDL permeability on water and thermal management in PEMFCs—I. Isotropic and anisotropic permeability. *International Journal of Hydrogen Energy* 2008; **33**(14):3767–3785.
10. Sun K, Wei TS, Ahn BY, Seo JY, Dillon SJ, Lewis JA. 3D printing of interdigitated Li-ion microbattery architectures. *Advanced Materials* 2013; **25**(33):4539–4543.
11. Sherwood TK, Pigford RL, Wilke CR. *Mass Transfer*. McGraw-Hill: New York, 1975; 39–43.
12. Boving TB, Grathwohl P. Tracer diffusion coefficients in sedimentary rocks: correlation to porosity and

hydraulic conductivity. *Journal of Contaminant Hydrology* 2001; **53**(1):85–100.
13. Tomadakis MM, Sotirchos SV. Transport properties of random arrays of freely overlapping cylinders with various orientation distributions. *The Journal of Chemical Physics* 1993; **98**(1):616–626.
14. Iversen N, Jørgensen BB. Diffusion coefficients of sulfate and methane in marine sediments: influence of porosity. *Geochimica et Cosmochimica Acta* 1993; **57**(3):571–578.
15. Nabovati A, Sousa ACM. Fluid flow simulation in random porous media at pore level using the lattice Boltzmann method. *Journal of Engineering Science and Technology* 2007; **2**(3):226–237.
16. Mason EA, Malinauskas AP, Evans Iii RB. Flow and diffusion of gases in porous media. *The Journal of Chemical Physics* 1967; **46**(8):3199–3216.
17. Van Brakel J, Heertjes PM. Analysis of diffusion in macroporous media in terms of a porosity, a tortuosity and a constrictivity factor. *International Journal of Heat and Mass Transfer* 1974; **17**(9):1093–1103.
18. Wiedenmann D, Keller L, Holzer L, Stojadinović J, Münch B, Suarez L, *et al.*. Three-dimensional pore structure and ion conductivity of porous ceramic diaphragms. *AICHE Journal* 2013; **59**(5):1446–1457.
19. Froning D, Gaiselmann G, Reimer U, Brinkmann J, Schmidt V, Lehnert W. Stochastic aspects of mass transport in gas diffusion layers. *Transport in Porous Media* 2014; **103**(3):469–495.
20. Darcy H. *Les Fontaines Publiques de la Ville de Dijon*. Victor Dalmont: Paris, 1856.
21. Forchheimer, P. (1914). Hydraulik. BG Teubner. Leipzig and Berlin, Chap. 15, Secc. pp. 116-118.
22. Ismail MS, Borman D, Damjanovic T, Ingham DB, Pourkashanian M. On the through-plane permeability of microporous layer-coated gas diffusion layers used in proton exchange membrane fuel cells. *International Journal of Hydrogen Energy* 2011; **36**(16):10392–10402.
23. Amara MEAB, Nasrallah SB. Numerical simulation of droplet dynamics in a proton exchange membrane (PEMFC) fuel cell micro-channel. *International Journal of Hydrogen Energy* 2015; **40**(2):1333–1342.
24. Succi S, Benzi R, Higuera F. The lattice Boltzmann equation: A new tool for computational fluid-dynamics. *Physica D: Nonlinear Phenomena* 1991; **47**(1–2):219–230.
25. Bhatnagar PL, Gross EP, Krook M. A model for collision processes in gases. I. Small amplitude processes in charged and neutral one-component systems. *Physical Review* 1954; **94**(3):511–525.
26. Gas diffusion layer (GDL) property sheets, FuelCellsEtc. Last access: 2016/05/02. http://fuelcellsetc.com/store/DS/gas-diffusion-layer-properties.pdf
27. Zou Q, He X. On pressure and velocity boundary conditions for the lattice Boltzmann BGK model. *Physics of Fluids* (1994-present) 1997; **9**(6):1591–1598.
28. Hirt L, Ihle S, Pan Z, Dorwling-Carter L, Reiser A, Wheeler JM, Spolenak R, Vörös J, Zambelli T. Template-free 3D microprinting of metals using a force-controlled nanopipette for layer-by-layer electrodeposition. *Advanced Materials* 2016; **28**:2311–2315.
29. Laleian A, Valocchi AJ, Werth CJ. An incompressible, depth-averaged lattice Boltzmann method for liquid flow in microfluidic devices with variable aperture. *Computation* 2015; **3**(4):600–615.
30. Portinari M. 2015 2-D and 3-D verification and validation of the lattice Boltzmann methods.
31. Singhal SC. Advances in solid oxide fuel cell technology. *Solid State Ionics* 2000; **135**(1):305–313.
32. Tsuchiya H, Kobayashi O. Mass production cost of PEM fuel cell by learning curve. *International Journal of Hydrogen Energy* 2004; **29**(10):985–990.
33. Kitahara T, Konomi T, Nakajima H. Microporous layer coated gas diffusion layers for enhanced performance of polymer electrolyte fuel cells. *Journal of Power Sources* 2010; **195**(8):2202–2211.
34. Shen L, Chen Z. Critical review of the impact of tortuosity on diffusion. *Chemical Engineering Science* 2007; **62**(14):3748–3755.
35. Millington RJ. Gas diffusion in porous media. *Science* 1959; **130**(3367):100–102.
36. Koponen A, Kataja M, Timonen J. Permeability and effective porosity of porous media. *Physical Review E* 1997; **56**(3):3319–3325.
37. Kim IC, Torquato S. Diffusion of finite-sized brownian particles in porous media. *The Journal of Chemical Physics* 1992; **96**(2):1498–1503.
38. Xu P, Yu B. Developing a new form of permeability and Kozeny–Carman constant for homogeneous porous media by means of fractal geometry. *Advances in Water Resources* 2008; **31**(1):74–81.
39. Ismail MS, Hughes KJ, Ingham DB, Ma L, Pourkashanian M. Effect of PTFE loading of gas diffusion layers on the performance of proton exchange membrane fuel cells running at high-efficiency operating conditions. *International Journal of Energy Research* 2013; **37**(13):1592–1599.
40. McGregor R. The effect of rate of flow on rate of dyeing II–the mechanism of fluid flow through textiles and its significance in dyeing. *Journal of the Society of Dyers and Colourists* 1965; **81**(10):429–438.
41. Van Doormaal MA, Pharoah JG. Determination of permeability in fibrous porous media using the lattice Boltzmann method with application to pem fuel cells. *International Journal for Numerical Methods in Fluids* 2009; **59**(1):75–89.

42. Tamayol A, Bahrami M. Transverse permeability of fibrous porous media. *Physical Review E* 2011; **84**(4, 046314).
43. Ismail MS, Damjanovic T, Hughes K, Ingham DB, Ma L, Pourkashanian M, Rosli M. Through-plane permeability for untreated and PTFE-treated gas diffusion layers in proton exchange membrane fuel cells. *Journal of Fuel Cell Science and Technology* 2010; **7**(5, 051016).
44. Liu X, Civan F, Evans RD. Correlation of the non-Darcy flow coefficient. *Journal of Canadian Petroleum Technology* 1995; **34**(10):50–54.

Paper IV

ECS Transactions, 75 (14) 521-530 (2016)
10.1149/07514.0521ecst ©The Electrochemical Society

Impact on Diffusion Parameters Computation in Gas Diffusion Layers, Considering the Land/Channel Region, Using the Lattice Boltzmann Method

M. Espinoza-Andaluz[a,b], B. Sundén[a] and M. Andersson[a]

[a] Department of Energy Sciences, Lund University, Lund, SE-221 00, Sweden
[b] Escuela Superior Politécnica del Litoral, ESPOL, PO Box 09-01-5863 Guayaquil, Ecuador

Diffusion phenomena through the gas diffusion layer (GDL) at the microscale are one of the most complex physical phenomena to be described in proton exchange fuel cell (PEFC) numerical models. Predicting transport parameter behavior in GDLs is a valuable stage to propose micro-architectural designs, which can improve the efficiency and performance of fuel cells (FCs). The purpose of this paper is to propose an expression to estimate parameters involved in the diffusion process such as gas-phase tortuosity and effective diffusion coefficient when the effects of the land/channel region are considered. Three-dimensional GDL approximations are generated considering real characteristics of micro-porous layers employed in FCs. The fluid behavior through the porous media is simulated using the Lattice Boltzmann method (LBM), and the mentioned parameters are studied. The incidence of the land/channel presence over the gas-phase tortuosity is determined, and its effects over the effective diffusion are estimated.

Introduction

There are several multi-physical phenomena that occur inside the FCs during the energy conversion process. These phenomena occur when the reactant gases pass through the diffusion media present in the FC layers, i.e., gas diffusion layer (GDL), catalyst layer (CL) or electrode support layer, and reach the active sites. Scanning electron microscope images of the porous media can be observed in (1) and (2). In PEFCs, the reactant gases must flow in the direction from the flow plates, specifically from the channel, to the active sites present in the interface CL/electrolyte to allow the electrochemical reactions. When the electrochemical reaction is carried out, the hydrogen molecules (H_2) are oxidized, the positive charge passes through the electrolyte, and the free electrons flow to the current collectors. These free electrons flow towards an external circuit, where they can be used in electric appliances. A simplified scheme of the different components of the proton exchange fuel cell (PEFC) anode is presented in Figure 1.

Given the anisotropic and morphological characteristics of the GDLs, a deep understanding of the fluid behavior through the diffusion media will help to improve the efficiency and to predict the performance of the FCs. However, describing the fluid flow through the diffusion media at the microscale is not an easy task, and computational approximations of this phenomenon can describe the fluid behavior through the

mentioned layers in a better way. From a microscale point of view several models related to FCs have been implemented using the LBM (3) - (5).

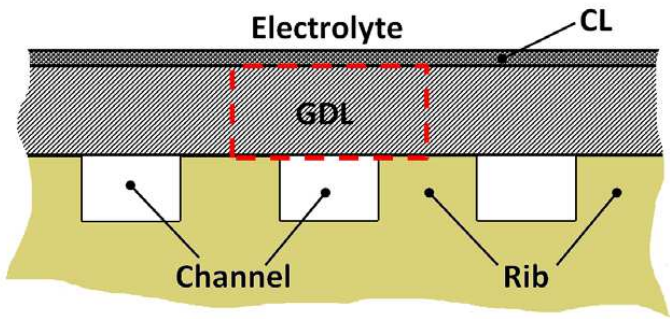

Figure 1. Schematic representing the different components in a PEFC anode. The region enclosed the dotted lines represents the modeled volume. Details about the modeled GDL are given in the Methodology section.

In porous media a fundamental property to be computed is the porosity, which represents the percentage of the total volume that can be occupied by the fluid. It can be determined numerically as:

$$\varepsilon = \frac{Void\ Volume}{Total\ Volume} \quad [1]$$

It is a dimensionless property, and for GDLs the porosity are commonly between 0.60 and 0.90 (5). Considering the anisotropic characteristic of the GDLs, the gas-phase tortuosity plays an important role in the gas diffusion phenomena. The gas-phase tortuosity is a measure of complexity of the medium, and it can be computed as (6):

$$\tau_{gas} = \frac{\sum_{i,j} u_{mag}(i,j)}{\sum_{i,j} |u_y(i,j)|} \quad [2]$$

where u_{mag} represents the magnitude of the fluid velocity through the porous medium, u_y corresponds to the velocity in the main flow direction, i.e., *y*-direction. The gas-phase tortuosity is a dimensionless value, and in any porous medium is expected to be always bigger than unity. Taking into account the two mentioned properties, and based on the study carried out by Mason et al. (7), the ratio between effective diffusion coefficient and the diffusion coefficient can be determined as:

$$\frac{D_{eff}}{D} = \frac{\varepsilon}{\tau_{gas}} \quad [3]$$

Most of the GDL models estimate the right hand side of equation [3] by means of the Bruggeman approximation (8), i.e., $\varepsilon^{3/2}$. However, in the current work the mentioned approximation is not used since all the porosity and gas-phase tortuosity values are computed for each GDL.

The purpose of this study is to determine the impact of the land/channel region over the diffusion parameters such as gas-phase tortuosity and the effective diffusion

coefficient. The modeled GDLs are generated based on a realistic porous material used in FCs considering the layer and fiber thickness as a constant value. The fluid flow behavior through the GDLs is obtained by the LBM, and the diffusion parameters are computed for each land/channel ratio. The simulated GDLs as well as the fluid behavior are computed in Matlab® R2015a, the complete code is developed by the authors. The rest of the paper is divided as follows: The second section is mainly devoted to the applied methodology, boundary conditions and GDL reconstruction. The third section presents the results obtained and the proposed expressions for the diffusion parameters. Finally, the conclusions are given.

Methodology

The LBM has been applied to compute the fluid flow behavior through the GDLs. Since this study is a three-dimensional case, the D3Q19 scheme is implemented, i.e., there are nineteen linked velocities connecting the lattice neighbors. In this study, one section of the complete GDL is considered as depicted in Figure 2.

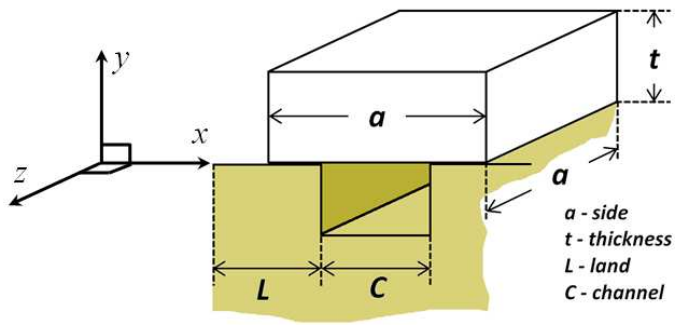

Figure 2. Schematic of the modeled volume considered in the current study. The cross-sectional area is given by a^2, and t is the thickness of the layers. L and C are the width of the land and channel, respectively. The inlet velocity is initially established in y-direction in the channel region.

The volume representing the GDLs is given by a^2 times t, which are constant during all the simulations. The inlet velocity through the channel region is kept at low values, considering that in GDLs the Reynolds number is expected to be lower than 10^{-4} respect to the fiber diameter (9). Each digitally generated GDL is subjected to the inlet flow only in the channel region, such inlet velocity is established in the y-direction. For the outlet boundary condition (upper side of the volume in Figure 2) the second derivative approximation is considered. Finally, on the other four sides of the volume, periodic boundary conditions are implemented. The digital re-construction of the GDLs is based on Figure 3. It can be described as an array of fibers arranged in a random manner, the fibers are aligned in the in-plane direction. In each simulation, one land/channel ratio is evaluated for their corresponding comparison. The first simulation is given when the land/channel ratio is not considered, and then the land/channel ratio is increased in steps of 0.1 until to reach the unity.

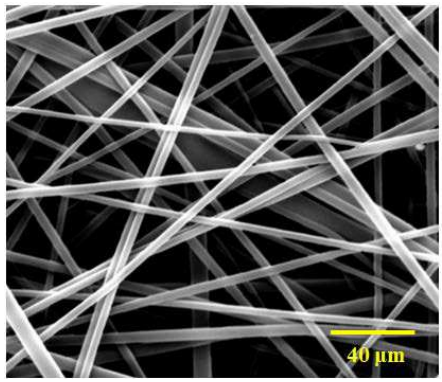

Figure 3. SEM image of a GDL used for gas diffusion media in FCs. The arrange of the fibers represents the patron considered for generating the GDLs in the current work. Credits: Dr Tingshuai Li, UESTC, China.

Fiber diameter, porosity and the length of the land and channel region are established from the values found in the literature: (4), (5), (10) and (11). For simulation purposes, the GDL fibers are considered infinitely long, i.e., limited only by the model domain. Values for the cross-sectional area, layer thickness and porosity are given in Table I.

TABLE I. Characteristics of the modeled domain.

	Length	**Values**
a	1600 µm	-
t	200 µm	-
L/C	-	No presence, 0.1 to 1 in steps of 0.1
Porosity	-	0.7416 – 0.7693

It is important to notice that the thickness of the GDLs in practical applications can range from dozens of micro-meters up to around 400 µm. However, the selected GDL thickness of this work corresponds to an average value. The fiber diameter is considered as a constant value for the whole domain.

Results and discussion

The first result obtained with the model is the porosity value. The fibers are placed randomly over the volume for emulating the GDLs, and due to the fact that the digital process determines the number of fibers, which can be different at each array. The porosity varies along the thickness as presented in Figure 4. The porosity is computed every 10 µm along the flow direction, the figure shows the porosity values for one of the samples.

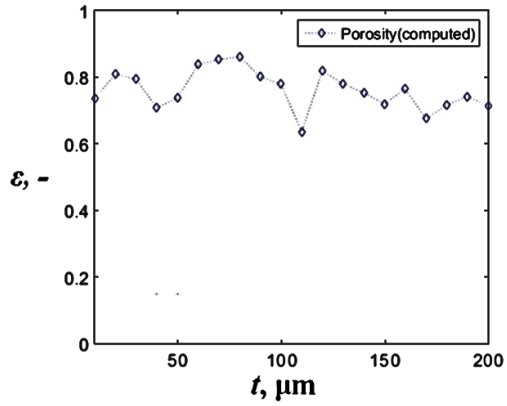

Figure 4. Porosity values along the flow direction for one of the GDL samples.

For the given example in Figure 4, the average porosity of the complete domain is 0.7620. The average porosity, corresponding to the porosity of the whole domain, for all GDLs is computed. The mean and standard deviation for all the GDLs are calculated to: 0.7555 ± 0.0139. A measure of dispersion of the data relative to the mean is the coefficient of variation, and it is defined as:

$$C_v = \frac{standard\ deviation}{mean\ value} \quad [4]$$

Considering the porosity values obtained from the GDLs, it can be seen that the dispersion of the computed porosity from the mean is not considerable since the coefficient of variation is low, i.e., 1.839 %. The average porosity for all the GDL samples is shown in Figure 5.

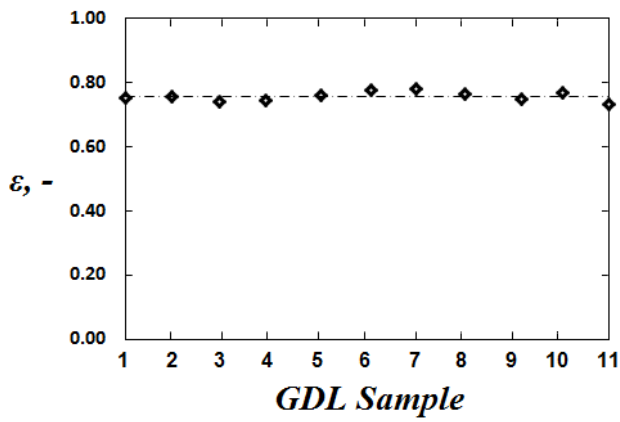

Figure 5. Computed porosity values for all the GDLs used in this work. There is no considerable dispersion in porosity values. GDL 1 corresponds to the GDL in which no L/C region is considered, whereas that in GDL 6 the L/C ratio is 0.5. For GDL 11, the L/C region is unity.

For GDL 1, i.e., the GDL sample in which no L/C region is considered, the gas-phase tortuosity is 1.1431 with a porosity of 0.7496. These values may be compared with

previous studies in which the tortuosity-porosity relationship is proposed. Previous proposed relationships, current computed porosity and gas-phase tortuosity and deviation error are presented in Table II.

TABLE II. Comparison of gas-phase tortuosity and porosity values of GDL 1 with previous proposed relationships.

Tortuosity-porosity relationship (Ref.)		Computed porosity GDL 1	Gas-phase tortuosity calculated with previous relationships	Computed gas-phase tortuosity GDL 1	Deviation error in gas-phase tortuosity values
$\tau = \frac{3-\varepsilon}{2}$	(12)		1.1252		+1.77%
$\tau = 2-\varepsilon$	(13)		1.2504		-8.42%
$\tau = \varepsilon^{-\frac{1}{2}}$	(8)	0.7476	1.1550	1.1431	-0.86%
$\tau = \varepsilon^{-\frac{1}{3}}$	(14)		1.1008		+4.02%
$\tau = 1 - Ln\,\varepsilon$	(15)		1.2882		-11.1%

The last column of Table II shows the deviation error between the gas-tortuosity value computed in the current work and the expected values using previous proposed relationships. With a maximum deviation of 12%, a reasonable agreement of the gas-phase tortuosity computation was attained.

The fluid behavior through the GDLs was computed using the LBM. Figures 6, 7 and 8 show the steady state solution of the fluid flow at three selected positions along the flow direction. As expected, the presence/absence of the land/channel region influences the fluid distribution. The scale bar in the following figures represents the normalized velocity values for the corresponding lattice element involved in the calculations where 1.0 represents the highest velocity and 0.0 the lowest velocity.

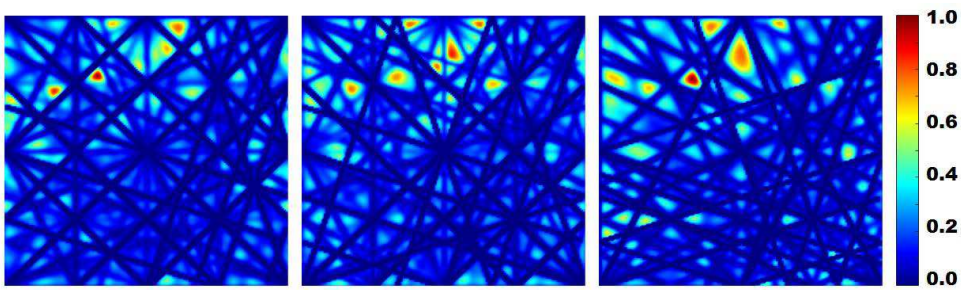

Figure 6. Cross-sectional view of the fluid distribution at three different positions when the land/channel region is not considered. Lower velocities are represented by blue color regions.

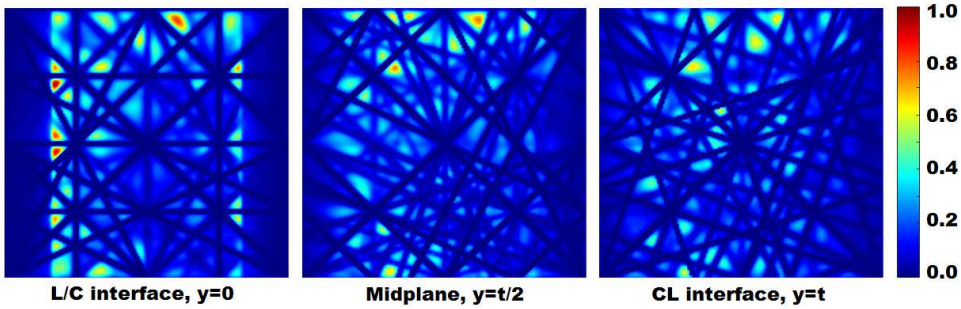

Figure 7. Cross-sectional view of the fluid distribution at three different positions when the land/channel ratio is 0.5.

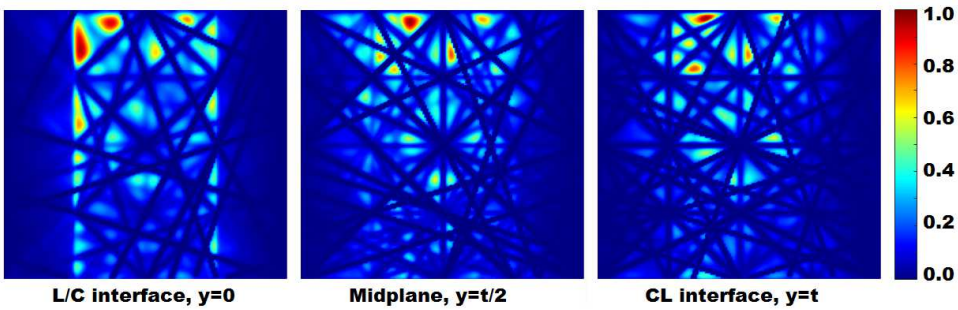

Figure 8. Cross-sectional view of the fluid distribution at three different positions when the land/channel ratio is 1.

Observing the previous figures, it is clear the incidence of the L/C region over the fluid distribution. The impact is observable not only in the fluid distribution near the flow plates (L/C interface), but it is also considerable near the electrolyte (CL interface). The effect of the L/C ratio on the gas-phase tortuosity and the diffusion coefficient is estimated by computing these variables for different L/C ratios. Gas-phase tortuosity values as a function of the L/C ratio is presented in Figure 9.

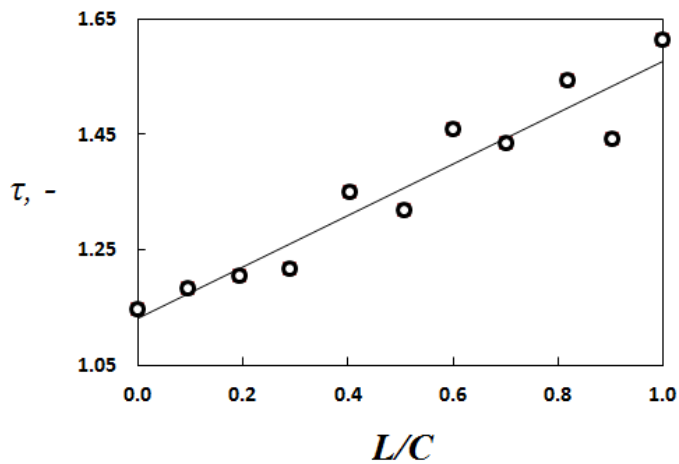

Figure 9. Gas-phase tortuosity behavior relative to the land/channel ratio.

According to the obtained values, if the land/channel region increases, the gas-phase tortuosity increases. Fitting the values to a curve, the expression that relates the gas-phase tortuosity and the land/channel region is approximated as:

$$\tau_{gas} = \tau_o + 0.4496 \left(\frac{L}{C}\right) \quad [5]$$

where τ_o represents the gas-phase tortuosity of the GDL when the L/C region is not considered, i.e., the gas-phase tortuosity of the GDL when the FC has not been assembled. The fitting gives to τ_o the value of 1.13, and the goodness of the fit is such as R-square is 0.909 that means that around 91 % of the gas-phase tortuosity values can be explained by the proposed relationship.

According to Van Brakel and P. M. Heertjes (14), the ratio between the effective diffusion coefficient and the diffusion coefficient can be named diffusibility (Q), and a simple approximation for Q is the ratio between the porosity and the gas-phase tortuosity. Similar to the comparison presented in Table II, the diffusibility computed in the current work is compared with previous studies. Table III presents several diffusibility-porosity relationships, and the diffusibility computed in this study.

TABLE III. Comparison of computed diffusibility of GDL 1 with previous proposed relationships.

Diffusibility-porosity relationship (Ref.)		Diffusibility calculated with previous relationships	Computed Diffusibility GDL 1	Deviation error in Diffusibility values
$Q = \frac{2\,\varepsilon}{3-\varepsilon}$	(16, 17)	0.6638	0.6540	-1.48%
$Q = \varepsilon^{\frac{3}{2}}$	(8, 18)	0.6464		+1.18%
$Q = \frac{\varepsilon}{1-\frac{1}{2}Ln\,\varepsilon}$	(19)	0.6527		+0.21%
$Q = \varepsilon^{\frac{4}{3}}$	(20)	0.6785		-3.61%

The last column of Table III shows the deviation error between the diffusibility value computed in the current work and the expected values using previous proposed relationships. With a deviation error ranging in ±5%, a reasonable agreement of the diffusibility computation was attained. The impact of the L/C region over Q is presented in Figure 10.

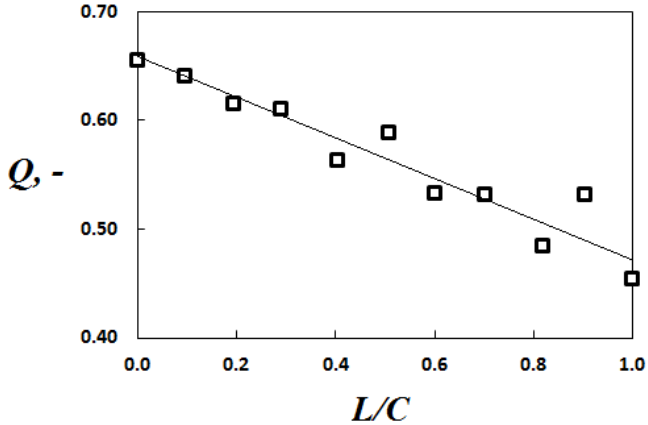

Figure 10. Diffusibility behavior relative to the land/channel ratio.

An expression that relates the diffusibility and the L/C ratios is obtained by fitting the computed values, and is expressed as follows:

$$Q = Q_o - 0.1839\left(\frac{L}{C}\right) \quad [6]$$

where, according to the fitted curve, Q_o is 0.6561. The R - square value found in this fitting is similar to the previous relationship, and therefore; the prediction of diffusibility using equation [6] is reasonably accurate.

The variation from the fitted curve observed in Figure 9 and 10 occur because the porous media representing the GDLs used to mimicking the fluid behavior are different. Although all the GDL samples are different, they are created following the same algorithm generation, and therefore the porosity variations are not considerable as shown in Figure 5.

It is important to notice that although the chanel region has been considered for computing the gas-phase tortuosity and diffusibility, the compression of the GDL when the assembly is effected has not been taken into account. If this scenario is considered, the porosity will vary non-uniformly, i.e., the porosity change rate in the land region is bigger than in the chanel region, and therefore; the gas-phase tortuosity and diffusibility will have different behavior.

Conclusions

The impact over diffusion parameters such as gas-phase tortuosity and diffusibility when the land/channel region is considered in GDL models has been estimated. Characteristics such as porosity, layer thickness, and fiber thickness of the GDLs are based on real porous layers for FCs. The fluid behavior through ten digitally generated GDLs has been obtained using the LBM approach, and relationships to approximate the gas-phase tortuosity and diffusibility taken into consideration the L/C ratio has been proposed.

Acknowledgments

Financial support for this work comes from Senescyt and Espol (Ecuador), which is very grateful. Also, the authors want to thank to VINNOVA (2015-01485) and the National Natural Science Foundation of China (Grant No. 51550110238).

References

1. Y. Chen, J. Bunch, T. Li, Z. Mao, and F. Chen, *Journal of Power Sources*, **213**, 93-99 (2012).
2. T. S. Li, C. Xu, T. Chen, H. Miao and W. G. Wang, *Journal of Solid State Electrochemistry*, **15**(6), 1077-1085 (2011).
3. M. Espinoza, B. Sundén, M. Andersson and J. Yuan, *ECS Transactions*, **65**(1), 59-73 (2015).
4. M. Espinoza, M. Andersson, J. Yuan and B. Sundén, *International Journal of Energy Research*, **39**(11), 1528-1536 (2015).
5. M. Espinoza, B. Sundén and M. Andersson, *In ASME 2014 International Mechanical Engineering Congress and Exposition*, (pp. V06AT07A058-V06AT07A058) (2014).
6. A. Nabovati and A. C. M. Sousa, *Journal of Engineering Science and Technology*, **2**(3), 226-237 (2007).
7. E. A. Mason, A. P. Malinauskas and R. B. Evans III, *The Journal of Chemical Physics*, **46**(8), 3199-3216 (1967).
8. V. D. Bruggeman, *Annalen der physik*, **416**(7), 636-664 (1935).
9. D. Froning, G. Gaiselmann, U. Reimer, J. Brinkmann, V. Schmidt and W. Lehnert, *Transport in porous media*, **103**(3), 469-495 (2014).
10. N. Limjeerajarus and P. Charoen-Amornkitt, *International Journal of Hydrogen Energy*, **40**(22), 7144-7158 (2015).
11. M. F. Mathias, J. Roth, J. Fleming and W. Lehnert, *Handbook of fuel cells* (2003).
12. K. A. Akanni, J. W. Evans and I. S. Abramson, *Chemical Engineering Science*, **42**(8), 1945-1954 (1987).
13. E. E. Petersen, *AIChE Journal*, **4**(3), 343-345 (1958).
14. J. Van Brakel and P. M. Heertjes, *International Journal of Heat and Mass Transfer*, **17**(9), 1093-1103 (1974).
15. M. M. Tomadakis and S. V. Sotirchos, *The Journal of chemical physics*, **98**(1), 616-626 (1993).
16. D.A. de Vries, *Meded. Landb. Hogesch. Wageningen*, **52**, pp. 1–73 (1952).
17. G.H. Neale, W.K. Nader, *A.I.Ch.E. Jl*, **19**, pp. 112–119 (1973).
18. T.J. Marshall, *Nature, Lond.*, **180**, pp. 664–665 (1957).
19. H.L. Weissberg, *J. Appl. Phys.*, **34**, pp. 2636–2639 (1963).
20. R.J. Millington, *Science, N.Y.*, **130**, pp. 100–102 (1959).

Paper V

INTERNATIONAL JOURNAL OF HYDROGEN ENERGY XXX (2017) 1–10

Available online at www.sciencedirect.com

ScienceDirect

journal homepage: www.elsevier.com/locate/he

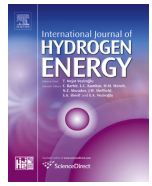

Comparing through-plane diffusibility correlations in PEFC gas diffusion layers using the lattice Boltzmann method

Mayken Espinoza-Andaluz [a,b,*], *Martin Andersson* [a], *Bengt Sundén* [a]

[a] *Lund University, Ole Römers väg 1, PO Box 118, 22100 Lund, Sweden*
[b] *Escuela Superior Politécnica del Litoral, Km 30.5 Vía Perimetral, PO Box 09-01-5863, Guayaquil, Ecuador*

ARTICLE INFO

Article history:
Received 19 December 2016
Received in revised form
2 February 2017
Accepted 13 February 2017
Available online xxx

Keywords:
Gas diffusion layer
Diffusibility
Lattice Boltzmann method
Polymer electrolyte fuel cell
Transport parameters

ABSTRACT

One of the key elements in a polymer electrolyte fuel cell (PEFC) is the gas diffusion layer (GDL). The GDL offers mechanical support to the cell and provides the medium for diffusing the reactant gases from the flow plates to the electrolyte enabling the electrochemical reactions, and therefore the energy conversion. At the same time, it has the task of transporting the electrons from the active sites, near to the electrolyte, towards the flow plates.

Describing the fluid flow and mass transport phenomena through the GDLs is not an easy task not only because of their complex geometries, but also because of these phenomena occur at microscale levels. Most of the PEFC models at cell scale make assumptions about certain microscale transport parameters, assumptions that can make a model less close to the reality. The purpose of this study is to analyze five different proposed correlations to estimate the through-plane (TP) diffusibility of digitally created GDLs and using lattice Boltzmann (LB) models. The correlations are ranked depending on their precision, accuracy and symmetry. The results show that the best estimation is given when the porosity and gas-phase tortuosity are taken into account in the correlation.

Introduction

Due to its clean nature and high efficiency, fuel cells (FCs) appear among the most convenient devices to reduce the emission of polluting gases to the environment. This device converts the chemical energy present in the supplied fuel into electrical and thermal energy by means of electrochemical reactions that occur in the active site regions inside the device. There are different types of FCs which can be grouped according to different variables such as: operating temperature, output power, applicability or electrolyte. The last mentioned characteristic is the most commonly used parameter to classify them.

According to the Fuel Cell Technologies Market Report [1], the polymer electrolyte fuel cell (PEFC) is the most widely applied FC type around the world, especially because of its applicability in the transportation market, mobile and stationary applications. Although the use of PEFC around the world has been increasing during the last years, its presence in comparison with other technologies is still small. This is mainly because of the material and production cost of the

* *Corresponding author*. Department of Energy Sciences, Lund University, PO Box 118, 22100 Lund, Sweden.
E-mail addresses: Mayken.Espinoza_Andaluz@energy.lth.se, masespin@espol.edu.ec (M. Espinoza-Andaluz).
http://dx.doi.org/10.1016/j.ijhydene.2017.02.096

Please cite this article in press as: Espinoza-Andaluz M, et al., Comparing through-plane diffusibility correlations in PEFC gas diffusion layers using the lattice Boltzmann method, International Journal of Hydrogen Energy (2017), http://dx.doi.org/10.1016/j.ijhydene.2017.02.096

PEFCs. A deep understanding of the complexity inside the PEFCs will help to find suitable materials and better microstructural configurations which lead to a better performance and cost reduction.

In brief, a PEFC consists of several layers, each one providing different mechanical, electrical and thermal support to the system. The electrolyte is a polymer membrane which allows only the passage of the positive ions resulting from the oxidation of hydrogen (H_2) molecules. This hydrogen oxidation is carried out in the active sites on the anode side of the FC. In a PEFC the hydrogen acts as a fuel, but before reaching the active sites present in the boundary between the catalyst layer (CL) and the electrolyte; it has to flow through a complex medium known as the gas diffusion layer (GDL). The fluid and mass transport phenomena through the GDL are concerns of the present study.

The morphological and complexity of GDLs make their study a non-easy task from an experimental point of view, especially because of the characteristic lengths involved. In this sense, a computational study at microscale can give us detailed information about the fluid and mass transport through this complex geometry. Fig. 1 shows a SEM (scanning electron microscopy) image of a GDL that is considered in this study.

There are three main types of GDL, carbon-paper, carbon-cloth and non-woven. Independently of the GDL type, this layer provides mechanical support to the PEFCs and is responsible for conduction of the free electrons from the active sites to the current collector. At the same time, the GDL plays an important role in the diffusion of the reactant gases from the flow plates to the three phase boundaries (TPB).

Although there are plenty of models describing a single channel or the whole PEFCs [2–5], most of these models rely on assumptions regarding the microscale behavior of the fluid and mass transfer through the layers. To obtain a detailed description of the phenomena through digitally created GDLs, the lattice Boltzmann method (LBM) is applied. LBM has been widely used to mimic the fluid and mass transport phenomena in different layers of PEFCs [6–8]. Froning et al. investigated the effect of compressed GDLs over the permeability and gas-phase tortuosity using the LBM [9]. A study of microstructural parameters in GDLs was carried out using a 2D lattice Boltzmann (LB) fluid model [10], and García-Salaberri et al. presented a detailed study about the effective diffusivity in partially-saturated GDLs [11]. Chen and Jiang applied the LBM to study the distribution of liquid–gas flow in simulated GDLs [12], while Wu and Jiang reconstructed CL and GDL to evaluate different parameters such as tortuosity and pore-size distribution [13]. In addition, an analytical study to determine the effective diffusivity of micro-porous layers has been carried out by Andisheh-Tadbir et al. [14]. However, an exhaustive comparative analysis of the ratio between the effective diffusion coefficient and the bulk diffusion coefficient considering the computation of transport parameters at microscale in GDLs has not been carried out yet.

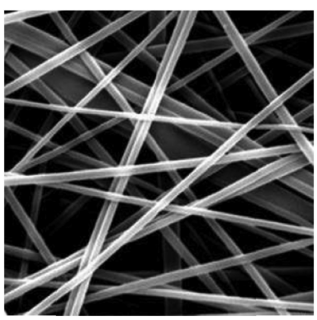

Fig. 1 – SEM image of a porous layer employed as GDL. This GDL corresponds to the carbon paper type.

This study aims, based on several stochastically created GDLs, to analyze and compare different proposed correlations to estimate the diffusibility from a microscale point of view. The degree of over- and underestimation is determined for each correlation, as well as their accuracy and precision to predict the mentioned diffusion parameter. At the end, all the correlations are ranked considering the accuracy, precision and estimation. The code for generating the GDLs and solving the fluid and mass transport have been completely developed by the authors.

The rest of the paper is divided as follows: in the second section, a review of the different diffusibility correlations is given. The methodology applied, which involve GDL generation, model solution and parameters computed is presented in Section "Methodology". Results and discussions are detailed in the fourth section. Finally, conclusions are presented in Section "Conclusions".

Diffusibility correlations

Due to the presence of solid obstacles which produce different flow paths of the gases, the mass diffusion coefficient in the free space (D_{bulk}) differs from the mass diffusion coefficient in porous media (D^{eff}). According to Hoogschagen [15], the ratio between the two mentioned parameters can be defined as diffusibility:

$$Q = \frac{D^{eff}}{D_{bulk}} \tag{1}$$

There have been several attempts to obtain a correlation that allows to determine the effective diffusion coefficient as a function of the bulk diffusion coefficient. From a modeling point of view, the widely accepted correlation to scale the effective and bulk diffusion coefficient is [16]:

$$\frac{D^{eff}}{D_{bulk}} = \frac{\varepsilon}{\tau_{gas}} \tag{2}$$

where ε is the porosity of the medium and τ_{gas} is the gas-phase tortuosity, both representing geometrical aspects of the porous media. However, from a cell scale analysis, to determine the gas-phase tortuosity value is not an easy task, and therefore; several correlations in which this variable is not involved have been proposed.

One of the first studies is based on the electrical conductivity of materials with a certain amount of non-conducting particles presented by Bruggeman [17]. In the mentioned study, the

Please cite this article in press as: Espinoza-Andaluz M, et al., Comparing through-plane diffusibility correlations in PEFC gas diffusion layers using the lattice Boltzmann method, International Journal of Hydrogen Energy (2017), http://dx.doi.org/10.1016/j.ijhydene.2017.02.096

sample consists of a group of particles classified as two different phases randomly distributed in the medium. Making an analogy between the electrical transport properties and mass transport properties, the Bruggeman approximation is written as:

$$\frac{D^{eff}}{D_{bulk}} = \varepsilon^{1.5} \tag{3}$$

Neale and Nader in their study [18], based on a geometrical model in which the porous medium is formed by a bed of impermeable spheres, proposed a rational function of the porosity to estimate the diffusibility. Their prediction model is independent of the size distribution of the spheres and can be applied to diffusion, electric conduction and fluid flow with similar success. The mentioned correlation is expressed as follows:

$$\frac{D^{eff}}{D_{bulk}} = \frac{2\varepsilon}{3-\varepsilon} \tag{4}$$

In studies in which the diffusibility is analyzed [19,20], the expression proposed by Das et al. [21] is also considered. Das et al. based their work on the Hashin–Shtrikman model to obtain a correlation to determine the diffusion parameters in CLs and GDLs. For the last mentioned layer, the simplified expression is expressed as:

$$\frac{D^{eff}}{D_{bulk}} = 1 - \left(\frac{3(1-\varepsilon)}{3-\varepsilon}\right) \tag{5}$$

However, applying simple mathematical rules and evaluating several porosity values into Eq. (5), the obtained diffusibility values from this equation are equal to those obtained from Eq. (4). Because of this issue, the relationship proposed by Das et al. is not considered in the current study.

Considering the orientation of the fibers and porosity of the porous domains, Tomadakis and Sotirchos [22] proposed a way to determine the effective diffusion coefficient. They calculated, in a computational study, the effective diffusion coefficients of fibrous beds using the mean-square displacement of random walkers. Based on the percolation theory, the expression obtained is as follows:

$$\frac{D^{eff}}{D_{bulk}} = \varepsilon\left(\frac{\varepsilon-\varepsilon_p}{1-\varepsilon_p}\right)^{\alpha} \tag{6}$$

where ε_p is the percolation threshold, and α is a parameter that depends on the spatial simulation approach, i.e., 1D, 2D or 3D. For the current study, the parameters for a 3D approach are considered.

Taking as a base the correlation proposed by Tomadakis and Sotirchos, Nam and Kaviany [23] proposed different values for ε_p and α. They studied 3D fibrous diffusion media by using network models for anisotropic solid structure, and based on the percolation theory they obtained the required values in the correlation, i.e., ε_p and α, to estimate the diffusibility. The applicable values for Eq. (6), considering the digitally constructed GDLs in the current study are presented in Table 1.

Table 1 – Percolation threshold and empirical values to be replaced in Eq. (6) according to different authors. Both studies are based on the percolation theory.

Authors	ε_p	α
Tomadakis and Sotirchos [22]	0.037	0.661
Nam and Kaviany [23]	0.110	0.785

Methodology

The methodology applied in the current study can be divided into three main stages. The first one related to the porous media generation which represents the GDLs. Once the porous media are generated, the LBM is applied to obtain the fluid flow and mass concentration through the GDLs. Finally, based on the obtained results, the transport parameters can be computed. Each of the stages is described in detail in the current section.

GDL generation

During the last years, there have been several attempts to reconstruct and analyze the properties of carbon paper GDLs as reported in Ref. [24]. From a microscopical point of view, a GDL can be represented as an array of fibers randomly placed in a 3D domain. To generate the solid/pore structure, Fig. 1 has been considered as the reference. The digital generation of the GDLs employed in the present work can be explained by means of the following steps:

(a) For each layer, randomly determine the center axis of the cylinders representing the fibers. The inclination of the axis of the fibers is related to the cross-sectional dimensions.
(b) Generate the 3D geometry around the center of the axis determined in step (a).
(c) Stack the group of layers until the desirable GDL thickness is reached.

The thickness of the modeled GDLs is established at 200 μm as an approximation of the real values found from the manufacture's data [25]. Based on the study presented by Inoue et al. [26], the cross-sectional area of the domain is determined as 200 × 200 μm^2. For all the generated GDLs, the simulation domain is represented by 120 × 120 × 120 voxels.

Although the mentioned characteristics can give a good reproducibility of structural properties, several assumptions are considered in the GDL generation as follows:

- Carbon fibers are considered infinitely long and only can be cut by the box domain.
- Carbon fibers are considered as undeformable cylinders with constant diameter.
- Fibers are not allowed to stay in the direction of the GDL thickness, but are allowed to penetrate when they found each other.
- Land channel region is not considered for both, compression effects or fluid distribution.

Considering the mentioned assumptions, a digital approximation of the GDL employed during the current study is presented in Fig. 2.

For all the modeled GDLs, the porosity was restricted to be between 0.70 and 0.76 as found in real cases and also used in previous studies [25,26]. As mentioned in the assumptions,

Please cite this article in press as: Espinoza-Andaluz M, et al., Comparing through-plane diffusibility correlations in PEFC gas diffusion layers using the lattice Boltzmann method, International Journal of Hydrogen Energy (2017), http://dx.doi.org/10.1016/j.ijhydene.2017.02.096

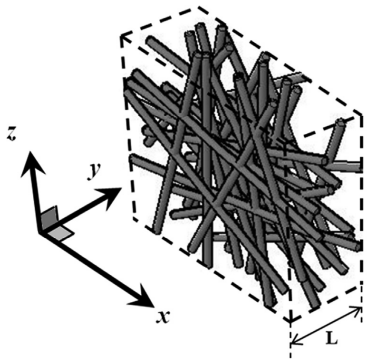

Fig. 2 – Digital representation of the generated GDLs used to compute the different transport parameters.

the fiber diameter is considered as constant based on [26,27], and equal to 7.0 μm.

Lattice Boltzmann method

To solve the fluid behavior and the mass transport phenomena through the modeled GDLs, the LBM is applied. The central basis of the LBM is the lattice Boltzmann equation (LBE) which is expressed as follows [28]:

$$\frac{\partial f_a(r,t)}{\partial t} + c_a \nabla f_a(r,t) = \frac{1}{\tau_R}\left[f_a^{eq}(r,t) - f_a(r,t)\right] \quad (7)$$

where f is the so-called particle distribution function (PDF), which is a function of the position r and the time t. In LBM the whole domain is divided into several lattice elements, and the connections between the lattice elements are the linked velocities entitled by c. To each discretized velocity is given a certain weight depending on the model to be obtained, the weight is assigned according to the linked lattice neighbor in the a-direction.

The right hand side of Eq. (7) is a result of the so-called Bhatnagar Gross & Krook (BGK) approximation [29], in which the equilibrium particle distribution, f^{eq}, should be defined according to the transport phenomenon to be solved. The relaxation parameter, τ_R, is also related to the viscosity and the mass diffusion parameter when the fluid flow and mass transport LB model is applied. For more detailed information about LBM, the readers are referred to [30].

Fluid flow LB model

The fluid flow behavior through the GDLs is recovered when the equilibrium distribution function defined by Ref. [31] is replaced in Eq. (7). Such an equilibrium distribution function is expressed as:

$$f_a^{eq} = \rho w_a\left[1 + \frac{c_a \cdot u}{{c_s}^2} + \frac{(c_a \cdot u)^2}{2\,{c_s}^4} - \frac{u^2}{2\,{c_s}^2}\right] \quad (8)$$

Here, ρ is the local density, w represents the weighting factor, c_s the lattice speed of sound and u is the velocity. Both, u and ρ are updated every iterative step, and can be obtained by the following expressions:

$$\rho = \sum_a f \quad (9)$$

$$\rho u = \sum_a c_a f_a \quad (10)$$

The treatment of the boundary conditions represents another important issue to be considered to obtain the fluid flow solution. At inlet and outlet, pressure boundary conditions are implemented according Zou and He [32]. In the other four sides of the domain, i.e., parallel to the main flow direction, periodic boundary conditions are implemented [28]. At the fluid–solid interface, the simple non-slip boundary condition is employed. The first author's code for solving the fluid flow LB model has been validated against benchmarked problems and also in porous media applications related to FCs [7,10,33]. During the simulation process, physical flow characteristics to mimic the fluid behavior through GDLs were considered. The Reynolds numbers related to the fiber diameter are computed, and in the current simulations these are smaller than 10^{-4} for each sample, which match with the ones found in PEFCs [34,35].

Mass transport LB model

According to the Fick's Law, from a macroscopic point of view, the mass concentration of gases, C, through the void space of the GDLs can be described as:

$$\nabla(D_{bulk}\nabla C) = S \quad (11)$$

where S is a source term, which due to the nature of the current work is set as zero. The mass transport LB model requires a modification of the equilibrium distribution function, and is expressed as [36]:

$$g_a^{eq} = C w_a\left[1 + \frac{3\,c_a \cdot u}{{c_s}^2}\right] \quad (12)$$

Similar to the fluid flow LB models, boundary conditions should be implemented. At the inlet and outlet, the mass concentration is prescribed according to [37]. When the fluid and solid are in contact, a simple bound-back boundary is applied. On the other four sides of the domain, periodic boundary conditions are imposed.

To validate the developed mass transport LB model, the mass diffusion in a 3D square duct is simulated. The analytical solution of Eq. (11), with no consideration of the source term and due to symmetry in only one direction, is given by the following linear function:

$$C(y) = -\frac{C_{in} - C_{out}}{L}y + C_{in} \quad (13)$$

Here, C_{in} and C_{out} are 1.0 and 0.1, respectively. The length of the square duct is given by L, which will represent the thickness of the GDLs. Fig. 3 shows a comparison between the mass concentration profile obtained from our mass transport LB model and the analytical solution, i.e., Eq. (13).

Results show a good agreement between the analytical and LBM simulations. The deviation error falls in the range of −1.17% and 0.52% with an absolute average deviation error of 0.33%.

Please cite this article in press as: Espinoza-Andaluz M, et al., Comparing through-plane diffusibility correlations in PEFC gas diffusion layers using the lattice Boltzmann method, International Journal of Hydrogen Energy (2017), http://dx.doi.org/10.1016/j.ijhydene.2017.02.096

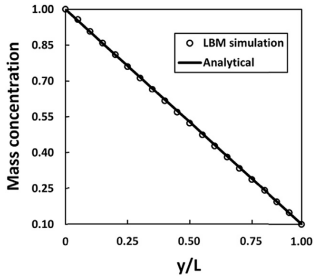

Fig. 3 – Comparison between the LBM simulation and the analytical solution for the mass concentration distribution.

Computed transport parameters

The first parameter to be computed is the porosity. Once GDLs are generated, giving the characteristics of the LBM, the whole domain is divided into small lattices. Each lattice is assigned zero or unity value to void space and solid material, respectively. The porosity is determined by:

$$\varepsilon = \frac{V_g}{V_T} \tag{14}$$

which represents the ratio of the void space (V_g), the volume of the material that can be occupied by the fluid, to the total volume (V_T).

The second parameter considered in the current study is the gas-phase tortuosity. The fluid behavior through the GDLs is computed with the LBM, as a result the velocity field can be obtained using Eq. (10). To determine the gas-phase tortuosity, the following expression is employed [38]:

$$\tau_g = \frac{\sum_{i,j,k} \boldsymbol{u}_{mag}(i,j,k)}{\sum_{i,j,k} |\boldsymbol{u}_y(i,j,k)|} \tag{15}$$

where u_{mag} represents the magnitude of the velocity in each position, and u_y corresponds to the velocity in the main flow direction.

Finally, based on the obtained results from the mass transport LB model, the diffusibility of the GDLs is computed. According to [11], the diffusibility can be determined as follows:

$$\frac{D^{eff}}{D_{bulk}} = \frac{\iint j \, dA}{A\left(\frac{D_{bulk}\,\Delta C}{L}\right)} \tag{16}$$

where j is the local diffusive flux which can be computed as explained by Ref. [39], A is the cross-sectional area of the analyzed GDL, L corresponds to the GDL thickness and ΔC is the concentration difference between the inlet and outlet.

It is important to notice that the gas-phase tortuosity and diffusibility are directional dependent. In this study, only the through-plane (TP) direction for both variables is considered due to the importance of the fluid and mass behavior between the flow plates and the electrolyte. From now on, when diffusibility and gas-phase tortuosity are mentioned, it should be noted that the through-plane direction is analyzed.

Results and discussions

The mentioned variables in the previous section are computed once the steady state has been reached, i.e., when the relative variation of the studied characteristic fall in a range below 10^{-6}. The diffusibility for all the digitally created GDLs is computed by using Eq. (16), and these values are taken as expected values to be compared with the other correlations in which the porosity and gas-phase tortuosity are involved.

To obtain the gas-phase tortuosity, the fluid flow LB model through the GDLs is applied. The velocity field is determined and the gas-phase tortuosity is computed by using Eq. (15). Fig. 4 shows the fluid behavior at three different positions in the main flow direction. Regions with higher velocities are red colored while regions with lower velocities are represented by blue color. As expected, the velocity is zero in the regions occupied by the fibers and high velocities are found in the pore space material.

Following the fluid flow LB model, the mass transport LB model is applied to the GDLs. The mass concentration in each lattice element is computed and the diffusibility is determined by using Eq. (16). Fig. 5 shows the mass concentration distribution for three different positions in the gradient

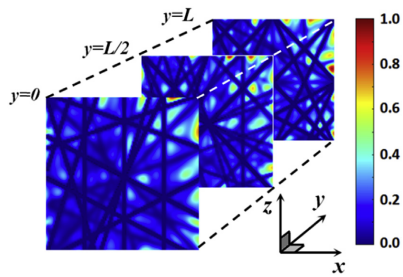

Fig. 4 – Digital representation of fluid flow velocity through a modeled GDL at three different positions in the main flow direction (y+).

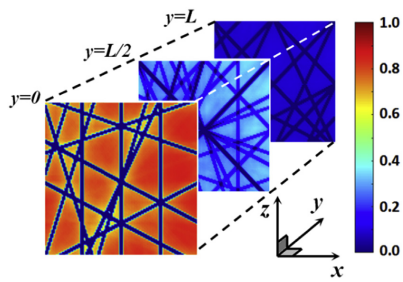

Fig. 5 – Digital representation of the mass concentration in the pore space through a modeled GDL at three different positions in the gradient concentration direction (y+).

Please cite this article in press as: Espinoza-Andaluz M, et al., Comparing through-plane diffusibility correlations in PEFC gas diffusion layers using the lattice Boltzmann method, International Journal of Hydrogen Energy (2017), http://dx.doi.org/10.1016/j.ijhydene.2017.02.096

concentration. In analogy to the previous description, higher concentrations are given by red color regions and lower concentration are represented in blue color regions. At the fiber positions, zero mass concentrations are found as expected.

Considering the computational nature of the current work and the randomness induced due to the GDL generation, the number of simulated GDLs should be limited to avoid waste of computational resources. The required number of samples to be implemented in this work is determined based on the cumulative standard deviation (CSD) and standard error of the mean (SEM), detailed information about these parameters is given in the appendix.

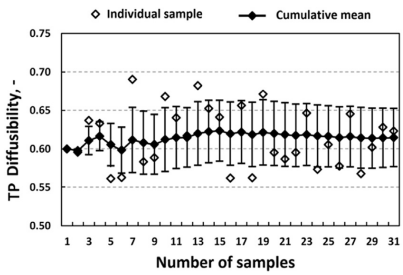

Fig. 6 – TP diffusibility values computed for each GDL sample. All the values fall in the range of 0.55 and 0.70.

The computed diffusibility for each sample, the diffusibility cumulative mean, and the cumulative standard deviation are presented in Fig. 6. Considering all the samples the diffusibility of the GDLs is 0.6144 ± 0.0377, while the obtained porosity is 0.7368 ± 0.0166. The computed GDL porosities agree with those found in real ones and in previous studies [21,22].

To determine the most suitable correlation to estimate the diffusibility, a comparison graph showing the computed diffusibility and each estimation relationship, i.e., Eqs. (2)–(4) and Eq. (6), is presented in Fig. 7. In each graph the vertical axis represents the values of the computed diffusibility, and on the horizontal axis the value obtained with the correlation is depicted. Additionally, a straight line is shown, the line of equality, which allows to evaluate the overprediction or underprediction of each relationship.

From a simple inspection of Fig. 7, the most suitable predictions are obtained in (a), (b) and (d). These are the relationship in which the porosity and gas-phase tortuosity are involved, the Bruggeman relationship and the one proposed by Tomadakis and Sotirchos, respectively.

Similarly, based on Fig. 7(f), it is easy to conclude that the relationship proposed by Neale and Nader overpredicts the diffusibility values for most of the samples, while the Nam and Kaviany relationship underpredicts the mentioned parameter for almost all of the GDL samples. In addition, although not so

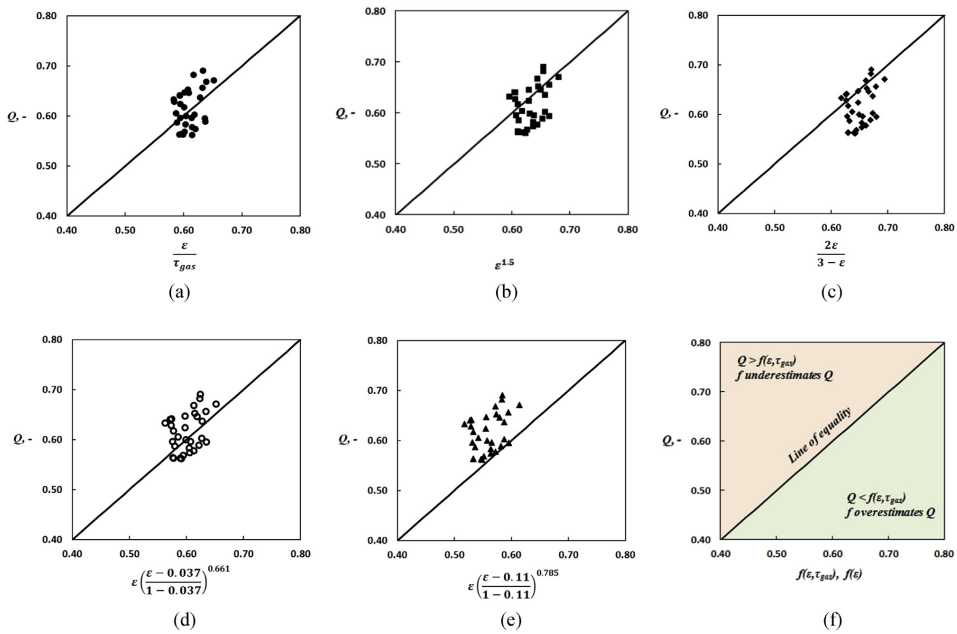

Fig. 7 – From (a)–(e): Comparison graph between the computed diffusibility values according to the mass transport LB model (vertical axis) and the previous proposed relations in which only transport parameters such as porosity and gas-phase tortuosity are involved (horizontal axis). (f) Under- and overestimation regions.

Please cite this article in press as: Espinoza-Andaluz M, et al., Comparing through-plane diffusibility correlations in PEFC gas diffusion layers using the lattice Boltzmann method, International Journal of Hydrogen Energy (2017), http://dx.doi.org/10.1016/j.ijhydene.2017.02.096

clear, the obtained values with the Nam and Kaviany relationship are the most dispersed diffusibility values.

To evaluate in detail the relationships in the current work, average, standard deviation and the degree of under/overestimation are determined. The corresponding values are presented in Table 2.

The computed standard deviations help us to evaluate the observations in Fig. 7. The most dispersed data are produced by the Nam and Kaviany relationship, i.e., the standard deviation of the diffusibility values computed with this relationship is the greatest. On the other hand, the less disperse diffusibility data are obtained when porosity and gas-phase tortuosity are considered, i.e., Eq. (2). The data dispersion is one of the parameters to be considered in order to find the most suitable relationship predicting the diffusibility. In measurements, the dispersion of the data is often called precision.

To determine the accuracy of the proposed relationships, the average of the diffusibility values obtained with the relationships is compared with the average of the diffusibility values obtained with Eq. (16). The most positive relative deviation error occurs when the Neale and Nader relationship is used, i.e., +6.00%, while the less negative deviation error occurs if the Nam and Kaviany relationship is used, i.e., −8.89%.

The last parameter to be considered to choose the best predictive relationship is related to the percentage of over- and underestimated values. An ideal relationship is considered to be one in which the number of overestimated diffusibility and the number of underestimated diffusibility values is the same, and it is named symmetry factor (SF). To determine SF, the following expression is used:

$$SF = \frac{MAX[over, under]}{Total - MAX[over, under]} \quad (17)$$

where, *over* and *under* correspond to the number of overestimation and underestimation, respectively. The mentioned values are determined for each relationship, and *MAX* is the function to choose the maximum value of these. According to this definition, the prediction is more symmetric when the *SF* is closer to unity. The *SF* is obtained from the data of the analyzed relationship, showing that the most symmetric is the one in which the porosity and gas-phase tortuosity are involved, i.e., $SF = 1.21$. In the opposite extreme, the less symmetric relationship is found by the proposed by Nam and Kaviany, i.e., $SF = 30.0$.

Considering the three mentioned characteristics, i.e., precision, accuracy and symmetry, the relationships can be ranked to analyze a suitable option. Fig. 8 shows the ranking of the five relationships analyzed in the current study. In all the parameters, the best ranked is the relationship in which the porosity and gas-phase tortuosity are considered in the estimation of the diffusibility.

Table 2 – Average, standard deviation and percentage of under- and overestimated TP diffusibility values according to the previously proposed relationships.

Relationship	Average	Standard deviation	% of predicted data	
			Over-	Under-
Eq. (2)	0.6096	0.0180	45.2	54.8
Eq. (3)	0.6326	0.0214	67.7	32.3
Eq. (4)	0.6513	0.0195	77.4	22.6
Eq. (6)*	0.6017	0.0226	41.9	58.1
Eq. (6)*	0.5598	0.0243	3.20	96.8

*See Table 1.

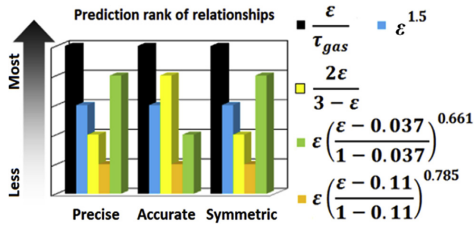

Fig. 8 – A ranking of the relationships analyzed in the current work considering the precision, accuracy and symmetry.

Conclusions

A detailed analysis of five different correlations to estimate the TP diffusibility has been carried out. The GDLs employed in this study have been digitally created by using an in-house code. Similarly, to obtain the fluid flow behavior and describe the mass transport phenomena through the GDLs, the fluid flow LB model and mass transport LB model were applied, respectively. All the simulations are carried out for single-phase flow, and therefore; no water content or water saturation is considered.

It has been demonstrated that the most suitable correlation to estimate the TP diffusibility in the GDLs is the one considering both transport parameters, i.e., porosity and gas-phase tortuosity. Its suitability is supported by three parameters: precision, accuracy and symmetry. If precision and symmetry are the parameters considered, the proposed relationship by Tomadakis and Sotirchos is ranked second. The correlation proposed by Neale and Nader ranks second if the accuracy is the only parameter analyzed. Among the five correlations analyzed in this work, the Bruggeman ranks in third place for all the considered parameters.

It is important to notice that the influence of the microporous layer (MPL) and the poly-tetrafluoroethylene (PTFE) content have not been considered in the current study. This will be analyzed in a further study taking into account that these variables can affect the flow paths of the fluid through the GDLs, and therefore influence the gas-phase tortuosity.

Acknowledgments

Financial support for this work comes from National Secretary of Higher Education, Science, Technology and Innovation, SENESCYT (Ecuador) and ESPOL, which is gratefully acknowledged.

Also, the authors want to thank Vinnova VINNMER (2015-01485) and the National Natural Science Foundation of China (Grant No. 51550110238).

Please cite this article in press as: Espinoza-Andaluz M, et al., Comparing through-plane diffusibility correlations in PEFC gas diffusion layers using the lattice Boltzmann method, International Journal of Hydrogen Energy (2017), http://dx.doi.org/10.1016/j.ijhydene.2017.02.096

Nomenclature

A	Cross-sectional area, Eq. (16)
1D, 2D, 3D	One-, two-, three-dimensional
BGK	Bhatnagar Gross & Krook
c	Discretized velocity, Eq. (7)
C	Concentration, Eq. (11)
CSD	Cumulative standard deviation
CL	Catalyst layer
D	Mass diffusion coefficient, $L^2\ T^{-1}$
f	Particle distribution function, Eq. (7)
FC	Fuel cell
g	Particle distribution function, Eq. (12)
GDL	Gas diffusion layer
i,j,k	x-, y-, z-position, Eq. (15)
j	Local diffusive flux, Eq. (16)
L	Length, thickness, L, Eq. (13)
LB	Lattice Boltzmann
LBM	Lattice Boltzmann method
LLN	Law of large number
m	Unit length, international system
MAX	Maximum value, Eq. (17)
MPL	Microporous layer
Over	Number of overestimated, Eq. (17)
PDF	Particle distribution function
PEFC	Polymer electrolyte fuel cell
PTFE	poly-tetrafluoroethylene
Q	Diffusibility, –
R	Position vector, Eq. (7)
S	Source term, Eq. (11)
SEM	Scanning electron microscopy
SEM	Standard error of the mean
SF	Symmetry factor, Eq. (17)
T	Time, Eq. (7)
TP	Through-plane
TPB	Three-phase boundary
u	Velocity vector, $M\ L^{-1}$, Eq. (8)
under	Number of underestimated, Eq. (17)
V	Volume, L^3, Eq. (14)
W	Weighting factor, Eq. (8)
Y	Flow direction position, Eq. (13)

Chemicals

H_2	Hydrogen

Greek symbols

α	Empirical value, Eq. (6)
Δ	Variable change, Eq. (16)
ε	Porosity, –
ρ	Density, $M\ L^{-3}$, Eq. (8)
τ	Tortuosity, –
τ	Relaxation parameter, Eq. (7)
μ	$\times 10^{-6}$

Subscripts

a	Lattice directions, Eq. (7)
bulk	Refer to bulk, Eq. (1)
g	Void space, Eq. (14)
gas	Gas-phase
in	Inlet, Eq. (13)
mag	Magnitude, Eq. (15)
out	Oulet, Eq. (13)
p	Percolation threshold, Eq. (6)
R	Relaxation parameter, Eq. (7)
s	Sound, Eq. (8)
T	Total, Eq. (14)
y	Main flow direction, Eq. (15)

Superscripts

Eff	Refer to effective, Eq. (1)
eq	equilibrium, Eq. (7)

Appendix. Determination of the number of samples

To determine the number of times that the model should be run, i.e., the number of GDL samples required in the study, an analysis of the cumulative standard deviation (CSD) and the standard error of the mean (SEM) was performed based on [40]. As observed in Fig. 9, the CSD seems to stabilize around the sample numbers 7 to 13. However, there is still a small variation around 0.040. Considering this variation, the runs continued until the value of the CSD was smaller than 0.040 for 5 consecutive samples.

Considering the CSD and the computed average, the coefficient of variation (CV) is determined. For all the samples, CV in percentage is equal to 6.14%, which is an acceptable value in engineering applications. The average and standard deviation of the diffusibility for all the samples is 0.6144 ± 0.0377. Based on the SEM obtained for all the samples, i.e., 0.0069, there is a probability that the true population mean falls between 0.60 and 0.63 with a 95% of confidence. This can be corroborated in Ref. [41]. Additionally, the change in the cumulative mean was analyzed as presented in Fig. 10. The trend is that the change in the cumulative mean decreases as the number of samples increases, which is compatible with the law of large numbers (LLN) in experiments.

The continuous line shows a curve approximation of the behavior of the change in the cumulative mean of each sample. The function can be expressed as follows:

$$f(n) = 0.009717^{-0.08375n} \tag{18}$$

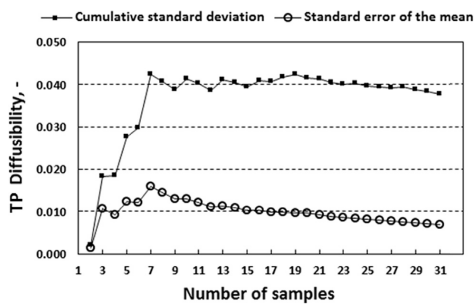

Fig. 9 – Behavior of the CSD and the SEM of the TP diffusibility from the computed GDL samples.

Please cite this article in press as: Espinoza-Andaluz M, et al., Comparing through-plane diffusibility correlations in PEFC gas diffusion layers using the lattice Boltzmann method, International Journal of Hydrogen Energy (2017), http://dx.doi.org/10.1016/j.ijhydene.2017.02.096

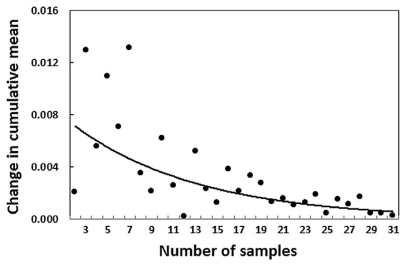

Fig. 10 – The evaluation of the cumulative mean shows a decreasing trend as the number of samples increases.

where n is the number of samples. As expected, when $n \to \infty$, the change in the cumulative mean approaches zero.

REFERENCES

[1] 2015 fuel cell technologies market report – department of energy. http://energy.gov/sites/prod/files/2016/10/f33/fcto_2015_market_report.pdf.
[2] Singdeo D, Dey T, Ghosh PC. Three dimensional computational fluid dynamics modelling of high temperature polymer electrolyte fuel cell. Appl Mech Mater 2014;492:365–9. http://dx.doi.org/10.4028/www.scientific.net/amm.492.365.
[3] Wang Y, Wang C-Y. Transient analysis of polymer electrolyte fuel cells. Electrochimica Acta 2005;50(6):1307–15. http://dx.doi.org/10.1016/j.electacta.2004.08.022.
[4] Jeon DH. Numerical study of serpentine flow-field cooling plates on PEM fuel cells performance. Int J Energy Res 2011;37(6):510–21. http://dx.doi.org/10.1002/er.1930.
[5] Obayopo SO, Bello-Ochende T, Meyer JP. Three-dimensional optimisation of a fuel gas channel of a proton exchange membrane fuel cell for maximum current density. Int J Energy Res 2011;37(3):228–41. http://dx.doi.org/10.1002/er.1935.
[6] Molaeimanesh GR, Saeidi Googarchin H, Qasemian Moqaddam A. Lattice Boltzmann simulation of proton exchange membrane fuel cells – a review on opportunities and challenges. Int J Hydrogen Energy 2016;41(47):22221–45. http://dx.doi.org/10.1016/j.ijhydene.2016.09.211.
[7] Espinoza M, Sunden B, Andersson M. Impact on diffusion parameters computation in gas diffusion layers, considering the Land/channel region, using the lattice Boltzmann method. ECS Trans 2016;75(14):521–30. http://dx.doi.org/10.1149/07514.0521ecst.
[8] Gao Y. Using MRT lattice Boltzmann method to simulate gas flow in simplified catalyst layer for different inlet–outlet pressure ratio. Int J Heat Mass Transf 2015;88:122–32. http://dx.doi.org/10.1016/j.ijheatmasstransfer.2015.04.031.
[9] Froning D, Yu J, Gaiselmann G, Reimer U, Manke I, Schmidt V, et al. Impact of compression on gas transport in non-woven gas diffusion layers of high temperature polymer electrolyte fuel cells. J Power Sources 2016;318:26–34. http://dx.doi.org/10.1016/j.jpowsour.2016.03.102.
[10] Espinoza M, Andersson M, Sundén B. Predicting transport parameters in PEFC gas diffusion layers considering micro-architectural variations using the Lattice Boltzmann method. Int J Energy Res 2016. http://dx.doi.org/10.1002/er.3661.
[11] García-Salaberri PA, Hwang G, Vera M, Weber AZ, Gostick JT. Effective diffusivity in partially-saturated carbon-fiber gas diffusion layers: effect of through-plane saturation distribution. Int J Heat Mass Transf 2015;86:319–33. http://dx.doi.org/10.1016/j.ijheatmasstransfer.2015.02.073.
[12] Chen W, Jiang F. Impact of PTFE content and distribution on liquid–gas flow in PEMFC carbon paper gas distribution layer: 3D lattice Boltzmann simulations. Int J Hydrogen Energy 2016;41(20):8550–62. http://dx.doi.org/10.1016/j.ijhydene.2016.02.159.
[13] Wu W, Jiang F. Microstructure reconstruction and characterization of PEMFC electrodes. Int J Hydrogen Energy 2014;39(28):15894–906. http://dx.doi.org/10.1016/j.ijhydene.2014.03.074.
[14] Andisheh-Tadbir M, El Hannach M, Kjeang E, Bahrami M. An analytical relationship for calculating the effective diffusivity of micro-porous layers. Int J Hydrogen Energy 2015;40(32):10242–50. http://dx.doi.org/10.1016/j.ijhydene.2015.06.067.
[15] Hoogschagen J. Diffusion in porous catalysts and adsorbents. Industrial Eng Chem 1955;47(5):906–12. http://dx.doi.org/10.1021/ie50545a016.
[16] Kaviany M. Principles of heat transfer in porous media. Mechanical engineering series. 1995. http://dx.doi.org/10.1007/978-1-4612-4254-3.
[17] Bruggeman DAG. Berechnung verschiedener physikalischer Konstanten von heterogenen Substanzen. I. Dielektrizitätskonstanten und Leitfähigkeiten der Mischkörper aus isotropen substanzen. Ann Der Phys 1935;416(7):636–64. http://dx.doi.org/10.1002/andp.19354160705.
[18] Neale GH, Nader WK. Prediction of transport processes within porous media: diffusive flow processes within an homogeneous swarm of spherical particles. AIChE J 1973;19(1):112–9. http://dx.doi.org/10.1002/aic.690190116.
[19] Zamel N, Li X, Shen J. Correlation for the effective gas diffusion coefficient in carbon paper diffusion media. Energy Fuels 2009;23(12):6070–8. http://dx.doi.org/10.1021/ef900653x.
[20] Yuan J, Sundén B. On mechanisms and models of multi-component gas diffusion in porous structures of fuel cell electrodes. Int J Heat Mass Transf 2014;69:358–74. http://dx.doi.org/10.1016/j.ijheatmasstransfer.2013.10.032.
[21] Das PK, Li X, Liu Z-S. Effective transport coefficients in PEM fuel cell catalyst and gas diffusion layers: beyond Bruggeman approximation. Appl Energy 2010;87(9):2785–96. http://dx.doi.org/10.1016/j.apenergy.2009.05.006.
[22] Tomadakis MM, Sotirchos SV. Ordinary and transition regime diffusion in random fiber structures. AIChE J 1993;39(3):397–412. http://dx.doi.org/10.1002/aic.690390304.
[23] Nam JH, Kaviany M. Effective diffusivity and water-saturation distribution in single- and two-layer PEMFC diffusion medium. Int J Heat Mass Transf 2003;46(24):4595–611. http://dx.doi.org/10.1016/s0017-9310(03)00305-3.
[24] Shojaeefard MH, Molaeimanesh GR, Nazemian M, Moqaddari MR. A review on microstructure reconstruction of PEM fuel cells porous electrodes for pore scale simulation. Int J Hydrogen Energy 2016;41(44):20276–93. http://dx.doi.org/10.1016/j.ijhydene.2016.08.179.
[25] Gas diffusion layer comparison table. http://fuelcellsetc.com/helpful-tools/gas-diffusion-layer-gdl-comparison-chart/.
[26] Inoue G, Yoshimoto T, Matsukuma Y, Minemoto M. Development of simulated gas diffusion layer of polymer electrolyte fuel cells and evaluation of its structure. J Power Sources 2008;175(1):145–58. http://dx.doi.org/10.1016/j.jpowsour.2007.09.014.

Please cite this article in press as: Espinoza-Andaluz M, et al., Comparing through-plane diffusibility correlations in PEFC gas diffusion layers using the lattice Boltzmann method, International Journal of Hydrogen Energy (2017), http://dx.doi.org/10.1016/j.ijhydene.2017.02.096

[27] Daino MM, Kandlikar SG. 3D phase-differentiated GDL microstructure generation with binder and PTFE distributions. Int J Hydrogen Energy 2012;37(6):5180–9. http://dx.doi.org/10.1016/j.ijhydene.2011.12.050.

[28] Mohamad AA. The Boltzmann equation. Lattice Boltzmann method. 2011. p. 15–24. http://dx.doi.org/10.1007/978-0-85729-455-5_2.

[29] Bhatnagar PL, Gross EP, Krook M. A model for collision processes in gases. I. Small amplitude processes in charged and neutral one-component systems. Phys Rev 1954;94(3):511–25. http://dx.doi.org/10.1103/physrev.94.511.

[30] Sukop M, Thorne D. Lattice Boltzmann modeling: an introduction for geoscientists and engineers. Berlin: Springer; 2006. p. 31–54. http://dx.doi.org/10.1007/3-540-27982-2_4.

[31] Qian YH, D'Humières D, Lallemand P. Lattice BGK models for navier-stokes equation. Europhys Lett (EPL) 1992;17(6):479–84. http://dx.doi.org/10.1209/0295-5075/17/6/001.

[32] Zou Q, He X. On pressure and velocity boundary conditions for the lattice Boltzmann BGK model. Phys Fluids 1997;9(6):1591. http://dx.doi.org/10.1063/1.869307.

[33] Espinoza Andaluz M. On microstructural analysis of porous media existing in fuel cells using the lattice Boltzmann method. Department of Energy Sciences, Lund University; 2015. http://dx.doi.org/10.13140/RG.2.2.33744.92167.

[34] Andersson M, Beale SB, Espinoza M, Wu Z, Lehnert W. A review of cell-scale multiphase flow modeling, including water management, in polymer electrolyte fuel cells. Appl Energy 2016;180:757–78. http://dx.doi.org/10.1016/j.apenergy.2016.08.010.

[35] Froning D, Gaiselmann G, Reimer U, Brinkmann J, Schmidt V, Lehnert W. Stochastic aspects of mass transport in gas diffusion layers. Transp Porous Media 2014;103(3):469–95. http://dx.doi.org/10.1007/s11242-014-0312-9.

[36] Yoshino M, Inamuro T. Lattice Boltzmann simulations for flow and heat/mass transfer problems in a three-dimensional porous structure. Int J Numer Methods Fluids 2003;43(2):183–98. http://dx.doi.org/10.1002/fld.607.

[37] Sukop M, Thorne D. Lattice Boltzmann modeling: an introduction for geoscientists and engineers. Berlin: Springer; 2006. p. 117–44. http://dx.doi.org/10.1007/3-540-27982-2_8.

[38] Nabovati A, Sousa ACM. Fluid flow simulation in random porous media at pore level using lattice Boltzmann method. New Trends Fluid Mech Res 2007:518–21. http://dx.doi.org/10.1007/978-3-540-75995-9_172.

[39] D'Orazio A, Succi S. Boundary conditions for thermal lattice Boltzmann simulations. Comput Sci — ICCS 2003;2003:977–86. http://dx.doi.org/10.1007/3-540-44860-8_101.

[40] Ritter FE, Schoelles MJ, Quigley KS, Klein LC. Determining the number of simulation runs: treating simulations as theories by not sampling their behavior. Human-in-the-loop simulations. 2011. p. 97–116. http://dx.doi.org/10.1007/978-0-85729-883-6_5.

[41] McCallum Layton & Co. Home page: https://www.mccallum-ayton.co.uk/tools/statistic-calculators/confidence-interval-for-mean-calculator/#confidence-interval-for-mean-calculator.

Please cite this article in press as: Espinoza-Andaluz M, et al., Comparing through-plane diffusibility correlations in PEFC gas diffusion layers using the lattice Boltzmann method, International Journal of Hydrogen Energy (2017), http://dx.doi.org/10.1016/j.ijhydene.2017.02.096

Notes

Mayken Stalin Espinoza-Andaluz has taught different courses related to Physics at undergraduate level since 2002 in his alma mater ESPOL (Ecuador). He ventured into the renewable energy research in 2008 during his scientific training in Germany, and during 2013; because of the need of increasing the technological and scientific skills in his home country, he decided to start his PhD studies in Sweden.

This book is his doctoral thesis, it was produced at the Department of Energy Sciences in 2017, Lund University.

Mayken Stalin Espinoza-Andaluz ha dictado diferentes cursos relacionados a ciencias Físicas a nivel de pregrado desde el 2002 en ESPOL (Ecuador), su alma mater. Incursionó en la investigación de las energías renovables en 2008 durante su entrenamiento científico en Alemania, y durante el 2013; debido a la necesidad de incrementar las destrezas científicas y tecnológicas de su país, dicidió iniciar sus estudios de PhD en Suecia.

Este libro es su tesis doctoral, fue producido en el Departamento de Ciencias Energéticas en 2017, Universidad de Lund.

Printed by Media-Tryck, Lund 2017 NORDIC ECOLABEL, 3041 0903

LUND UNIVERSITY

Lund University
Faculty of Engineering
Department of Energy Sciences
ISBN 978-91-7753-236-1
ISRN LUTMDN/TMHP-17/1129-SE